The Amplitude Formalism

for

Pattern-Forming Systems

with

Spontaneously Broken Isotropy

and some Applications

Von der Universität Bayreuth
zur Erlangung der Würde eines
Doktors der Naturwissenschaften (Dr. rer. nat.)
genehmigte Abhandlung

von

Axel G. Roßberg

geboren in Essen

1. Gutachter:	Prof. L. Kramer, Ph.D.
2. Gutachter:	Prof. Dr. F. Busse
Tag der Einreichung:	12. 11. 1997
Tag des Kolloquiums:	27. 01. 1998

Der Amplitudenformalismus
für
musterbildende Systeme
mit
spontan gebrochener Isotropie
und einige Anwendungen

Zusammenfassung

Der Amplitudenformalismus ist ein wichtiges Hilfsmittel zum Verständnis der raum-zeitlichen Dynamik komplexer nichtlinearer Systeme. Insbesondere bei der Beschreibung von Systemen, die selbstständig Strukturen (Muster) in ihrem Innern ausbilden, ohne daß diese von außen vorgegeben wären, hat sich diese Methode als recht erfolgreich herausgestellt [10].

Ein Beispiel: die reelle Ginzburg-Landau-Gleichung

Ein typisches Beispiel für eine Amplitudengleichung ist die reelle Ginzburg-Landau-Gleichung

$$\tau \partial_t A = \varepsilon A + \xi_{xx}^2 \partial_x^2 A + \xi_{yy}^2 \partial_y^2 A - g|A|^2 A. \tag{1}$$

Die Koeffizienten τ, ε, ξ_{xx}^2, ξ_{yy}^2 und g seien dabei auf positive reelle Werte beschränkt, während $A = A(x, y, t)$ eine komplexwertige Funktion ist (einige Autoren lassen unter diesem Namen auch für A nur reelle Werte zu). Die Größe A steht in diesem Fall für Amplitude und Phase einer räumlich periodischen, selbstorganisierten Struktur ("Rollen") in einem homogenen, anisotropen System. Die periodischen Variationen selbst wurden dabei, grob gesagt, bereits als ein Faktor $\exp(iq_c x)$ abgespalten. Auch leichte Verzerrungen der Rollen sowie Defekte (Dislokationen) in der Rollenstruktur sind zugelassen. Die Eigenschaften der reellen Ginzburg-Landau-Gleichung und ihrer Lösungen sind weitgehend verstanden [24, 10]. Dies liegt zu einem nicht unwesentlichen Teil daran, daß sich die Dynamik von A aus einem Potential

$$\mathfrak{U} = \int\!\!\int -|A|^2 + |\partial_x A|^2 + |\partial_y A|^2 + \frac{1}{2}|A|^4 \, dx \, dy$$

ableiten läßt und deshalb alle Lösungen von Gl. (1) zu einfachen, stationären Zuständen relaxieren.

Der Amplitudenformalismus

Amplitudengleichungen stehen ihrem Charakter nach zwischen einfachen asymptotischen Entwicklungen (Störungsrechnung), vereinfachten theoretischen Modellen, wie etwa dem Van-der-Waals-Gas, und den Normalformen der Bifurkationstheorie gewöhnlicher Differentialgleichungen [14].

Gemäß der Art ihrer Herleitung gehören Amplitudengleichungen zweifellos in den Bereich asymptotischer Methoden. Entsprechend gibt es auch einen gewissen Limes ($\varepsilon \to 0$ in Gl. 1), in dem sie als eine exakte Beschreibung des zu modellierenden Systems betrachtet werden können und einen quantitativen Vergleich mit dem Experiment zulassen.

Andererseits haben Amplitudengleichungen oft eine sehr einfache Struktur. Diese ermöglicht es, mit der Trennschärfe und Allgemeinheit analytischer Methoden Schlußfolgerungen zu ziehen. Im Idealfall lassen sich so gewonnene Erkenntnisse modellhaft auf komplexere reale Systeme übertragen, auch wenn man den asymptotischen Gültigkeitsbereich der Gleichungen bereits verlassen hat. Manchmal liefert das Modell erst die begriffliche Basis, um physikalische Effekte intuitiv zu verstehen oder auch nur zu beschreiben.

Eine Beziehung zu den Normalformen besteht insofern, als daß man auch für Amplitudengleichungen erwartet, daß Beschreibungen verschiedenster physikalischer Systeme sich in eine kleine Zahl relevanter Klassen einordnen lassen, die unterschiedlichen Symmetrietypen entsprechen. Innerhalb einer Klasse sind die Gleichungen formal äquivalent und unterscheiden sich nur in der Größe einiger freier Parameter. Anders als bei gewöhnlichen Differentialgleichungen scheint es jedoch nicht möglich, durch geeignete nichtlineare Variablentransformationen den Bereich ihrer exakten Gültigkeit *in der universellen, einfachen Form* bis zu einem endlichen Abstand vom Entwicklungspunkt zu erweitern (s. z.B. [28]).

Für alle diese Aspekte wird es in der vorliegenden Arbeit Beispiele geben.

Eine neue Symmetrieklasse

Die der reellen Ginzburg-Landau-Gleichung zugrundeliegende Anisotropie wird als von außen fest vorgegeben betrachtet. In der gegenwärtigen Arbeit soll nun der Fall untersucht werden, daß die Symmetriebrechung inhärent und spontan ist. Das System als ganzes bleibt deshalb weiterhin isotrop. Insbesondere kann die durch die Symmetriebrechung ausgezeichnete Richtung selbst räumlich und zeitlich variieren. Wir werden diese Richtung im Folgenden als "Direktor" bezeichnen und durch den Winkel $\varphi = \varphi(x, y, t)$ beschreiben, in dem sie zur x-Achse des Koordinatensystems steht.

Bei der Entwicklung der Amplitudengleichungen zur Beschreibung der gekoppelten Dynamik von Rollenamplitude A und Direktor φ stößt man zunächst auf ein eher formales Problem. Bei der reellen Ginzburg-Landau-Gleichung war die Richtung des Wellenvektors der zugrundeliegenden Modulationen noch im wesentlichen vorgegeben (hier die x-Richtung), und es mußten nur kleine Abweichungen davon berücksichtigt werden. In unserem Fall definiert sich der bevorzugte Wellenvektor von Modulationen jedoch nur relativ zum Direktor. Eine Herleitung der Gleichungen durch Entwicklung um einen Zustand (eigentlich eine Eigenfunktion) mit fest vorgegebenem Wellenvektor bräche künstlich die Isotropie, was sich durch einen Verlust an Symmetrie in den Amplitudengleichungen wiederspiegeln würde.

Deshalb werden, nach einer eingehenden Beschreibung des die neue Symmetrieklasse charakterisierenden Transformationsverhaltens, in Abschnitt 1.1 Definitionen für A und φ eingeführt (Gl. (1.19,1.18)), die auf Grund ihrer Symmetrieeigenschaften inhärent rotationsinvariante Amplitudengleichungen erzwingen. Für "Normalrollen" (s.u.) ergeben sich diese (Abschnitt 1.2) als

$$\tau\partial_t A = \Big[\varepsilon + \xi_{xx}^2\partial_x^2 + \xi_{yy}^2(\partial_y - iq_c\varphi)^2 - g|A|^2 + i\beta_y\varphi_{,y}\Big]A, \tag{2}$$

$$\tilde{\gamma}_1\partial_t\varphi = K_1\partial_y^2\varphi + K_3\partial_x^2\varphi - \tilde{\chi}_a H^2\varphi + \frac{\Gamma}{4}(-iq_cA^*(\partial_y - iq_c\varphi)A + \text{c.c.}). \tag{3}$$

Die Rotationsinvarianz drückt ich hier im Auftreten der Kombination $(\partial_y - iq_c\varphi)$ aus, die für den Winkel zwischen Direktor und lokalem Wellenvektor steht. Der Term $-\tilde{\chi}_a H^2\varphi$ bricht diese Isotropie und wurde hinzugefügt, um die Lösungen der Gleichungen zu stabilisieren (Abschnitt 1.4.1). Die Gültigkeit von Gln. (2,3) ist auf kleine Winkel φ beschränkt. Eine Erweiterung zu beliebig großen Winkeln ist jedoch möglich (Gln. (1.130,1.131)).

Ähnlich lassen sich Gleichungen für "Schrägrollen" aufstellen. Schrägrollen unterscheiden sich von Normalrollen dadurch, daß bei ihnen der bevorzugte Wellenvektor weder parallel noch senkrecht zum Direktor steht. Sie treten aus Symmetriegründen immer mit zwei möglichen Wellenvektoren auf (s. Abschnitt 1.1.4).

Die neue Definition der Amplitude A macht es nötig, auch den gängigen Formalismus der asymptotischen Entwicklung zu überdenken, der von den Grundgleichungen des zu beschreibenden physikalischen Systems letztendlich zur Bestimmung der Koeffizienten der Amplitudengleichungen führt (Abschnitt 1.3). Es zeigt sich jedoch, daß sich (in niedrigster Ordnung) keine wesentlichen Änderungen ergeben.

Die Lösungen der Amplitudengleichungen

In Abschnitt 1.4 werden die neuen Gleichungen und ihre Lösungen in qualitativer Hinsicht untersucht. Zwei wichtige Ergebnisse für Normalrollen sollen hier hervorgehoben werden:

- Ist $\Gamma < 0$ in Gl. (3), so erhält das System, im Gegensatz zur reellen Ginzburg-Landau-Gleichung, einen starken Nichtpotential-Charakter.
- Auch für kleine ε skalieren die Beiträge der einzelnen Terme der Normalrollen-Gleichungen (abgesehen von dem zusätzlichen symmetriebrechenden Term) so, daß alle von der gleichen Größenordnung sind und zur Dynamik beitragen können.

Die Kombination dieser beiden Eigenschaften ist wohl die Grundlage für die überraschende Vielfalt an Strukturen, die man in numerischen Lösungen der Gln. (2,3) findet (s. Abb. 4.2).

Bei Schrägrollen gehen diese Eigenschaften zum Teil verloren. Trotzdem scheint es auch hier mindestens zwei verschiedene Typen dynamischer Zustände zu geben: "Rotating-Rolls" (Abb. 1.2) und "Swinging-Rolls" (Abb. 1.4–1.6), wie in Abschnitt 1.4.2 ausgeführt wird.

Kapitel 2 ist der analytischen Untersuchung homogener (idealer) Rollenlösungen und ihrer Stabilität gewidmet. Insbesondere für Normalrollen konnte die komplizierte Struktur des Stabilitätsbereiches zu großen Teilen aufgeklärt werden (z.B. Abb. 2.1). In vielen Fällen ist der stabile Bereich in ε von oben beschränkt. Dann enthalten die Amplitudengleichungen schon alle Effekte, die für die Stabilität homogener Rollen relevant sind. Auch bei Schrägrollen kommt man in der wichtigen Frage der Stabilität der schnellstwachsenden Mode zu einem handhabbaren Kriterium (Gl. 2.54).

Experimentelle Bezüge

Der in den vorangegangenen Kapiteln entwickelte Formalismus wird nun in Kapitel 3 auf ein experimentelles Modellsystem angewandt. Die Ergebnisse werden zum einen mit direkten numerischen Rechnungen [16], zum anderen mit einigen experimentellen Arbeiten verglichen. In weiten Bereichen wird eine gute Übereinstimmung erzielt.

Das letzte Kapitel gibt eine detaillierte Beschreibung einer Klasse komplexer dynamischer Lösungen von Gln. (2,3). Sie ist dadurch gekennzeichnet, daß die Größe φ räumlich periodisch variiert und Defekte (Nullstellen von A) sich in parallelen Ketten anordnen. Diese sogenannten "Chevron"-Muster sind deshalb von besonderem Interesse, da sie in engem Zusammenhang mit einer gleichnamigen, seit langem bekannten Erscheinung bei der Elektrokonvektion von Flüssigkristallen zu stehen scheinen. Es wird eine Erklärung des Phänomens vorgeschlagen, die auf der Abstraktion von der Amplitude A auf die Positionen von Defekten beruht. Dabei werden die Defekte selbst auch nur in ihrer kollektiven Dynamik in Form von Defektdichten beschrieben. Das sich ergebende mathematische Modell ist äquivalent zu einem Reaktions-Diffusions-System [10]. Entsprechend können sich sowohl die räumlich-periodischen Turing-Mustern ausbilden, die mit den Chevrons identifiziert werden, als auch homogene Oszillationen. Letztere wurden in Simulationen der Gln. (2,3) tatsächlich gefunden, ihr Nachweis im Experiment steht jedoch noch aus.

⋆ ⋆ ⋆

carpe diem

Abstract and Reading Guide

A well known example for an amplitude equation is the real Ginzburg-Landau equation [24, 10]

$$\tau \partial_t A = \varepsilon A + \xi_{xx}^2 \partial_x^2 A + \xi_{yy}^2 \partial_y^2 A - g|A|^2 A. \tag{1a}$$

The coefficients τ, ε, ξ_{xx}^2, ξ_{yy}^2, and g are real positive numbers, while $A = A(x, y, t)$ is a complex valued function (some authors allow only real values for A under this name). The quantity A represents amplitude and phase of some spatially periodic, self-organized structure ("rolls") that is evolving in a homogeneous, anisotropic environment. The actual periodicity of the structure has already been eliminated from this representation by, roughly speaking, splitting off a factor $\exp(iq_c x)$ from the amplitude A. Equation (1a) describes the evolution of imperfections of the roll structure, such as a bend of the rolls or point defects (dislocations). It is exact in the limit that the control parameter ε approaches zero.

In Eq. (1a) the anisotropy is assumed to be imposed by some external condition. In contrast, the current work is centered around an adaptation of Equation (1a) to the case where the isotropy is broken internally and spontaneously, while the system as a whole remains isotropic. We will call the direction selected by this process the "director" of the system. The angle $\varphi = \varphi(x, y, t)$ between the director and the x-axis becomes an additional dynamical variable.

Chapter 1 is concerned with the construction of an appropriate set of amplitude equations that describes the mutual interaction of the roll amplitude A and the director. The first three sections of this chapter do therefore have a very formal character. Though required for a systematic approach, they do not contribute much to an intuitive understanding. For the latter Section 1.4 may be useful.

Before setting up the equations, a technical problem has to be solved. For the Ginzburg-Landau equation (1a) the wave vector of the underlying modulations is basically fixed to be parallel to the x-axis. Only small deviations have to be taken into account. In our case, however, the direction of the preferred wave vector of modulations is only given relative to the director. A derivation of the equations by an expansion around a state (better: an eigenfunction) with a fixed wave vector would artificially break the isotropy. This would be reflected in a loss of symmetry in the amplitude equations.

The aim of Section 1.1 is twofold. One is to solve above-mentioned problem by introducing definitions of A and φ that are designed to enforce inherently rotationally-invariant amplitude equations. The other is to give a detailed account of the relation between the symmetries of the system as a whole and of the linear modes associated with A and φ.

In Section 1.2 these results are used for a formal construction of the equations. For "normal rolls" (see below) one gets

$$\tau\partial_t A = \left[\varepsilon + \xi_{xx}^2\partial_x^2 + \xi_{yy}^2(\partial_y - iq_c\varphi)^2 - g|A|^2 + i\beta_y\varphi_{,y}\right]A, \tag{2a}$$

$$\tilde{\gamma}_1\partial_t\varphi = K_1\partial_y^2\varphi + K_3\partial_x^2\varphi - \tilde{\chi}_a H^2\varphi + \frac{\Gamma}{4}(-iq_c A^*(\partial_y - iq_c\varphi)A + \text{c.c.}). \tag{3a}$$

The rotational invariance expresses itself by the appearance of the combination $(\partial_y - iq_c\varphi)$, which represents the angle between the director and the local wave vector of the rolls. The term $-\tilde{\chi}_a H^2\varphi$ breaks the isotropy. It was added to stabilize the solutions of the equations. In the form given above these equations are only valid for small angles φ, but an extension for arbitrarily large φ can be constructed (Eqs. (1.130,1.131)).

Similar equations are obtained for "oblique rolls" (Eqs. (1.73,1.138)). Oblique rolls are distinguished from normal rolls by having a preferred wave vector that is neither normal nor parallel to the director. Symmetry requires then that the preferred wave vector is twofold degenerate.

The newly introduced definition for the amplitude A requires a revision of the asymptotic expansion formalism that leads from the basic equations of the underlying physical system to the coefficients in the amplitude equations. In Section 1.3, however, it is argued that, for an expansion to lowest order as in Eqs. (2a,3a), there are basically no changes.

Section 1.4 discusses some qualitative features of Eqs. (2a,3a), the corresponding oblique-roll system, and their solutions. For normal rolls two simple but important results shall be mentioned.

- When $\Gamma < 0$ in Eq. (3a) the system has a strong non-potential character, which is a major distinction from the real Ginzburg-Landau equation.

- For $H^2 = 0$ the relative contribution to the dynamics is of the same order of magnitude for all terms of Eqs. (2a,3a), even as $\varepsilon \to 0$.

The combination of these properties seems to be the basis for the rich variety of structures that can be found in numerical solutions of the equations (see Fig. 4.2).

In the oblique-roll range these properties get partially lost. Nevertheless there seem to be at least two different types of dynamic states: "rotating rolls" and "swinging rolls", as is explained in Section 1.4.2.

Chapter 2 depends on the previous chapters only in so far, as the rescaled forms of the amplitude equations, that were constructed in Section 1.4, are used. It is devoted to an analytic characterization of homogeneous (i.e. ideal) roll solutions and their stability. In particular for normal rolls the complicated structure of the stable range could be disentangled (e.g.. Fig. 2.1). In many cases an upper limit for ε is found, above which homogeneous rolls are unstable. Then the amplitude equations do already contain all effects that are relevant for the stability of homogeneous rolls. For oblique rolls the important question of the stability of the fastest growing mode could also be reduced to a simple inequality (2.54).

The link between the amplitude formalism and an experimental model is provided by Chapter 3. The theory is compared to direct numerical calculations [16] and some experimental works. In the course of this chapter, most of the important theoretical results are touched. It may also be read as a summary.

The last chapter is again rather independent. Only Section 1.4.1 is needed as a background. It gives a detailed description of a certain type of complex dynamic solutions of Eqs. (2a,3a). The "chevron" patterns are characterized by a spatially periodic variation of φ and the formation of parallel chains of defects. They are of particular interest, because similar structure are well known to appear in electroconvection experiments in liquid crystals. An explanation in terms of the collective dynamics of defects and their interaction with the director is proposed.

Contents

Chapter 1

The Amplitude Formalism

In this chapter we develop the amplitude formalism describing the pattern dynamics in pattern-forming systems with spontaneously broken isotropy. It may sometimes appear rather formal, in particular since large parts lack mathematical rigor. However, the formalism makes it easier to specify the assumptions necessary to obtain the amplitude equations and to point out distinctions from other systems. Besides, the formal approach allows an easy generalization of the results to the more complicated situations, such as Hopf bifurcations to traveling or standing waves, or to systems or ground states that lack inversion symmetry, none of which will be discussed here. For a rigorous approach to the problem of constructing amplitude equation in the case of a simple isotropic ground state, see [29] and references therein.

1.1 Symmetry relations

1.1.1 A Pattern-Forming Layer

Assume that the complete state U of the system under consideration and its evolution are described by N real field variables within a layer which extends infinitely in the x- and y-direction and is of constant thickness d in the z-direction, i.e.

$$U : (x, y, z, t) \in \mathbb{R}^2 \times [-d/2, d/2] \times \mathbb{R} \longrightarrow U(x, y, z, t) \in \mathbb{R}^N . \qquad (1.1)$$

Define summation and multiplication with a scalar on such functions U in the usual way.

The dynamics of the system shall be defined by a set of N partial differential equations (supplemented with a suitable set of boundary conditions) for which we introduce the abstract notation

$$\partial_t U = F(U), \tag{1.2}$$

where F contains no time derivatives.

Assume F to commute with certain symmetry operations G, i.e. $\mathsf{G}F(U) = F(\mathsf{G}U)$. G may be one of the following[1]:

- an in-plane translation T_{x_0,y_0} for any $x_0, y_0 \in \mathbb{R}$, which maps the point (x, y, z, t) to $(x + x_0, y + y_0, z, t)$,
- a time translation T_{t_0} for any $t_0 \in \mathbb{R}$, mapping $(x, y, z, t) \rightarrow (x, y, z, t+t_0)$,
- an in-plane rotation R_α $(\alpha \in \mathbb{R})$, $(x, y, z, t) \rightarrow (x \cos\alpha - y \sin\alpha, x \sin\alpha + y \cos\alpha, z, t)$,
- reflection at the $y = 0$ plane S_y, $(x, y, z, t) \rightarrow (x, -y, z, t)$,
- rotation by π around the y-axis R_y, $(x, y, z, t) \rightarrow (-x, y, -z, t)$.

The action of the symmetry operations on states U shall be a "physical action" in a sense similar to the definition in [29]: It may be seen as a combination of two operations: A "motion" of the local field values, as if they were rigidly connected to space, and possibly an internal transformation, e.g. a rotation of the field vector in the case of a vector field. Formally[2]: if G maps $(x, y, z, t) \rightarrow (x', y', z', t')$ then $(\mathsf{G}U)(x', y', z', t') = \overline{\mathsf{G}}(U(x, y, z, t))$ with $\overline{\mathsf{G}} : \mathbb{R}^N \rightarrow \mathbb{R}^N$. In particular, let $\overline{\mathsf{G}} = 1$ for $\mathsf{G} = \mathsf{T}_{x_0,y_0}, \mathsf{T}_{t_0}$. In order to keep the formalism simple we will assume the action of the symmetry operators on states U to be linear.

1.1.2 The Degenerate Ground State

As usual in the amplitude-equation approach we assume that there is always at least one homogeneous, time-independent solution U_g to Eq. (1.2), the *ground state* ($\mathsf{T}_{x_0,y_0}U_g = U_g$, $\mathsf{T}_{t_0}U_g = U_g$).

The present work focuses on the situation where the ground state is degenerate due to a spontaneous breaking of isotropy. Then one has a family of ground states $\mathsf{R}_\alpha U_g$ that can be generated by in-plane rotation of U_g by arbitrary angles α.

The degeneracy of the ground state implies that U contains some internal degree of freedom relating to direction.

We will only consider the case where the symmetry with respect to R_y is preserved by the ground state, such that $\mathsf{R}_y \mathsf{R}_{\alpha_s} U_g = \mathsf{R}_{\alpha_s} U_g$ for a suitable choice

[1] The elements of the Euclidean group are identified with their actions on states U.

[2] Notice the distinction between a function U and its value $U(x, y, z, t)$ at some point in space and time.

of α_s. Without loss of generality assume α_s=0. In this sense U_g will be said to be "oriented along the x-axis". The symmetry $\mathsf{S}_y U_g = U_g$ will also be assumed. We do not assume symmetry with respect to a half rotation around the z-axis R_π, that maps $(x, y, z, t) \to (-x, -y, z, t)$, but it will be shown that the latter would not influence the form of the resulting amplitude equations, i.e. it would not impose further restrictions on the allowed terms.

1.1.3 Perturbations of the Ground State

In order to investigate the transition from the homogeneous ground state to a spatially and/or temporally structured state we consider spatially uniformly bounded perturbations V of the ground state

$$U = U_g + V \tag{1.3}$$

Equation (1.2) may then be expanded in orders of V.

$$\partial_t V = F(U_g + V) = LV + N(V|V) + M(V|V|V) + \dots \tag{1.4}$$

with each of the operators $N, M, \dots$ being linear in each of its arguments and fully symmetric with respect to permutations of the arguments. The latter serves only to simplify some formulas. A symbol | is used to separate the arguments in order to underline the linearity of each "slot".

Since $\mathsf{G}F(U_g + V) = F(\mathsf{G}(U_g + V)) = F(\mathsf{G}U_g + \mathsf{G}V) = F(U_g + \mathsf{G}V)$ if G is one of T_{x_0,y_0},T_{t_0}, S_y, R_y, the equation of motion for V (1.4) is symmetric under these operations.

1.1.4 Active Modes

Now we are ready for a description of the linearized dynamics of perturbations V of U_g. We look for solutions of $\partial_t V = \sigma V = LV$, i.e. eigenvectors of L. The spatial and temporal translation symmetry of L generally implies that the eigenvectors of L are of the form $V(x, y, z, t) = W_{q,p,m}(z) \exp(\sigma t + i(qx + py))$, with $W_{q,p,m} \in \mathbb{C}^N$, $m \in \mathbb{N}$. The boundedness of V restricts q and p to real numbers; $\sigma = \sigma_m(q, p)$ may be complex and is in general analytic in q and p.

The amplitude formalism is used to deal with the situation where most of the linear modes are quickly decaying (stable), while only for a few m and a small (not necessarily connected) area in q-p-space the real parts of the growth rates $\mathrm{Re}[\sigma_m(q, p)]$ are close to zero[3]. The quickly decaying modes may then

[3]The rather vague language used here reflects the fact that due to the continuity of the spectrum in q and p a direct application of the center manifold theorem is impossible. The problem is discussed in detail in [29] and is not subject of the present work.

be eliminated from the equations of motion to obtain new effective dynamic equations for the slow modes.

In the present case there is always one such set of slow modes in the vicinity of the Goldstone mode

$$V_G := \frac{d}{d\alpha} R_\alpha U_g \Big|_{\alpha=0} \tag{1.5}$$

associated with the homogeneous ($q, p = 0$) rotation of the ground state. The growth rate of the Goldstone mode itself is zero.

We consider the situation where, due to a particular choice of the system, there are other slow modes[4]. Let $\sigma_A(q,p) := \sigma_{n_A}(q,p)$ for some branch $n_A \in \mathbb{N}$ and let $\mathrm{Re}[\sigma_A(q,p)]$ be small for wave vectors close to $(q,p) = \vec{q}_c := (q_c, p_c)$. To be specific, $\mathrm{Re}[\sigma_A(q,p)]$ shall be *maximal* at $\vec{q}_c$. For later use, define

$$W_{q,p,A} := W_{q,p,n_A}. \tag{1.6}$$

The current work considers only the situation where the translational symmetry is broken ($\vec{q}_c \neq 0$) by the latter mode such that a "pattern" appears. Referring to the case of convection we will talk of these structures as "rolls".

Enumeration of Patterning Modes

Along with the solution

$$W_A(z) := W_{q_c,p_c,A}(z), \tag{1.7}$$
$$V_A(x,y,z,t) := W_A(z)\exp(\sigma_A(q_c,p_c)t + i(q_c x + p_c y)), \tag{1.8}$$

there is always the solution that can be obtained from it by complex conjugation[5]. Translations in space and/or time and their linear combinations are just equivalent to multiplications with a scalar, but application of R_y and S_y may also lead to new solutions. In this section we shall be mainly concerned with the question of how many solutions one can expect to obtain altogether.

It will now be argued that, in general, V_A is degenerate with respect to the symmetries $\mathsf{G} = \mathsf{R}_y, \mathsf{S}_y, \mathsf{R}_y\mathsf{S}_y$ if and only if V_A and $\mathsf{G}V_A$ have different wave vectors (the "proof" ends at #). Degeneracy means that V_A and $\mathsf{G}V_A$ are linearly independent. In this case one can construct a G-symmetric solution $V_+ = V_A + \mathsf{G}V_A$ and a G-antisymmetric solution $V_- = V_A - \mathsf{G}V_A$. Since V_+ and V_- are qualitatively different with respect to G, one would generally expect

[4] When a system is capable of having additional slow modes at all, there is usually a co-dimension-1 condition on some system parameters (e.g. the voltage or the temperature difference) to obtain a situation as described here.

[5] Complex conjugation will be indicated by a star * superscript, addition of the complex conjugate by the expression $+c.c.$

their dynamics to be unrelated. This is a contradiction, because G commutes with L and thus V_A and $\mathsf{G}V_A$ have the same growth rate. Therefore $\mathsf{G}V_A = cV_A$ with some $c \in \mathbb{C}$ ($\mathsf{G}^2 = 1$ requires $c = \pm 1$). However, this argument becomes invalid if

$$\mathsf{H}V_- = cV_+ \tag{1.9}$$

for some $c \in \mathbb{C}$ and some symmetry H that commutes with the linear operator L. Then the claim of "qualitative difference" cannot be held. Contrarily, the growth rates are equal by definition of H. Equation (1.9) implies $\mathsf{GH}V_- = \mathsf{G}cV_+ = cV_+$ and $\mathsf{HG}V_- = -\mathsf{H}V_- = -cV_+$, hence H and G do not commute. But only if H contains a spatial translation it can have this property, and only if V_A and $\mathsf{G}V_A$ have different wave vectors spatial translation can act in a nontrivial way. Thus the case (1.9) is impossible if the wave vectors are equal. Conversely, V_A and $\mathsf{G}V_A$ are of course linearly independent if they have different wave vectors[6]. The same argument holds for $\mathsf{G} = \mathsf{R}_\pi$ and its combinations with R_y and S_y, if R_π is a symmetry of the ground state. It does not go through with G containing the complex conjugation operator $\mathsf{C}V := V^*$ because then Eq. (1.9) is satisfied trivially with $\mathsf{H} = 1$, $c = i$. #

In the case that V_A and $\mathsf{G}V_A^*$ ($\mathsf{G} = \mathsf{R}_y, \mathsf{S}_y, \mathsf{R}_y\mathsf{S}_y$) have the same wave vector, they may or may not be linearly dependent. If

$$\mathsf{G}V_A^* = cV_A \tag{1.10}$$

for any $c \in \mathbb{C}$ ($|c| = 1$ since $(\mathsf{GC})^2 = 1$) one can construct a G-symmetric, real-valued roll solution $c^{1/2}V_A + c.c.$ which is related to its G-antisymmetric form $ic^{1/2}V_A + c.c.$ by a translation in space. Equation (1.10) implies that V_A is non-oscillatory ($\mathrm{Im}[\sigma_A(q_c, p_c)] = 0$). On the contrary, if Eq. (1.10) cannot be satisfied, there are the two degenerate real-valued roll solutions $V_A + c.c.$ and $\mathsf{G}V_A + c.c.$. In general these are oscillatory solutions that travel in opposite directions. Traveling rolls will not be considered in this work. Therefore Eq. (1.10) should always hold if an appropriate G exists. Now notice that $\mathsf{R}_y\mathsf{S}_y$ is the 3-dimensional inversion $(x, y, z, t) \to (-x, -y, -z, t)$, and $\mathsf{R}_y\mathsf{S}_y V_A^*$ and V_A do always have the same wave vector. Hence we can assume without (further) loss of generality

$$\mathsf{R}_y\mathsf{S}_y V_A = V_A^*, \tag{1.11}$$

where the factor c in Eq. (1.10) has been eliminated by absorbing a factor $c^{1/2}$ into the definition of W_A. In the presence of an R_π-symmetric ground state V_A may be either symmetric or antisymmetric under $\mathsf{R}_\pi\mathsf{R}_y\mathsf{S}_y$, i.e. $(x, y, z, y) \to (x, y, -z, t)$, because this operation also leaves the wave vector unchanged.

[6]If the wave vectors are opposite, this may be the trivial degeneracy due to complex conjugation $\mathsf{G}V_A = cV_A^*$, which is discussed below.

The transformations of the Goldstone mode are readily calculated.

$$\begin{aligned} \mathsf{R}_y V_G = \mathsf{R}_y \frac{d}{d\alpha} R_\alpha U_g = \frac{d}{d\alpha} \mathsf{R}_y \mathsf{R}_\alpha U_g = \frac{d}{d\alpha} \mathsf{R}_{-\alpha} \mathsf{R}_y U_g = \\ \frac{d}{d\alpha} \mathsf{R}_{-\alpha} U_g = -\frac{d}{d\alpha} \mathsf{R}_\alpha U_g = -V_G \end{aligned} \tag{1.12}$$

and similarly $\mathsf{S}_y V_G = -V_G$, and in case of R_π-symmetry $\mathsf{R}_\pi V_G = V_G$.

In conclusion, there are three cases of possible roll modes: "normal rolls" with $q_c \neq 0$, $p_c = 0$, "parallel rolls" with $q_c = 0$, $p_c \neq 0$ and "oblique rolls" with $q_c \neq 0$, $p_c \neq 0$. Oblique rolls are twofold degenerate. From the "zig" solution $V_A + c.c.$ one can construct the "zag" solution $\mathsf{S}_y V_A + c.c.$ with wave vector $\pm(q_c, -p_c)$. Normal rolls (parallel rolls) are in general either S_y-symmetric (R_y-symmetric) or antisymmetric, since S_y (R_y) does not change the wave vector of normal (parallel) rolls. Assume $q_c, p_c \geq 0$ without loss of generality in all cases.

1.1.5 Reduction to Amplitudes

We will now establish the connection from the physical state of the system U to the modulated amplitudes of the roll mode $A(x,y,t) \in \mathbb{C}$ (or the amplitudes A_1 and A_2 in case of oblique rolls) and of the Goldstone mode $\varphi(x,y,t) \in \mathbb{R}$. The postulate of a homogeneous ground state, oriented along the x-direction, will therefore be relaxed. Instead, its orientation locally has an angle $\varphi(x,y,t)$ with the x-axis, a notion that will be made precise in Eq. (1.18). For the moment φ shall not be too large, such that the ground state is only weakly perturbed and decomposition (1.17) below is possible. Later, in Section 1.4.1 this restriction will be relaxed to allow arbitrarily large values of φ.

The definitions and calculations in the following part will only be done for normal rolls. The adaptation to the oblique-roll and parallel-roll cases is obvious. For these only the results will be given.

Define

$$(V_1 | V_2) := \int_{-\infty}^{+\infty} dx \int_{-\infty}^{+\infty} dy \int_{-d/2}^{+d/2} dz V_1(x,y,z,t=0)^* \cdot V_2(x,y,z,t=0) \tag{1.13}$$

and

$$\langle W_1 | W_2 \rangle := \int_{-d/2}^{+d/2} dz W_1(z)^* \cdot W_2(z), \tag{1.14}$$

where the dot denotes, as usual, the sum over pairwise products of the N components.

Let V_A^+ be the adjoint eigenfunction of L to V_A with respect to $(\cdot|\cdot)$. As in Eq. (1.7) define

$$W_A^+(z) := V_A^+(0,0,z,0). \tag{1.15}$$

Normalize V_A^+ such that $\langle W_A^+ \,|\, W_A \rangle = 1$. Similarly define V_G^+ and

$$W_G(z) := V_G(0,0,z,0),\ W_G^+(z) := V_G^+(0,0,z,0),\ \langle W_G^+ \,|\, W_G \rangle = 1. \tag{1.16}$$

Decomposability

As modes with wave vectors not too close to $\pm(q_c, 0)$ or $(0,0)$ decay rapidly, it is fair to assume that (after a transient) they are only weakly excited through nonlinear interaction with the active modes close to $\pm(q_c,0)$ and $(0,0)$. The excitation is strongest close to the wave vectors $(nq_c, 0)$, the higher harmonics, with small $n \in \mathbb{N}$, $|n| \geq 2$, because these modes are excited by interactions at a relatively low order (n-th order; recall that a multiplication in real space corresponds to a convolution in Fourier space). Other modes, for example those with wave vectors $((n+1/2)q_c, 0)$ can only be excited by very high order interactions. In fact, for the complex Ginzburg-Landau equation[7] (and therefore for all systems that it approximates), it has been shown that, on the average, the Fourier modes decay exponentially like $\exp(-akl)$ with the distance k from the main peek, where $a > 0$ is some constant, and l is the typical length scale of modulations[8]. A similar result should hold for our system. The length scale l is here given by the inverse of the extension of the range of active modes around q_c, which is supposed to be small. Hence l is large. We will therefore assume that modes of U in the vicinity of $(\pm q_c, 0)$ and $(0,0)$ can be separated like

$$U(x,y,z,t) = \sum_{n=-1,0,+1} U_n(x,y,z,t)e^{inq_cx} \ + \ U_{\text{rest}} \tag{1.17}$$

where the Fourier modes of the U_n are negligible for wave vectors larger than $q_c/2$, while U_{rest} contains only contributions at higher harmonics (see also Fig-

[7]Equation (1a) with complex valued ξ_{xx}^2, ξ_{yy}^2 and g and the corresponding equations in 1-d and higher dimensions are called "complex Ginzburg-Landau equations".

[8]According to [53] the solution $\psi(x)$ of the complex Ginzburg-Landau equation (for simplicity $x \in \mathbb{R}$) has, after a transient, an analytic continuation $\psi(z)$ to a stripe of half-width b in the complex plane ($z = x + iy$, $|y| < b$), where b is some positive constant. When introducing the Fourier transform $\tilde{\psi}(k)$ of $\psi(x)$, one gets as a corollary

$$|\psi(z)| = (2\pi)^{-1/2} \left| \int_{-\infty}^{\infty} \exp(ikx)\exp(-ky)\tilde{\psi}(k)\,dk \right| < \infty$$

for $|y| < b$. In order for the integral to remain finite, $\tilde{\psi}(k)$ must on the average decay like $\exp(-b|k|)$ or faster. The relation $b \sim l$ can be obtained by a simple scaling argument.

ure 1.4.1 on page 39).

When the Fourier transforms of the U_n decay at least exponentially with the wavenumber, decomposition (1.17) defines the functions U_n up to an uncertainty of order $\exp(-a|q_c|l/2)$, that results from the "overlap" of the harmonics in Fourier space. The convergence as $l \to \infty$ is faster than any power of l. The rather clumsy definitions of A and φ given below are aimed to preserve this accuracy for the transformation laws derived from these definitions. This allows to construct amplitude equations truncated at any desired order in the spatial derivatives.

Definition of the Amplitudes A and φ

Define $\varphi(x, y, t)$ by

$$0 = \left\langle W_G^+(z) \middle| \overline{\mathsf{R}}_{-\varphi(x,y,t)}(U_0(x, y, z, t)) \right\rangle, \tag{1.18}$$

with U_0 given by Eq. (1.17). In fact, there may be several solutions to this equation, even within the interval $\varphi(x, y, t) \in [-\pi, \pi[$. Of course, the one for which $U_0(x, y, z, t)$ is locally similar to $\overline{\mathsf{R}}_{\varphi(x,y,t)} U_g(x, y, z, t)$ has to be chosen.

Using φ, we can define the pattern amplitude $A(x, y, t)$ as

$$A(x, y, t) = \left\langle W_A^+(z) \middle| \overline{\mathsf{R}}_{-\varphi(x,y,t)}(U_1(x, y, z, t)) \right\rangle. \tag{1.19}$$

Putting the parts together again, one obtains

$$U = U_{A,\varphi} + R \tag{1.20}$$

where

$$\begin{aligned} U_{A,\varphi}(x, y, z, t) = {} & \overline{\mathsf{R}}_{\varphi(x,y,t)}(U_g(x, y, z, t)) + \\ & + \left(A(x, y, t)\overline{\mathsf{R}}_{\varphi(x,y,t)}\left(W_A(z)\right) e^{iq_c x} + c.c.\right) \end{aligned} \tag{1.21}$$

and the rest term R contains contributions that drop out in the projections (1.18, 1.19) as well as higher harmonics. Actually, the knowledge of R is decisive for understanding the dynamics of A and φ. We will come back to this problem in Section 1.3. For the formal construction of the amplitude equations it is sufficient to assume that some reasonable function R can be constructed if the functions A and φ are given. In particular R shall not break any of the remaining symmetries of the system[9].

[9] This is not trivial. In fact, secondary symmetry-breaking bifurcations often occur when the modulation amplitude A becomes too large. In the case of isotropic Rayleigh-Bénard convection (a different symmetry class) a well known example is the cross-roll instability [7].

1.1.6 Transformation Laws for the Amplitudes

The aim of the following calculations is to show that definitions (1.18,1.19) are consistent with intuition and to demonstrate how the symmetries of V_A and U_g affect the symmetry properties of A and φ.

Rotation

Assume the fields A and φ to be known for a given solution U of Eq. (1.2). After a rotation R_δ by an infinitesimal angle δ the state U becomes $U' = \mathsf{R}_\delta U$. We will now calculate the fields A' and φ' corresponding to U'.

Since R_δ maps $(x + \delta y, y - \delta x, z, t) \to (x, y, z, t)$,

$$U'(x, y, z, t) = (\mathsf{R}_\delta U)(x, y, z, t) = \overline{\mathsf{R}}_\delta(U(x + \delta y, y - \delta x, z, t)). \tag{1.22}$$

Equating the harmonics in Eq. (1.17) we obtain

$$U'_n(x, y, z, t) = \overline{\mathsf{R}}_\delta(U_n(x + \delta y, y - \delta x, z, t))e^{inq_c\delta y}. \tag{1.23}$$

The defining equation for φ'

$$\begin{aligned} 0 &= \left\langle W_G^+(z)\right| \overline{\mathsf{R}}_{-\varphi'(x,y,t)}\overline{\mathsf{R}}_\delta(U_0(x + \delta y, y - \delta x, z, t))\right\rangle && (1.24)\\ &= \left\langle W_G^+(z)\right| \overline{\mathsf{R}}_{-\varphi'(x,y,t)+\delta}(U_0(x + \delta y, y - \delta x, z, t))\right\rangle && (1.25)\end{aligned}$$

is solved by

$$\varphi'(x, y, t) = \varphi(x + \delta y, y - \delta x, t) + \delta. \tag{1.26}$$

Finally

$$\begin{aligned} A'(x, y, t) &= \left\langle W_A^+(z)\right| \overline{\mathsf{R}}_{-\varphi'(x,y,t)}(U'_1(x, y, z, t))\right\rangle \\ &= \left\langle W_A^+(z)\right| \overline{\mathsf{R}}_{-\varphi(x+\delta y,y-\delta x,t)-\delta}(\overline{\mathsf{R}}_\delta(U_1(x + \delta y, y - \delta x, z, t)))e^{iq_c\delta y}\right\rangle \\ &= \left\langle W_A^+(z)\right| \overline{\mathsf{R}}_{-\varphi(x+\delta y,y-\delta x,t)}(U_1(x + \delta y, y - \delta x, z, t))\right\rangle e^{iq_c\delta y} \qquad (1.27)\\ &= A(x + \delta y, y - \delta x, t)e^{iq_c\delta y}. \end{aligned}$$

The last chain of equations illustrates why the rotation operator in definition (1.19), which is not included in the traditional approach, is necessary to obtain clean transformation laws.

3-d Inversion

As another example consider the transformation $\mathsf{P} := \mathsf{R}_y \mathsf{S}_y$. Notice that the adjoints inherit symmetries, e.g. Eq. (1.11) implies $\mathsf{P}^+ V^+ = (V^+)^*$, where $(\mathsf{P}^+ U_1 | \, U_2) := (U_1 | \, \mathsf{P} U_2)$ for any U_1, U_2. The "local" transformation behavior can be found like this: Observe that for any U

$$\left(V_A^+ \middle| \, \overline{\mathsf{P}}(U(-x,-y,-z,0))\right) = \left(V_A^+ \middle| \, (PU)(x,y,z,0)\right) = \left((V_A^+)^* \middle| \, U\right), \qquad (1.28)$$

and use Dirac δ-functions to define $U(x,y,z,0) = \delta(x)\delta(y)W(z)$ for some $W(z)$. Then

$$\left\langle W_A^+(z) \middle| \, \overline{\mathsf{P}}(W(-z))\right\rangle = \left\langle W_A^+(z)^* \middle| \, W(z)\right\rangle . \qquad (1.29)$$

Similarly

$$\left\langle W_G^+(z) \middle| \, \overline{\mathsf{P}}(W(-z))\right\rangle = \left\langle W_G^+(z) \middle| \, W(z)\right\rangle . \qquad (1.30)$$

Proceeding as for the rotation,

$$U'_n(x,y,z,t) = \overline{\mathsf{P}}(U_{-n}(-x,-y,-z,t)) = \overline{\mathsf{P}}(U_n(-x,-y,-z,t)^*) \qquad (1.31)$$

and Eq. (1.18) becomes

$$\begin{aligned} 0 &= \left\langle W_G^+(z) \middle| \, \overline{\mathsf{R}}_{-\varphi'(x,y,t)}(U'_0(x,y,z,t))\right\rangle && (1.32)\\ &= \left\langle W_G^+(z) \middle| \, \overline{\mathsf{R}}_{-\varphi'(x,y,t)}\overline{\mathsf{P}}(U_0(-x,-y,-z,t))\right\rangle && (1.33)\\ &= \left\langle W_G^+(z) \middle| \, \overline{\mathsf{P}}\,\overline{\mathsf{R}}_{-\varphi'(x,y,t)}(U_0(-x,-y,-z,t))\right\rangle && (1.34)\\ &= \left\langle W_G^+(z) \middle| \, \overline{\mathsf{R}}_{-\varphi'(x,y,t)}(U_0(-x,-y,z,t))\right\rangle , && (1.35) \end{aligned}$$

which is solved by

$$\varphi'(x,y,t) = \varphi(-x,-y,t). \qquad (1.36)$$

Using this result,

$$\begin{aligned} A'(x,y,t) &= \left\langle W_A^+(z) \middle| \, \overline{\mathsf{R}}_{-\varphi'(x,y,t)}(U'_1(x,y,z,t))\right\rangle && (1.37)\\ &= \left\langle W_A^+(z) \middle| \, \overline{\mathsf{R}}_{-\varphi(-x,-y,t)}\overline{\mathsf{P}}(U_1(-x,-y,-z,t)^*)\right\rangle && (1.38)\\ &= \left\langle W_A^+(z) \middle| \, \overline{\mathsf{P}}\,\overline{\mathsf{R}}_{-\varphi(-x,-y,t)}(U_1(-x,-y,-z,t)^*)\right\rangle && (1.39)\\ &= \left\langle W_A^+(z)^* \middle| \, \overline{\mathsf{R}}_{-\varphi(-x,-y,t)}(U_1(-x,-y,z,t)^*)\right\rangle && (1.40)\\ &= A(-x,-y,t)^*. && (1.41) \end{aligned}$$

Reduction to Substitution Rules

These transformation laws lead to invariance conditions for the amplitude equations. We want to formulate these transformation laws in such a way that they can be evaluated more or less mechanically. Therefore we let a coordinate transformation follow the symmetry operations above. For example, in the case of rotation define

$$\tilde{x} := x + \delta y, \quad \tilde{y} := y - \delta x, \tag{1.42}$$

which implies

$$\partial_x = \partial_{\tilde{x}} - \delta \partial_{\tilde{y}}, \quad \partial_y = \partial_{\tilde{y}} + \delta \partial_{\tilde{x}}. \tag{1.43}$$

All together, rotation by a small angle δ can be expressed by the substitution

$$\begin{gathered} x \to \tilde{x} - \delta\tilde{y}, \quad y \to \tilde{y} + \delta\tilde{x}, \\ \partial_x \to \partial_{\tilde{x}} - \delta\partial_{\tilde{y}}, \quad \partial_y \to \partial_{\tilde{y}} + \delta\partial_{\tilde{x}}, \\ A(x,y,t) \to A(\tilde{x},\tilde{y},t)e^{i\delta q_c \tilde{y}}, \quad \varphi(x,y,t) \to \varphi(\tilde{x},\tilde{y},t) + \delta. \end{gathered} \tag{1.44}$$

In what follows we drop the tilde ˜ and suppress the arguments of $A(x,y,t)$ and $\varphi(x,y,t)$.

The action of P is equivalent to[10]

$$x \to -x,\ y \to -y,\ A \to A^*. \tag{1.45}$$

φ is formally unchanged. Furthermore S_y leads to

$$y \to -y,\ \varphi \to -\varphi,\ A \to \pm A, \tag{1.46}$$

where the $+$ and $-$ on A correspond to S_y-symmetric and S_y-antisymmetric V_A respectively. Similarly, $\mathsf{R}_\pi \mathsf{R}_y \mathsf{S}_y$ can be expressed as

$$A \to \pm A \tag{1.47}$$

in the case of R_π-symmetry. Translations in space T_{x_0,y_0} and time T_{t_0} result in

$$x \to x + x_0,\ y \to y + y_0,\ A \to Ae^{-iq_c x_0} \tag{1.48}$$

and

$$t \to t + t_0. \tag{1.49}$$

The corresponding results for parallel rolls can be obtained from (1.44–1.49) by the substitution $q_c \to p_c$, $x \to y$, $y \to -x$, $R_y \to S_y$, $S_y \to R_y$. Formally parallel rolls appear as normal rolls turned by $\pi/2$. Because of this equivalence we will only relate to normal rolls from now on.

[10] Of course, derivatives change their sign as the corresponding coordinates.

1.1.7 Oblique Rolls

In the case of oblique rolls a state decomposable as

$$U(x,y,z,t) = \sum_{n=-1,0,1} \sum_{m=-1,0,1} U_{n,m}(x,y,z,t) e^{in(q_c x + p_c y) + im(q_c x - p_c y)} + U_{\text{rest}}, \tag{1.50}$$

in the same sense as (1.17) is assumed. Then the amplitudes of zig and zag mode are defined by

$$A_1(x,y,t) = \left\langle W_A^+(z) \middle| \overline{\mathsf{R}}_{-\varphi(x,y,t)}(U_{1,0}(x,y,z,t)) \right\rangle \tag{1.51}$$

and

$$A_2(x,y,t) = \left\langle W_A^+(z) \middle| \overline{\mathsf{S}}_y \ \overline{\mathsf{R}}_{-\varphi(x,y,t)}(U_{0,1}(x,y,z,t)) \right\rangle . \tag{1.52}$$

The amplitude equations should be invariant under the substitutions

$$\begin{aligned} & x \to x - \delta y, \quad y \to y + \delta x, \\ & \partial_x \to \partial_x - \delta \partial_y, \quad \partial_y \to \partial_y + \delta \partial_x, \\ & A_{1/2} \to A_{1/2} e^{i\delta(q_c y \mp p_c x)}, \quad \varphi \to \varphi + \delta, \end{aligned} \tag{1.53}$$

corresponding to a rotation and

$$x \to -x,\ y \to -y,\ A_{1/2} \to A_{1/2}^* \quad \text{for } \mathsf{P}, \tag{1.54}$$

$$y \to -y,\ \varphi \to -\varphi,\ A_{1/2} \to A_{2/1} \quad \text{for } \mathsf{S}_y, \tag{1.55}$$

$$A_{1/2} \to \pm A_{1/2} \quad \text{for } \mathsf{R}_\pi \mathsf{R}_y \mathsf{S}_y \text{ (if applicable)}, \tag{1.56}$$

$$x \to x + x_0,\ y \to y + y_0,\ A_{1/2} \to A_{1/2} e^{-i(q_c x_0 \pm p_c y_0)} \quad \text{for } \mathsf{T}_{x_0,y_0}, \tag{1.57}$$

$$t \to t + t_0 \quad \text{for } \mathsf{T}_{t_0}. \tag{1.58}$$

1.2 Construction of the Amplitude Equations

The transformation rules (1.44-1.49) for normal rolls and (1.53-1.58) for oblique rolls can be used to construct the general form of amplitude equations that are compatible with the symmetries of the "microscopic" equations as described in Section 1.1.1. For the normal-roll case, this procedure will be described in detail, while, as before, only the result will be given for the oblique-roll case.

1.2.1 The Phenomenological Approach

Since one may feel uneasy with the idea of "deriving" statements about a "macroscopic" system (A, φ in the present case) with little or no reference to the underlying "microscopic" equations (here Eq. (1.2)), some words must be said about the approach used here to construct the amplitude equations describing the evolution of A and φ.

Three different methods to obtain physical equations may be distinguished:

1. Fitting experimental data. This is the only thing that can be done if all background information is missing, or if the methods described below fail to work. A typical example is the friction law

$$F_{\text{friction}} = cF_{\text{normal}} \tag{1.59}$$

for surfaces gliding on each other.

2. Deriving the equation from a more basic one using controlled approximations. In most cases the approximations are based on smallness assumptions, and usually a clear statement can be made that some quantity a must be considerably smaller than some quantity b for the approximation to be good. The form of the terms entering the final result and their coefficients are obtained in a single step. A prominent result of this kind is Fermi's Golden Rule

$$w_{a\rightarrow b} = \frac{2\pi}{\hbar} \left|\langle a|V|b\rangle\right|^2 \delta(E_a - E_b - \omega\hbar), \tag{1.60}$$

which is valid for measurements on time scales much larger than ω^{-1}.

3. Using symmetry considerations and smallness and regularity assumptions to obtain the form of the macroscopic equations. This is sometimes called the "phenomenological" approach. Usually only a list of relevant terms is obtained, while the coefficients connecting them are left unknown. They may afterwards be determined experimentally or be calculated from the microscopic equations. In both cases the necessary work is highly reduced compared to the direct approaches 1 and 2, because only a small set of coefficients has to be found instead of the complete equation. The smallness assumptions, which are made in order to restrict the number of relevant terms, are of a different kind than those made in 2. For example, terms like $c_i x^i$, $(i \geq 2)$ can be neglected compared to a term $c_1 x$ when x is small enough. But there is no statement on how small x must be. One may try to calculate some of the coefficients c_i in order to obtain an inequality for x. However, in many cases it will be found that the higher the

index i, the tighter the bound on x. *A priori* it can only be said that the omission of the higher order terms is justified in the limit $x \rightarrow 0$. A clear answer to the question about the range of validity can only be given by other (non-perturbative) methods or, which is often simpler, an experimental test. Assuming that the equations are valid in this sense, it is often possible, using analytic methods, to understand some of their important implications, even when the coefficients are unknown. A typical case is the material equation of electrodynamics

$$\vec{P} = (\underline{\underline{\varepsilon}} - 1)\varepsilon_0 \vec{E}, \tag{1.61}$$

where the form of the dielectric tensor $\underline{\underline{\varepsilon}}$ reflects the symmetries of the material it describes.

We will use method number 3, the phenomenological approach.

1.2.2 Supplementary Conditions

Apart from having the right symmetries, the equations must have some other properties that are implied in the definitions of A and φ in Sec. 1.1.

1. The growth rate $\sigma_A(q_c, 0)$ of A must be small. In fact, it will be assumed that $\sigma_A(q_c, 0)$ can be changed by adjusting some system parameter ε, which is defined in such a way that $\varepsilon \sim \sigma_A$ for small $|\varepsilon|$.

2. Since A and φ correspond to eigenmodes of perturbations of the ground state, they do not couple at linear order (in fact, this follows also from symmetry arguments).

3. At $\varepsilon < 0$ the ground state $\varphi = const.$, $A = 0$ is stable. For A this follows from the fact that σ_A is maximal at $(q_c, 0)$. If the ground state was unstable against modulations of its orientation φ, the fastest growing mode of such modulations would have a finite wave vector, since for homogeneous rotations the growth rate is zero. In general this maximal rate will not be small for small ε, which is in contradiction to postulates made (page 11).

4. There is no coupling to the "fast" modulation of the (imperfect) roll state (1.17), i.e. no terms like $\exp(iq_c x)$ are contained in the equation. Assuming that the expansion of the evolution equation (1.4) terminates after a small number of terms $N(\ldots), M(\ldots), \ldots$, it can be seen by inserting Eq. (1.17) in Eq. (1.4) that this fact follows from the postulate of decomposability of the roll state.

5. The equations must reflect the condition that the number of active modes, i.e. the area covered by them in Fourier space, is small. In order to make

the amplitude formalism work, this condition must be strengthened to the postulate that the distance of the wave vector of the active modes from $\pm(q_c, 0)$ or $(0, 0)$ respectively must be small. This is a major problem in the case of simple isotropic pattern-forming systems that are described by the Newel-Whitehead-Segel equation, because in this case the critical modes are degenerated to lie on a circle of radius q_c in Fourier space, the mode associated with $A = const.$ being only one of them. In the present case such difficulties can be avoided by a smallness assumption for φ (see below). The assumption that only modes close to $A = const.$ and $\varphi = const.$ are involved in the dynamics can be expressed formally by considering operators ∂_x and ∂_y applied to A and φ as "small" quantities.

Based on property number 4 the invariance conditions (1.46–1.48) can be simplified. From the nontrivial terms explicitly containing x and y only those containing factors like e^{iq_cx} could be invariant under a translation (1.48). As these are disallowed by property 4, condition (1.48) can be reformulated to forbidding any explicit x and y dependence *and* requiring invariance under

$$A \to Ae^{i\theta} \tag{1.62}$$

for any $\theta \in \mathbb{R}$. This invariance can be interpreted in the sense that the phase of the roll pattern has no influence on the dynamics. As a consequence the changes of signs of A in conditions (1.46) and (1.47) play no role for the form of the amplitude equations. In particular (1.47) has become redundant and, as mentioned before, the additional symmetry R_π has also no effect on the form of the amplitude equations. Invariance under (1.46) becomes equivalent to invariance under

$$y \to -y,\ \varphi \to -\varphi. \tag{1.63}$$

A last condition necessary to limit the number of terms in the amplitude equation is that A, and in a first step also φ, are small. Notice that for the formulation of the decomposability assumption (p. 14) φ was also assumed to be small. But the smallness condition we employ now is stronger. Before, φ was only assumed not to exceed some finite bound, now it must be infinitesimally small. The smallness of A does not follow from assumptions made in Section 1.1 either, but it may be a natural consequence of the dynamics.

All together, the quantities

$$\partial_t, A, \varphi, \varepsilon, \partial_x, \partial_y \tag{1.64}$$

are assumed to be small. As is typical for the phenomenological approach, nothing can be said about how small they should be. Instead, this has to be understood in a way that, if a term T_1 is a product of a term T_2 and some factors of the list (1.64), then $T_1 \ll T_2$, no matter what the prefactor is, provided only that all factors in (1.64) are small enough. In order to obtain simple equations, a term like T_1 will be discarded if it appears in a sum together with T_2.

1.2.3 Formal Construction

The rest is only formal work. In order to obtain the evolution equation for A, we assume the equation to be written as (or expandable to) a sum of products of the elements (1.64), one of the addends being $\partial_t A$. We will suppress possible real valued coefficients (which are *not* small), because they are not useful at this point. The term $\partial_t A$ is turned into its complex conjugate by substitution (1.45). This can be compensated by taking the complex conjugate of the complete equation. In this sense substitution (1.45) may be rewritten as

$$x \to -x,\ y \to -y,\ i \to -i. \tag{1.65}$$

Products invariant under (1.62,1.63,1.65) are

$$\partial_t,\ \varepsilon,\ i\partial_x,\ \partial_y^2,\ i\partial_y\varphi,\ \varphi^2,\ |A|^2 \tag{1.66}$$

and combinations thereof. The only way to obtain dynamics which is also invariant under a phase shift (1.62) is to include in each term exactly one factor A and an arbitrary number of invariants (1.66). The simplest form

$$\partial_t A = A \tag{1.67}$$

violates property number 1 above. Thus other terms containing invariants (that would have been too small to appear in (1.67)) must be included.

$$\partial_t A = \varepsilon A + i\partial_x A + \partial_y^2 A + i\partial_y \varphi A + \varphi^2 A + |A|^2 A. \tag{1.68}$$

The term $i\partial_x A$, with $A = A_0 \exp(iQx)$ and $Q > 0$ or $Q < 0$ depending on the sign of the (suppressed) coefficient, destroys property number 3. After erasing this, the term $-(i\partial_x)^2 = \partial_x^2$ becomes relevant. Notice that the combination $i\partial_y\varphi A$ can appear in two ways, with ∂_y being applied either to A or to φ. In the second case it will be written as $i\varphi_{,y}A$. This results in

$$\partial_t A = \varepsilon A + \partial_x^2 A + \partial_y^2 A + i\varphi\partial_y A + \varphi^2 A + i\varphi_{,y} A + |A|^2 A. \tag{1.69}$$

Now consider the substitutions corresponding to rotation (1.44). An additional factor $e^{i\delta q_c y}$ appears at A. In the course of factoring it out of the equation, additional terms resulting from the commutation with ∂_y are obtained. These terms can be absorbed into the substitution rule (1.44) as

$$\partial_y \to \partial_y + \delta\partial_x + i\delta q_c \quad \text{(applied to } A\text{)}, \quad \partial_y \to \partial_y + \delta\partial_x \quad \text{(applied to } \varphi\text{)}, \tag{1.70}$$

$$\partial_x \to \partial_x - \delta\partial_y, \quad \varphi \to \varphi + \delta.$$

In these substitution rules, the terms linear in δ contain always one or none of the factors ∂_x, ∂_y or φ. At first order in δ, the total number of the factors ∂_x, ∂_y, φ in the new terms generated by applying substitutions (1.70) to (1.69) is therefore one or two. Terms with two such factors are also generated by applying (1.70) to terms with three factors[11] ∂_x, ∂_y or φ and do not have to be balanced at the order considered here. For balancing those with only one such factor, it is sufficient to choose the combination $\partial_y^2 A + i\varphi\partial_y A + \varphi^2 A$ to be of the form $(\partial_y - iq_c\varphi)^2 A$ (recall that ∂_y does not operate on φ here). In order to write down the final result, the (unknown) coefficients will be introduced. Following common practice, the coefficient at εA is set to one.

$$\tau\partial_t A = \Big[\varepsilon + \xi_{xx}^2\partial_x^2 + \xi_{yy}^2(\partial_y - iq_c\varphi)^2 - g|A|^2 + i\beta_y\varphi_{,y}\Big]A. \tag{1.71}$$

In order to obtain property number 3, the coefficients τ, ξ_{xx}^2 and ξ_{yy}^2 must be positive, g and β_y may be either positive or negative. Usually ε will also be positive.

The equation containing $\partial_t\varphi$,

$$\tilde{\gamma}_1\partial_t\varphi = K_1\partial_y^2\varphi + K_3\partial_x^2\varphi + \frac{\Gamma}{4}(-iq_cA^*(\partial_y - iq_c\varphi)A + \text{c.c.}), \tag{1.72}$$

can be constructed using similar ideas. Again, at linear order the signs of the coefficients are known ($\tilde{\gamma}_1, K_1, K_3 > 0$) while the sign of Γ remains undetermined.

For oblique rolls the same procedure leads to

$$\begin{aligned}\tau\partial_t A_{1/2} = \Big[\,&\varepsilon + \xi_{xx}^2(\partial_x \pm ip_c\varphi)^2 + \xi_{yy}^2(\partial_y - iq_c\varphi)^2 \\ &\pm 2\xi_{xy}^2(\partial_x \pm ip_c\varphi)(\partial_y - iq_c\varphi) - g|A_{1/2}|^2 \\ &-h|A_{2/1}|^2 \pm i\beta_x\varphi_{,x} + i\beta_y\varphi_{,y}\Big]A_{1/2},\end{aligned} \tag{1.73}$$

$$\tilde{\gamma}_1\partial_t\varphi = K_1\partial_y^2\varphi + K_3\partial_x^2\varphi + \frac{\Gamma q_c p_c}{2}(|A_1|^2 - |A_2|^2). \tag{1.74}$$

A discussion of Eqs. (1.71–1.74) must be postponed to Section 1.4. First we need to finish the construction work.

---

[11] Such terms, consistent with symmetry, do always exist. Consider for example those obtained from replacing δ with φ in the terms obtained using (1.70).

1.3 The Coefficients of the Amplitude Equation

In this section we show how the coefficients in the amplitude equations (1.71,1.72) can be calculated from the "microscopic" equations (1.2). The procedure for calculating the coefficients in an amplitude equation is well known [51, 34, 5, 27]. Only the new definitions of the amplitudes (1.18,1.19) require the reconsideration of these procedures. For the reader not interested in the details, this section can be skipped without any losses.

The coefficients must be chosen such that they give asymptotically as $A, \varphi, \varepsilon, \partial_x, \partial_y \to 0$ the same dynamics for A and φ as the microscopic equation (1.2) together with definitions (1.18,1.19). Of course the microscopic dynamics can only be found if the rest term R in Eq. (1.20) can be reconstructed consistent with A and φ. It will be shown that adiabatic elimination of R is sufficiently accurate in our case.

1.3.1 General Framework

Before starting we introduce some notation. Sometimes it is convenient to apply L directly to "z-profiles" of Fourier modes, like $W_A(z)$ or $W_G(z)$. The information about the wavenumber of the mode must then be passed explicitly to L. We define

$$L_{q,p} := e^{-i(qx+py)} L e^{i(qx+py)} \tag{1.75}$$

and introduce the convention that a differential operator applied to a z-profile acts as if it was constant in the x-y-plane, e.g. $L_{q_c,0} W_A = 0$, $L_{0,0} W_G = L W_G = 0$. Furthermore we write (a little sloppy)

$$L_q := L_{q,0}, \quad \partial_p L_q := \frac{d}{dp} L_{q,p}\Big|_{p=0}, \quad \partial_p^2 L_q := \frac{d^2}{dp^2} L_{q,p}\Big|_{p=0}. \tag{1.76}$$

The microscopic equation of motion and its expansion around U_g, Eq. (1.4) will be evaluated at $\varepsilon = 0$, except for the following definition: $\partial_\varepsilon L := (d/d\varepsilon) L\Big|_{\varepsilon=0}$. Below, the function arguments x, y will be summarized to $\vec{r}$ and all arguments t will be dropped.

For functions decomposable like (1.17) let a projector E, that selects the fast dynamics of the system, be defined as

$$\begin{aligned}(E_\varphi U)(\vec{r},z) &:= U(\vec{r},z)\\ &-\overline{\mathsf{R}}_{\varphi(\vec{r})} W_G(z)\left\langle W_G^+(z)\right|\overline{\mathsf{R}}_{-\varphi(\vec{r})}(U_0(\vec{r},z))\rangle \\ &-\left[\overline{\mathsf{R}}_{\varphi(\vec{r})} W_A(z) e^{iq_c x}\left\langle W_A^+(z)\right|\overline{\mathsf{R}}_{-\varphi(\vec{r})}(U_1(\vec{r},z))\rangle + c.c.\right].\end{aligned} \quad (1.77)$$

The statement made in Section 1.1, that R contains contributions that "drop out" in the projections (1.18,1.19) can now be made precise (we use the notation of Eqs. (1.20,1.21)):

$$R = EU = EEU = ER. \quad (1.78)$$

Differentiation in time gives[12]

$$\dot{R} = \dot{E}U + E\dot{U} = \dot{E}(U_{A,\varphi} + R) + EF(U_{A,\varphi} + R). \quad (1.79)$$

One may look at this equation as a definition of R as a function of A and φ. Such a definition requires that Eq. (1.79) has a unique solution $R = ER$ for any given A and φ. We cannot address the question of the solvability of Eq. (1.79) in this work. Instead, Eq. (1.79) will be used as an ansatz for a perturbative scheme starting at

$$R \equiv 0 \quad \text{for} \quad A, \varphi \equiv 0, \quad (1.80)$$

where spatial and temporal derivative operators applied to A and φ will be considered as small perturbations, as well as ε and A and φ themselves. This is, of course, just an adaptation of the usual perturbation scheme for constructing amplitude equations (see e.g. [27]) to the new definition of the amplitude.

In order to do a meaningful reduction of coordinates, it must be shown that, for small A and φ, R relaxes on a fast time scale. For example, assume R to contain a Fourier mode $W_r(z)\exp(i(q_c x + py))$. To linear order in R one has by Eq. (1.79)

$$\begin{aligned}\dot{W}_r e^{i(q_c x+py)} &= E\left[L W_r e^{i(q_c x+py)}\right] + O(A) + O(\varphi) \quad (1.81)\\ &= e^{i(q_c x+py)} L_{q_c} W_r + pE\left[e^{i(q_c x+py)}\partial_p L_{q_c} W_r\right]\\ &\quad + O(p^2) + O(A) + O(\varphi). \quad (1.82)\end{aligned}$$

According to Eq. (1.78) W_r is orthogonal to the slow eigenmode W_A of L_{q_c}. All eigenmodes but W_A of L_{q_c} relax quickly. Since p is small, the terms of order p and higher are only small corrections. Hence W_r relaxes quickly towards its equilibrium value given by A and φ.

[12] The dot $\dot{}$ denotes a time derivative.

In the present approach the "fast variables" selected by the projector E do not lie in eigenspaces of L. As a consequence A and φ are slightly excited during the eventual fast relaxation of R.

As mentioned, for the accuracy required for the coefficients of Eqs. (1.71,1.72), an adiabatic elimination of R is sufficient, i.e. the term $\dot{R}$ on the l.h.s. of Eq. (1.79) can be neglected.

To see this, notice that, as usual, the error in R due to adiabatic elimination is of order $O(\partial_t A) + O(\partial_t \varphi)$. It must be shown that the contribution of R to the dynamics of A and φ is $O(Rf)$, where f is one of the small factors $A, \varphi, \varepsilon, \partial_x, \partial_y, R$. Then the total error from the adiabatic elimination in the dynamics of A and φ (i.e. to $\partial_t A$ and $\partial_t \varphi$) is $O(f\partial_t A) + O(f\partial_t \varphi)$. This is sufficient for calculating the coefficient of a term T in the amplitude equations as long as it is possible to construct a situation where T contributes at leading order to the dynamics, i.e. $\partial_t A, \partial_t \varphi = O(T)$. This is always the case in our calculations. For the same reason any other correction terms to $\partial_t A$ and $\partial_t \varphi$ of lower order than $\partial_t A$ or $\partial_t \varphi$ may be discarded.

We will need the evolution equation of A and φ. For given R they can read off from the definitions,

$$
\begin{aligned}
\dot{A}(\vec{r}) &= \partial_t \left\langle W_A^+(z) \middle| \overline{\mathsf{R}}_{-\varphi(\vec{r})}(U_1(\vec{r},z)) \right\rangle \\
&= \left\langle W_A^+(z) \middle| \dot{\varphi}(\vec{r})(\frac{d}{d\varphi}\overline{\mathsf{R}}_{-\varphi(\vec{r})})(U_1(\vec{r},z)) \right\rangle && (1.83)\\
&\quad + \left\langle W_A^+(z) \middle| \overline{\mathsf{R}}_{-\varphi(\vec{r})}(\dot{U}_1(\vec{r},z)) \right\rangle \\
&= \left\langle W_A^+(z) \middle| \overline{\mathsf{R}}_{-\varphi(\vec{r})}(\dot{U}_1(\vec{r},z)) \right\rangle + h.o.t., && (1.84)
\end{aligned}
$$

with "$h.o.t.$" standing for higher order terms, and

$$
\begin{aligned}
0 &= \partial_t \left\langle W_G^+(z) \middle| \overline{\mathsf{R}}_{-\varphi(\vec{r})}(U_0(\vec{r},z)) \right\rangle \\
&= \dot{\varphi}(\vec{r}) \left\langle W_G^+(z) \middle| (\frac{d}{d\varphi}\overline{\mathsf{R}}_{-\varphi(\vec{r})})(U_0(\vec{r},z)) \right\rangle && (1.85)\\
&\quad + \left\langle W_G^+(z) \middle| \overline{\mathsf{R}}_{-\varphi(\vec{r})}(\dot{U}_0(\vec{r},z)) \right\rangle .
\end{aligned}
$$

It follows from Eq. (1.21) that $U_0 = \overline{\mathsf{R}}_\varphi U_g + O(R)$. Hence

$$
\frac{d}{d\varphi}\overline{\mathsf{R}}_{-\varphi(\vec{r})}(U_0(\vec{r},z)) = \frac{d}{d\alpha}\overline{\mathsf{R}}_{-\alpha}\Big|_{\alpha=0} U_g(\vec{r},z) + O(R) = -W_G(z) + O(R) \quad (1.86)
$$

according to definitions (1.5,1.16). Making use of $\langle W_G^+ | W_G \rangle = 1$, Eq. (1.85) may then be rewritten as

$$\dot{\varphi}(\vec{r}) = \left\langle W_G^+(z) \middle| \overline{\mathsf{R}}_{-\varphi(\vec{r})}(\dot{U}_0(\vec{r},z)) \right\rangle (1 + O(R)). \tag{1.87}$$

The term $O(R)$ is only a small correction and can be dropped.

We go back to the problem of adiabatic elimination. It will only be made sure that the contribution at order Rf^0 vanishes (the linear dependence of the leading contribution on the small factors f is then obvious), i.e. if R has only Fourier modes at $(\pm q_c, 0)$, $(0,0)$ and at higher harmonics $(\partial_x, \partial_y = 0)$ and is, for the moment, considered to be independent of A and φ, there is, at zeroth order in A, φ, no linear contribution of R to the evolution of the amplitudes.

Consider Eq. (1.84). With W_r symbolizing the Fourier mode or R at $(q_c, 0)$, the decisive contribution would be

$$\dot{A}(\vec{r}) = \langle W_A^+(z) | \overline{\mathsf{R}}_0(L_{q_c} W_r(z)) \rangle + O(A) + O(\varphi) \tag{1.88}$$

$$= \langle W_A^+(z) | L_{q_c} W_r(z) \rangle + O(A) + O(\varphi) \tag{1.89}$$

$$= 0 \quad \text{by definition of } W_A^+. \tag{1.90}$$

For $\dot{\varphi}$ the argument is similar.

With the adiabatic elimination, the defining equation for R, Eq. (1.79) becomes

$$0 = EF(U_{A,\varphi} + R). \tag{1.91}$$

The rotation operators $\overline{\mathsf{R}}_{-\varphi(\vec{r})}$ in Eqs. (1.84,1.87) may be dropped while calculating coefficients of up to first order in φ. Again we use Eq. (1.84) as example. Contributions to $\dot{U}_1$ that are not removed by R according to Eq. (1.91) are of the form $\dot{U}_1(\vec{r}, z) = g(\vec{r})\overline{\mathsf{R}}_{\varphi(\vec{r})} W_A(z)$, with some $g(\vec{r}) \in \mathbb{C}$. The rotations in this expression for $\dot{U}_1$ and the rotation in Eq. (1.84) just cancel each other, i.e.

$$\dot{A}(\vec{r}) = \langle W_A^+(z) | g(\vec{r}) W_A(z) \rangle . \tag{1.92}$$

If the rotation in Eq. (1.84) is dropped, one gets

$$\dot{A}(\vec{r}) = \langle W_A^+(z) | g(\vec{r}) \overline{\mathsf{R}}_{\varphi(\vec{r})} W_A(z) \rangle \tag{1.93}$$

instead. Now expand the rotation operator:

$$\overline{\mathsf{R}}_{\varphi(\vec{r})} = 1 + \varphi(\vec{r}) \frac{d}{d\alpha} \overline{\mathsf{R}}_\alpha \Big|_{\alpha=0} + O(\varphi^2). \tag{1.94}$$

At first order in φ,

$$\begin{aligned}\left\langle W_A^+ \middle| \frac{d}{d\alpha}\overline{\mathsf{R}}_\alpha\Big|_{\alpha=0} W_A \right\rangle &= \left\langle W_A^+ \middle| \overline{\mathsf{S}}_y \overline{\mathsf{S}}_y \frac{d}{d\alpha}\overline{\mathsf{R}}_\alpha\Big|_{\alpha=0} W_A \right\rangle \\ &= -\left\langle W_A^+ \middle| \overline{\mathsf{S}}_y \frac{d}{d\alpha}\overline{\mathsf{R}}_\alpha\Big|_{\alpha=0} \overline{\mathsf{S}}_y W_A \right\rangle \\ &= -\left\langle W_A^+ \middle| \frac{d}{d\alpha}\overline{\mathsf{R}}_\alpha\Big|_{\alpha=0} W_A \right\rangle \\ &= 0.\end{aligned} \tag{1.95}$$

All together

$$\left\langle W_A^+(z) \middle| \overline{\mathsf{R}}_{\varphi(\vec{r})}(\dot{U}_1(\vec{r},z)) \right\rangle = \left\langle W_A^+(z) \middle| \dot{U}_1(\vec{r},z) \right\rangle + O(\varphi^2). \tag{1.96}$$

Summarizing we can say that, to the order considered, we might also have chosen definitions like

$$A(x,y,t) = \left\langle W_A^+(z) \middle| U_1(x,y,z,t) \right\rangle, \quad \varphi(x,y,t) = \left\langle W_G^+(z) \middle| U_0(x,y,z,t) \right\rangle, \tag{1.97}$$

and Eq. (1.91). Next, some examples for calculating the coefficients will be given.

1.3.2 τ

The determination of τ in Eq. (1.71) is standard. Let the “test configuration” be $\varepsilon \neq 0$, $A = const.$, $\varphi = 0$. To first order in ε and to first order in A,

$$\dot{U} = F(U) = (L + \varepsilon\partial_\varepsilon L)(AV_A + R), \tag{1.98}$$

with R satisfying

$$O(\varepsilon A) = E\left[L(AV_A + c.c. + R)\right] = E\left[LR\right], \quad (1-E)R = 0, \tag{1.99}$$

which is trivially solved by $R \equiv 0$. Equation (1.84) becomes

$$\dot{A}(\vec{r}) = \left\langle W_A^+(z) \middle| \dot{U}(\vec{r},z) \right\rangle = \varepsilon \left\langle W_A^+ \middle| (\partial_\varepsilon L A V_A)(\vec{r},z) \right\rangle = \varepsilon \left\langle W_A^+ \middle| \partial_\varepsilon L_{q_c} A W_A \right\rangle \tag{1.100}$$

In order to match terms with Eq. (1.71), i.e.

$$\tau\dot{A} = \varepsilon A + h.o.t., \tag{1.101}$$

choose

$$\tau^{-1} = \left\langle W_A^+ \middle| \partial_\varepsilon L_{q_c} W_A \right\rangle. \tag{1.102}$$

1.3.3 ξ_{yy}^2

The coefficient ξ_{yy}^2 is usually [5, 10] defined as

$$\xi_{yy}^2 = -\frac{\tau}{2}\partial_p^2 \sigma_A(q_c, p), \tag{1.103}$$

with σ_A as in Section 1.1. It will be shown that our approach gives the same result. Assume $\varepsilon = 0$ (from now on), and $\varphi = 0$, $A = A_0 \exp(ipy)$. R must satisfy

$$O(p^2) = E\left[L(W_A A_0 e^{ipy} + c.c. + R)\right], \tag{1.104}$$

which is solved by $R(\vec{r}, z) = pA(\vec{r})\partial_p W_A(z) + c.c.$, where "$\partial_p W_A$" is defined by

$$L_{q_c}\partial_p W_A = -\partial_p L_{q_c} W_A, \tag{1.105}$$

$$\left\langle W_A^+ \middle| \partial_p W_A \right\rangle = 0. \tag{1.106}$$

Since L_{q_c} has a nontrivial kernel W_A, the solvability Eq. (1.105) is not guaranteed. Instead there is a compatibility condition that a solution $\partial_p W_A$ only exists if the r.h.s. is orthogonal to W_A^+,

$$\left\langle W_A^+ \middle| \partial_p L_{q_c} W_A \right\rangle = 0. \tag{1.107}$$

The latter is equivalent to $\left(V_A^+ \middle| \frac{d}{dp} e^{-ipy} L e^{ipy} V_A \right) \Big|_{p=0} = 0$, which can be shown to hold using a symmetry argument as in Eq. (1.95). In fact, if a compatibility condition like Eq. (1.107) was not satisfied when solving for R at some order in the perturbation scheme, there would be a contribution to $\dot{A}$ or $\dot{\varphi}$ at this order instead. But in our case R is only needed up to orders lower than the terms appearing in the amplitude equation. Therefore the compatibility condition will always be satisfied. From the family $\partial_p W_A + cW_A$, $c \in \mathbb{C}$, of solutions to Eq. (1.105), condition (1.106) selects the one that guarantees condition (1.78) to be fulfilled. Of course $\partial_p W_A = (\partial/\partial p) W_{q_c,p,A}\big|_{p=0} + cW_A$ with $W_{q,p,A}$ as defined in Eq. (1.6). This can be seen from the expansion of the eigenvalue equation

$$\begin{aligned} \sigma_A(q_c, p) W_{q_c,p,A} &= (0 + O(p^2)) W_{q_c,p,A} = L_{q_c,p} W_{q_c,p,A} \\ &= p\partial_p L_{q_c} W_A + p L_{q_c} \left(\frac{\partial}{\partial p} W_{q_c,p,A} \right)_{p=0} \end{aligned} \tag{1.108}$$

(recall that σ_A is maximal and analytic at $(q_c, 0)$) and comparing with Eq. (1.105).

Proceeding as for τ,

$$\begin{aligned}
\dot{A}(\vec{r}) &= \left\langle W_A^+(z) \middle| \dot{U}_1(\vec{r},z) \right\rangle \\
&= \left\langle W_A^+ \middle| L_{q_c,p}(AW_A + pA\partial_p W_A) \right\rangle + h.o.t. \qquad (1.109)\\
&= \left\langle W_A^+ \middle| L_{q_c}AW_A + p\partial_p L_{q_c}AW_A + L_{q_c}Ap\partial_p W_A + p\partial_p L_{q_c}Ap\partial_p W_A \right.\\
&\qquad \left. + \frac{1}{2}p^2\partial_p^2 LAW_A \right\rangle \\
&= \left\langle W_A^+ \middle| p\partial_p L_{q_c}Ap\partial_p W_A + \frac{1}{2}p^2\partial_p^2 L_{q_c}AW_A \right\rangle .
\end{aligned}$$

The fact that terms at order p^0 and p^1 drop out can be read off from the amplitude equation (1.71). Matching with $\tau\dot{A} = -p^2\xi_{yy}^2 A$ yields

$$\xi_{yy}^2 = -\tau \left\langle W_A^+ \middle| \partial_p L_{q_c}\partial_p W_A + \frac{1}{2}\partial_p^2 L_{q_c} W_A \right\rangle . \qquad (1.110)$$

In order to compare with Eq. (1.103), notice that, using the adjoint $W^+_{q_c,p,A}$ of $W_{q_c,p,A}$ with respect to $L_{q_c,p}$ normalized to $\left\langle W^+_{q_c,p,A} \middle| W_{q_c,p,A} \right\rangle = 1$, it is possible to write

$$\sigma_A(q_c,p) = \left\langle W^+_{q_c,p,A} \middle| L_{q_c,p} W_{q_c,p,A} \right\rangle . \qquad (1.111)$$

Differentiation on both sides of the equation leads to

$$\begin{aligned}
\partial_p^2\sigma_A(q_c,p) = &\left\langle \partial_p^2 W^+_{q_c,p,A} \middle| L_{q_c,p} W_{q_c,p,A} \right\rangle + \left\langle W^+_{q_c,p,A} \middle| L_{q_c,p}\partial_p^2 W_{q_c,p,A} \right\rangle \\
&+2\left\langle \partial_p W^+_{q_c,p,A} \middle| \partial_p L_{q_c,p} W_{q_c,p,A} \right\rangle +2\left\langle \partial_p W^+_{q_c,p,A} \middle| L_{q_c,p}\partial_p W_{q_c,p,A} \right\rangle \\
&+2\left\langle W^+_{q_c,p,A} \middle| \partial_p L_{q_c,p}\partial_p W_{q_c,p,A} \right\rangle + \left\langle W^+_{q_c,p,A} \middle| \partial_p^2 L_{q_c,p} W_{q_c,p,A} \right\rangle .
\end{aligned} \qquad (1.112)$$

At $p = 0$ the first two terms vanish because $L_{q_c}W_{q_c,0,A} = L^+_{q_c}W^+_{q_c,0,A} = 0$, the terms in the second line cancel each other because of Eq. (1.108), and the remaining two terms differ from the r.h.s. of Eq. (1.110) (times $-2/\tau$) at most by a term $\left\langle W_A^+ \middle| \partial_p L_{q_c} c W_A \right\rangle$, which vanishes according to Eq. (1.107).

For ξ_{xx}^2 a formula similar to Eq. (1.110) can be obtained.

1.3.4 β_y

As another example, we will construct a formula for the coefficient β_y in Eq. (1.71). Assume $A = const.$, $\varphi = \varphi_0 \exp(ipy) + c.c.$. We are looking for $\dot{A}$ at first order in A, in φ_0 and in p. At this order the two Fourier modes of φ do not interact. It is therefore sufficient to consider the $\exp(ipy)$ mode. The contributions to R at order $A\varphi_0$ and $p\varphi_0$ will be needed (there is no contribution at order pA). They are given by $R = A\varphi_0 r_1 \exp(i(q_c x + p_y)) + c.c. + p\varphi_0 \partial_p W_G \exp(ipy) + h.o.t.$ with

$$L_{q_c} r_1 = -2N_{0,0;q_c,0}(W_G|W_A) - L_{q_c} \frac{d}{d\alpha} \overline{\mathsf{R}}_\alpha W_A \Big|_{\alpha=0} \tag{1.113}$$

and

$$L_0 \partial_p W_G = -\partial_p L_0 W_G. \tag{1.114}$$

The nonlinear operator in Eq. (1.113) is an extension of the "z-profile" notation to the operator $N(\ldots)$ appearing in Eq. (1.4) (below it will also be introduced for $M(\ldots)$). The second term on the r.h.s. of Eq. (1.113) comes from the rotation in Eq. (1.21). The relevant contributions to U_1 are

$$\begin{aligned} \dot{U}_1 = pA\varphi_0 e^{i(q_c x + py)} \Big(& \partial_p L_{q_c} r_1 + 2N_{0,0;q_c,0}(\partial_p W_G|W_A) \qquad (1.115) \\ & + 2\partial_p N_{0,p;q_c,0}(W_G|W_A) + \partial_p L_{q_c} \frac{d}{d\alpha} \overline{\mathsf{R}}_\alpha W_A \Big|_{\alpha=0} \Big). \end{aligned}$$

Using this, the coefficient β_y comes out as

$$\beta_y = -(pA\varphi_0)^{-1} \, \tau \left\langle W_A^+(z) \middle| \dot{U}_1(0,z) \right\rangle. \tag{1.116}$$

In order to write the result in a more compact form notice that using the adjoint form of definition (1.105), and then Eq. (1.113),

$$\begin{aligned} \langle W_A^+ | \, \partial_p L_{q_c} r_1 \rangle &= - \langle \partial_p W_A^+ | \, L_{q_c} r_1 \rangle \qquad (1.117) \\ &= \left\langle \partial_p W_A^+ \middle| 2N_{0,0;q_c,0}(W_G|W_A) + L_{q_c} \frac{d}{d\alpha} \overline{\mathsf{R}}_\alpha W_A \Big|_{\alpha=0} \right\rangle. \end{aligned}$$

After doing a similar operation for the last term in Eq. (1.115) the two contributions containing the rotation operator cancel out. Hence (using an obvious extension of notation) β_y can be expressed as

$$\beta_y = -\tau \frac{d}{dp} \langle W_{q_c,p}^+ | \, 2N_{0,p;q_c,0}(W_{0,p,G}|W_A) \rangle \Big|_{p=0}. \tag{1.118}$$

1.3.5 g, h

As for the real Ginzburg-Landau equation (Eq. (1a)) the coefficient g in Eq. (1.71) is

$$g = -\tau \left\langle W_A^+ \right| 3M_{q_c;q_c;-q_c}(W_A|W_A|W_A^*) + 2N_{0;q_c}(r_0|W_A) + 2N_{2q_c;-q_c}(r_2|W_A^*) \rangle , \tag{1.119}$$

with

$$Lr_0 = -2N_{-q_c;q_c}(W_A^*|W_A), \tag{1.120}$$
$$Lr_2 = -N_{q_c;q_c}(W_A|W_A). \tag{1.121}$$

Similarly, obtaining the nonlinear coupling coefficient h requires to first calculate all second order (i.e. $N(\cdot|\cdot)$) terms that can be obtained by combining the linear modes with wave vectors (q_c, p_c), $(-q_c, p_c)$, $(q_c, -p_c)$. Their sum provides the inhomogeneity for the linear equation that determines the rest term R. Applying N again to all combinations of R with one of the three modes, adding the direct third order contributions (from $M(\cdot|\cdot|\cdot)$), and projecting on V_A^+, yields h up to the factor $-\tau$.

1.3.6 Γ

The coefficients in the equation for φ, Eq. (1.72) are determined only up to a common factor. To be specific, we choose $\tilde{\gamma}_1 = 1$.

The linear terms in Eq. (1.72) provide no difficult. In order to obtain a formula for Γ choose $A = A_0 \exp(ipy)$, $\varphi = 0$. To the required order, $R = pA_0 \partial_p W_A \exp(i(q_c x + py)) + c.c. + |A_0|^2 r_0$, where $\partial_p W_A$ and r_0 are given by Eqs. (1.105) and (1.120). However, since r_0 does not carry a modulation, it cannot contribute to $\partial_t \varphi$ at order $p|A_0|^2$. We are left with

$$\begin{aligned} \frac{1}{2} q_c \Gamma &= \left\langle W_G^+ \right| 2N_{q_c,0;-q_c,0}(\partial_p W_A|W_A^*) + c.c. + 2\partial_p N_{q_c,p;-q_c,-p}(W_A|W_A^*) \rangle \\ &= \frac{d}{dp} \left\langle W_G^+ \right| 2N_{q_c,p;-q_c,-p}(W_{q_c,p,A}|W^*_{q_c,p,A}) \rangle \Big|_{p=0} . \end{aligned} \tag{1.122}$$

1.4 Interpretation of the Amplitude Equations

This section collects some information about the amplitude equations and their solutions that can be obtained without much analytic work.

1.4.1 The Normal-Roll Equations

The Meaning of the Terms

By setting $\varphi \equiv 0$ in Eq. (1.71) the real Ginzburg-Landau equation is recovered [even with $\varphi \equiv const.$ and a substitution $A \rightarrow A\exp(i\varphi y)$]. The interpretation of the relaxation time τ, the coherence lengths ξ_{xx}^2 and ξ_{yy}^2, and the Landau coefficient g are the same for both equations and needs no further explanation (see e.g. [24, 27]). The combination $(\partial_y - iq_c\varphi)$ in Eqs. (1.71,1.72) must be understood as a measure for the angle between the local in-plane director $\hat{c} := (\cos\varphi, \sin\varphi)$ (i.e. the orientation of the ground state) and the local wave vector $\vec{q}_{loc} = \vec{q}_c + \mathrm{Im}[(\nabla A)/A]$. In contrast to the simple anisotropic case described by the real Ginzburg-Landau equation, Eq. (1.72) selects modulations with a wave vector parallel to $\hat{c}$ instead of parallel to the x-axis. The term containing β_y controls the drift of phase (i.e. lines of constant $\arg(A)$) induced by modulations of φ along the y-direction. For the in-plane director such a modulation corresponds to a splay [11]. By a splay the positive and negative x-direction do indeed become distinguishable, which naturally leads to the drift.

In Eq. (1.72) the linear coefficients $\tilde{\gamma}_1$, K_3, and K_1 can be understood in analogy to liquid-crystal theory [11] as rotational viscosity, and bend and splay elastic constants. At linear order, the dynamics of φ is simply diffusive. The nonlinear term containing Γ can be interpreted like this: Assuming $A \equiv A_0 = const.$, it reduces to $-(1/2)\Gamma q_c |A_0|^2 \varphi$ and may be seen as a correction to the linear dynamics of φ in the presence of a roll pattern. In fact, a roll pattern breaks the rotational symmetry. Thus φ cannot be expected to be neutrally stable anymore. If $\Gamma > 0$, φ is stabilized by the roll pattern, while for $\Gamma < 0$ a solution $\varphi \equiv 0$ becomes unstable. In the case of arbitrary A the nonlinear term can be interpreted as an interaction between the local wave vector $\vec{q}_{loc}$ and $\hat{c}$. The director $\hat{c}$ may be attracted ($\Gamma > 0$) or repelled ($\Gamma < 0$) by $\vec{q}_{loc}$. In the case of repulsion the interaction terms in Eq. (1.72) and Eq. (1.71) are strongly counteracting each other: Though rolls tend to align their wave vectors parallel to $\hat{c}$, such a configuration is not favored by the dynamics of φ. Because of this frustration no simple, stable, time-independent solution of Eqs. (1.71,1.72) exists. Presumably there is no stable, steady-state solution at all.

The Rescaled Form

By rescaling length, time, A, and φ, Eqs. (1.71,1.72) can be simplified to

$$\check{\tau}\partial_{\check{t}}\check{A} = \left[1 + \partial_{\check{x}}^2 + (\partial_{\check{y}} - i\check{\varphi})^2 - \mathrm{sign}(g)\,|\check{A}|^2 + i\check{\beta}_y\,\check{\varphi}_{,\check{y}}\,\right]\check{A}, \tag{1.123}$$

$$\partial_{\check{t}}\check{\varphi} = \partial_{\check{y}}^2\check{\varphi} + \check{K}_3\partial_{\check{x}}^2\check{\varphi} + \check{\Gamma}\,(-i\check{A}^*(\partial_{\check{y}} - i\check{\varphi})\check{A} + \mathrm{c.c.}). \tag{1.124}$$

The new variables and coefficients, indicated by a caret $\check{}$, are given by

$$\begin{aligned} A = (\varepsilon/|g|)^{1/2}\check{A}, \quad x = \xi_{xx}\varepsilon^{-1/2}\check{x}, \quad y = \xi_{yy}\varepsilon^{-1/2}\check{y}, \\ \varphi = \varepsilon^{1/2}\check{\varphi}/(\xi_{yy}q_c), \quad t = \tilde{\gamma}_1\xi_{yy}^2\check{t}/(\varepsilon K_1), \quad \check{\beta}_y = \beta_y/(\xi_{yy}^2 q_c), \\ \check{K}_3 = K_3\xi_{yy}^2/(K_1\xi_{xx}^2), \quad \check{\Gamma} = q_c^2\xi_{yy}^2\Gamma/(4|g|K_1), \quad \check{\tau} = K_1\tau/(\tilde{\gamma}_1\xi_{yy}^2). \end{aligned} \tag{1.125}$$

Notice that ε has been removed completely from Eqs. (1.123,1.124) and the coefficients. It can be concluded that solutions to Eqs. (1.71,1.72) do not change their qualitative character when ε approaches zero. In fact, if there is a solution to Eqs. (1.123,1.124) with sufficiently slowly varying and bounded $\check{A}$ and $\check{\varphi}$, scaling properties (1.125) guarantee that the smallness assumptions made for $\partial_t, A, \varphi, \varepsilon, \partial_x, \partial_y$ are satisfied arbitrarily well when $\varepsilon \to 0$. In this sense, solutions $\check{A}$, $\check{\varphi}$ are exact descriptions of the dynamics of the original system (1.2) in the limit $\varepsilon \to 0$.

Unfortunately, the conditions that φ is bounded and A is slowly varying will generally not be satisfied for solutions of Eqs. (1.123,1.124), in particular if they are spatially and/or temporally chaotic. As a consequence of the rotational invariance of the original system, Eqs. (1.123,1.124) are invariant under $\varphi \to \varphi + \delta$, $A \to A\exp(i\delta y)$. In analogy to the Mermin-Wagner theorem [30], that forbids long range correlations in 2-dimensional (equilibrium) systems with a continuous symmetry, it must be expected that fluctuations $|\varphi(\vec{r},t) - \varphi(0,0)|$ become arbitrarily large for sufficiently large $\vec{r}$ or t (see also the coarse-grained Eq. (1.129) below with $H^2 = 0$).

The Symmetry-Breaking Term

One approach to resolve this problem may be to introduce an additional, small, symmetry-breaking term[13] $-\tilde{\chi}_a H^2\varphi$ in Eq. (1.72), i.e. to replace it by

$$\tilde{\gamma}_1\partial_t\varphi = K_1\partial_y^2\varphi + K_3\partial_x^2\varphi - \tilde{\chi}_a H^2\varphi + \frac{\Gamma}{4}(-iq_cA^*(\partial_y - iq_c\varphi)A + \text{c.c.}). \tag{1.126}$$

Correspondingly Eq. (1.124) then becomes

$$\partial_{\check{t}}\check{\varphi} = \partial_{\check{y}}^2\check{\varphi} + \check{K}_3\partial_{\check{x}}^2\check{\varphi} - \varepsilon^{-1}\check{H}^2\check{\varphi} + \check{\Gamma}\,(-i\check{A}^*(\partial_{\check{y}} - i\check{\varphi})\check{A} + \text{c.c.}), \tag{1.127}$$

with $\check{H}^2 = \chi_a\xi_{yy}^2/K_1 H^2$ being ε-independent.

[13] The coefficient $\tilde{\chi}_a H^2$ is chosen in analogy to the dynamic equations of nematic liquid crystals [11], where it describes the influence of an external magnetic field.

Some care is required, because we want to make a statement about the limit of small $\check{H}^2$ *and* small ε. We will show that under certain conditions the limit $\varepsilon^{-1}\check{H}^2 \longrightarrow 0$ of system (1.123,1.127) can give a meaningful description of the original system. Assume that $\check{H}^2 \sim \varepsilon^\alpha$ with some positive α as $\varepsilon \longrightarrow 0$. In order to make the additional term in Eq. (1.127) small, we must choose $\alpha > 1$. Now assume that the behavior of $\check{\varphi}$, apart from being chaotic on scales $\check{x}, \check{y}, \check{t} = O(1)$, is basically relaxational on some very large scales X, Y, T. The chaotic small-scale dynamics causes fluctuations in $\check{\varphi}$ around its equilibrium value, e.g.

$$\left\langle \check{\varphi}^2 \right\rangle \sim \varepsilon H^{-2} \sim \varepsilon^{1-\alpha} \tag{1.128}$$

as $\varepsilon \longrightarrow 0$. Such a scaling can be motivated by thinking of an effective dynamic equation[14] for $\check{\varphi}$

$$\partial_T \check{\varphi} = D_X \partial_X^2 \check{\varphi} + D_Y \partial_Y^2 \check{\varphi} - C\varepsilon^{-1}\check{H}^2 \check{\varphi} + \eta + h.o.t.\,. \tag{1.129}$$

with a noise term η representing the chaotic motion on smaller scales. In terms of φ, relation (1.128) means $\left\langle \varphi^2 \right\rangle \sim \left\langle \check{\varphi}^2 \right\rangle \varepsilon \sim \varepsilon^{2-\alpha}$. Hence, when $\alpha < 2$, $\varphi \longrightarrow 0$ as $\varepsilon \longrightarrow 0$, and we are in the range of validity of Eq. (1.126). For $1 < \alpha < 2$ it would then be meaningful to consider the limit $\varepsilon^{-1}\check{H}^2 \longrightarrow 0$ in Eq. (1.127). It is fair to assume that most of the properties found for the attractor of Eqs. (1.123,1.127) in this limit (e.g. the values of the diffusion constants D_X and D_Y in Eq. (1.129)) have a direct correspondence in the original system (1.71,1.126) even when $\check{H}^2 = 0$ and $\varepsilon \longrightarrow 0$. However, the details of this relationship have not yet been worked out. The important point of the ideas described above is that letting $\varepsilon^{-1}\check{H}^2 \longrightarrow 0$ is not necessarily connected with $\varphi \longrightarrow \infty$ and a loss of validity of Eqs. (1.123,1.127).

Part of this work will be concerned with Eqs. (1.123,1.127) at finite $\varepsilon^{-1}\check{H}^2$. There are several reasons for doing so. In the experimental systems described in Chapter 3 the isotropy is easily broken by applying an external magnetic field in the plane of the layer. By adjusting the strength of the magnetic field, the degree of isotropy breaking can be chosen nearly arbitrarily. The study of the case of finite $\varepsilon^{-1}\check{H}^2$ in experiments allows a verification of large parts of the theory without having to confront the difficulties appearing when $\varepsilon^{-1}\check{H}^2 \longrightarrow 0$, which have been sketched above. In fact, H^2 may be seen as an additional "small quantity" in the sense of Section 1.2. From this point of view the (rotation) symmetry-breaking term appears naturally in Eq. (1.72). In order to avoid terms like $H^2 A$ or $iH^2\partial_x A$ in Eq. (1.71), we will adopt the convention that the threshold of instability $\varepsilon = 0$ and the wave vector q_c are defined with respect to the given value of H^2. Thus ε and q_c are really functions of H^2. There are

[14] Of course, in order to obtain the scaling behavior for $\check{\varphi} \longrightarrow \infty$, a knowledge of the higher order terms in Eq. (1.129) is required. We are just guessing here. However, in Chapter 4 some steps towards an equation like (1.129) are done.

also systems that naturally include an externally broken isotropy. For example, liquid crystal convection experiments are often done with anisotropic boundary conditions for the director at the plates confining the liquid crystal layer (e.g. "planar alignment"). For such systems Eqs. (1.123,1.127) can only be seen as a model system, because the limit $\check{H}^2 \to 0$ cannot be taken. However, many aspects of the dynamics of liquid crystal convection under planar alignment (see e.g. [37], Chapter 4, or the defect lattice in Fig. 4.2, that is well known from experiments [32]) can be reproduced by Eqs. (1.123,1.127) or Eqs. (1.71,1.126) respectively. Finally, recall that in the limit $\varepsilon^{-1}\check{H}^2 \to \infty$ (e.g. with fixed $\check{H}^2$ and $\varepsilon \to 0$) Eq. (1.127) reduces to $\check{\varphi} = 0$, and Eq. (1.123) becomes the well known real Ginzburg-Landau equation as mentioned above. By gradually lowering $\varepsilon^{-1}\check{H}^2$ it is therefore possible to make a continuous transition towards the not yet fully understood system (1.123,1.124).

An Explicitly Rotationally Invariant Form

Another method to deal with the unbounded fluctuations of φ is to cast Eqs. (1.71,1.126) into a manifestly rotationally invariant form. This can be achieved by reintroducing the fast variation ($\tilde{A} = Ae^{i\vec{q}_c\cdot\vec{r}}$) and rewriting derivatives and the H^2-term in vector notation. One possible form would be [We write $\hat{c}_\perp = \hat{z} \times \hat{c} = (-\sin\varphi, \cos\varphi)$. As a convention, $\partial_{\vec{r}} = (\partial_x, \partial_y)$ operates only on $\tilde{A}$ and $\nabla = (\partial_x, \partial_y)$ only on φ. $\vec{H} = (H, 0)$]:

$$\tau\partial_t\tilde{A} = \Big[\varepsilon + \xi_{xx}^2(\hat{c}\cdot\partial_{\vec{r}} - iq_c)^2 + \xi_{yy}^2(\hat{c}_\perp\cdot\partial_{\vec{r}})^2 \qquad (1.130)$$

$$-g|\tilde{A}|^2 + i\beta_y\hat{c}_\perp\cdot\nabla\varphi\Big]\tilde{A},$$

$$\tilde{\gamma}_1\partial_t\varphi = K_3\hat{c}_\perp\cdot\nabla^2\hat{c} + (K_1 - K_3)\hat{c}_\perp\cdot\nabla(\nabla\cdot\hat{c}) \qquad (1.131)$$

$$+\tilde{\chi}_a(\hat{c}\cdot\vec{H})(\hat{c}_\perp\cdot\vec{H}) + \frac{\Gamma}{4}(-iq_c\tilde{A}^*(\hat{c}_\perp\cdot\partial_{\vec{r}})\tilde{A} + \text{c.c.}).$$

So far this has only been a formal rearrangement. At the accuracy in ∂_t, A, φ, ε, ∂_x, ∂_y, H^2 obtained in Eqs. (1.71,1.126), the two systems are equivalent to each other. It shall now be argued that, as long as ε is small and $H^2 = 0$, the additional terms in Eqs. (1.130,1.131) give a correct extension of the description of the long term dynamics to the case of large φ.

There were two reasons why the formalism was not set up in a manifestly rotationally invariant form from the beginning. Firstly, it was necessary for identifying the relevant terms in amplitude equation. But this task has been

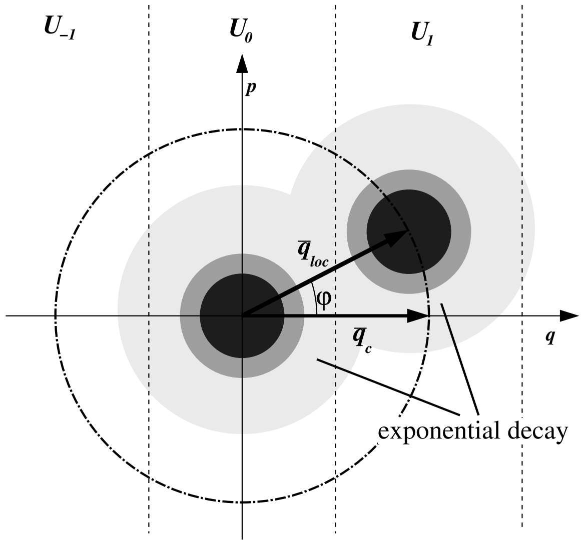

Figure 1.1: *Fourier space with large, but not too large φ. The active modes, indicated by the dark circles, can still clearly be associated to either U_0 or U_1. Only small parts of the exponentially decaying "halo" of slaved modes around the active peaks cross the line separating U_0 and U_1.*

completed. Secondly, it was required for doing decomposition (1.17), which allows a mapping of a state U and its dynamics to the amplitudes A, φ. As long as φ is small compared to one (e.g. $|\varphi| < 1/4$), the deviation of $\vec{q}_{loc}$ from $\vec{q}_c$ will also be sufficiently small compared to q_c, that it can clearly be associated to the modulated part U_1 of U instead of U_0 (see Fig. 1.4.1). Then the statement made in Section 1.1.5, that the uncertainty in the decomposition decays faster than any power of the inverse of the characteristic length l still holds [l in turn increases as $\varepsilon^{-1/2}$, see (1.125)]. If the distances over which φ varies by an amount $O(1)$ are large enough, it will be possible to divide the plane into different patches of roughly constant φ and perform the decomposition for every patch separately after a suitable rotation. Now notice that the diffusive nature of Eqs. (1.123,1.127) guarantees that variations of $\check{\varphi}$ of order O(1) occur on length scales not smaller than $\check{x}, \check{y} = O(1)$. In terms of the unscaled variables this means: φ varies by $O(\varepsilon^{1/2})$ on scales $x, y = O(\varepsilon^{-1/2})$. Consequently, variations of φ by $O(1)$ occur on scales $x, y = O(\varepsilon^{-1})$. Extraction of patches of such a size introduces an uncertainty in the wavenumber of order $\delta q = O(\varepsilon)$. Since this is small compared to the typical width $\delta q = O(\varepsilon^{1/2})$ of the peaks contributing to $U_{\pm 1}, U_0$ [see the scaling laws (1.125)], it does not impose a threat to the accuracy of the decomposition.

By allowing arbitrary rotations of the state in the plane, the distinction between ground states with or without R_π-symmetry, which was found to have no influence on the level of the amplitude equations in Section 1.2, becomes relevant. In the R_π-symmetric case φ and $\pi + \varphi$ are equivalent, while in the asymmetric case only φ and $2\pi + \varphi$ must be identified. This is important for determining the type of point defect (disclination, umbilic) that may occur in the director field. But point defects in the director field cannot be described by a continuous variable φ and therefore cannot be described by Eqs. (1.130,1.131). As long as ε is small, $H^2 = 0$, and $g > 0$, their numerical solutions seem always to remain in the range of validity of the equations. It can be concluded that disclinations cannot be generated dynamically under these conditions.

The form of the symmetry-breaking term $\tilde{\chi}_a(\hat{c} \cdot \vec{H})(\hat{c}_\perp \cdot \vec{H})$ is not unique. For example, a term $-\tilde{\chi}_a H^2 \hat{e}_y \cdot \hat{c}$ [with $\hat{e}_y = (0,1)$] would also be possible, at least in the absence of an R_π-symmetry. Notice also, that walls in the φ-field separating domains of $\varphi = n\pi$ and $\varphi = m\pi$ $(n \neq m)$ give rise to spatial variations in φ that do not become slower when $H^2 > 0$ is fixed and $\varepsilon \to 0$.

It must be mentioned that the extension of the amplitude equations introduced in Eqs. (1.130,1.131) lifts the restriction to small ∂_t, A, φ, ε, ∂_x, ∂_y, H^2 only by allowing an additional *joined* rotation of A and φ (which is equivalent to a rotation of the coordinates by some angle α and a subsequent substitution $\varphi \to \varphi - \alpha$). In particular $\vec{q}_{loc} = \mathrm{Im}[(\partial_{\vec{r}}\tilde{A})/\tilde{A}]$ must be close to the local critical wavenumber $q_c\hat{c}$. Of course, after a transient the system will naturally adjust to satisfy this condition if ε is small. In order to illustrate these limitations in the validity of Eqs. (1.130,1.131), expand the term $e^{iq_c x} T := \xi_{xx}^2 (\hat{c} \cdot \partial_{\vec{r}} - iq_c)^2 \tilde{A}$ occurring in Eq. (1.130) up to a slightly higher order than its original form $\xi_{xx}^2 \partial_x^2 A$:

$$T = \xi_{xx}^2 \left(\partial_x + \varphi \partial_y - \frac{i}{2} q_c \varphi^2 \right)^2 A. \tag{1.132}$$

A systematic extension of the amplitude equation in the sense of Section 1.2 would allow any term like

$$\xi_{xx}^2 \left(\partial_x + ia\partial_x^2 + ib(\partial_y - iq_c\varphi)^2 - \frac{i}{2q_c}\partial_y^2 \right)^2 A \tag{1.133}$$

with real coefficients a and b. As long as the terms ∂_x^2 and $(\partial_y - iq_c\varphi)^2$ are considered to be negligible small, their coefficients can be chosen arbitrarily. In Eq. (1.132) T corresponds to the choice $a = 0$, $b = 1/(2q_c)$.

Another problem of Eqs. (1.130,1.131) is that the inclusion of the fast variation $e^{iq_c x}$ makes numerical simulations more time consuming, in particular for small ε. Such a simulation requires a spatial resolution $O(q_c^{-1})$, which has to be compared to the resolution needed for simulations of Eqs. (1.71,1.126) [or equivalently Eqs. (1.123,1.127)] which is $O((\xi_{xx}^2 + \xi_{yy}^2 + K_3 + K_1)^{1/2}\varepsilon^{-1/2})$.

Though Eqs. (1.130,1.131) are slightly more general, we will speak in the language of Eqs. (1.123,1.127) whenever possible.

Potential Properties

If $\breve{\beta}_y = -1$ (or $\beta_y = -\xi_{yy}^2 q_c$) Eqs. (1.123,1.127) can be derived from a potential (we suppress the caret $\breve{}$ in this section)

$$\mathfrak{U} = \mathfrak{U}(A, A^*, \varphi) = \int\!\!\int -|A|^2 + |\partial_x A|^2 + |(\partial_y - i\varphi)A|^2 + \frac{1}{2}\mathrm{sign}(g)\,|A|^4 + \frac{1}{2\Gamma}\left(K_3|\partial_x\varphi|^2 + |\partial_y\varphi|^2 + \frac{H^2}{\varepsilon}|\varphi|^2\right) dx\, dy \quad (1.134)$$

in the sense that

$$\dot{A}(\vec{r},t) = -\frac{\delta\mathfrak{U}(A, A^*, \varphi)}{\delta A^*(\vec{r},t)}, \quad \dot{A}^*(\vec{r},t) = -\frac{\delta\mathfrak{U}(A, A^*, \varphi)}{\delta A(\vec{r},t)}, \quad \dot{\varphi}(\vec{r},t) = -\Gamma\frac{\delta\mathfrak{U}(A, A^*, \varphi)}{\delta\varphi(\vec{r},t)}. \quad (1.135)$$

If $\Gamma > 0$ and $g > 0$ then $\mathfrak{U}$ is a Lyapunov functional because

$$\frac{d\mathfrak{U}}{dt} = \int\!\!\int \frac{\delta\mathfrak{U}}{\delta A}\dot{A} + \frac{\delta\mathfrak{U}}{\delta A^*}\dot{A}^* + \frac{\delta\mathfrak{U}}{\delta\varphi}\dot{\varphi}\, dx\, dy \quad (1.136)$$

$$= -\int\!\!\int 2\left|\frac{\delta\mathfrak{U}}{\delta A}\right|^2 + \Gamma\left|\frac{\delta\mathfrak{U}}{\delta\varphi}\right|^2 dx\, dy \quad (1.137)$$

$$< 0$$

and $\mathfrak{U}$ is bounded from below. Then the dynamics of A and φ is relaxational.

If $\Gamma < 0$ and $g > 0$ then $\mathfrak{U}$ is still a Lyapunov functional for fixed φ as well as $-\mathfrak{U}$ is for fixed A, A^*. It can be concluded that if $\beta_y = -1$ the time scales for the dynamics of A and φ must be the same [up to fast relaxations of one of the variables, when a (quasi-)equilibrium configuration gets unstable due to slow changes of the other]. But the general effect of $\Gamma < 0$ is to give the system a strongly non-potential character, which is capable of driving it into complicated dynamic solutions (see e.g. Chapter 4).

1.4.2 The Oblique-Roll Equations

The most important difference between the normal- and the oblique-roll equation is the form of the Γ-term in the equation for the dynamics of φ. The reason for the difference becomes clear by replacing $A \longrightarrow A_1 \exp(ip_c y)$ in the Γ-term of Eq. (1.126). Of course, when p_c is large, we are outside the range of validity of the normal-roll equations, but it is fair to assume that we still get a qualitatively correct picture. In the resulting expression $(1/2)\Gamma q_c p_c |A_1|^2 + (1/4)\Gamma(-iq_c A_1^*(\partial_y - iq_c\varphi)A_1 + c.c.)$, the second part becomes negligible compared to the first when $A_1, \partial_y, \varphi \longrightarrow 0$. Therefore only a term of the form of the first part is kept in Eq. (1.73).

As a consequence of the form of the Γ-term in Eq. (1.74) there is no simple roll solution $|A_1|^2 = const.$, $|A_2|^2 = 0$, $\varphi = const.$ to the oblique-roll equations (1.73,1.74). The Γ-term cannot be compensated. Again, a symmetry-breaking term is introduced in order to simplify dynamics. For completeness, we rewrite Eq. (1.74):

$$\tilde{\gamma}_1 \partial_t \varphi = K_1 \partial_y^2 \varphi + K_3 \partial_x^2 \varphi - \tilde{\chi}_a H^2 \varphi + \frac{\Gamma q_c p_c}{2}(|A_1|^2 - |A_2|^2). \tag{1.138}$$

The structure of the equations for A_1 and A_2 (1.73) has not changed much from that of the corresponding normal-roll equation. It just contains some more terms due to the lower symmetry. In the vicinity of the transition to normal rolls or parallel rolls the coefficient h must approach the value $2g$ for continuity[15]. Thus a situation with $h < g$ should rather be considered as an exception (see [39] for an example where it *does* occur).

As for normal rolls, Eqs. (1.73,1.74) can be put into a rotationally invariant form:

$$\begin{aligned}\tau \partial_t \tilde{A}_{1/2} = \Big[& \varepsilon + \xi_{xx}^2 (\hat{c} \cdot \partial_{\vec{r}} - iq_c)^2 + \xi_{yy}^2 (\hat{c}_\perp \cdot \partial_{\vec{r}} \mp ip_c)^2 \\ & \pm 2\xi_{xy}^2 (\hat{c} \cdot \partial_{\vec{r}} - iq_c)(\hat{c}_\perp \cdot \partial_{\vec{r}} \mp ip_c) - g|\tilde{A}_{1/2}|^2 \\ & -h|\tilde{A}_{2/1}|^2 \pm i\beta_x \hat{c} \cdot \nabla\varphi + i\beta_y \hat{c}_\perp \cdot \nabla\varphi \Big] \tilde{A}_{1/2},\end{aligned} \tag{1.139}$$

[15] For only slightly oblique rolls the nonlinear interactions of A_1 with itself and A_2 (and vice versa) should all be based on similar mechanisms and would be describable by a single equation $\partial_t A_1 \exp(ip_c y) + \partial_t A_2 \exp(-ip_c y) \approx \ldots - g|A_1 \exp(ip_c y) + A_2 \exp(-ip_c y)|^2 (A_1 \exp(ip_c y) + A_2 \exp(-ip_c y)) = \ldots - g(|A_1|^2 + 2|A_2|^2) A_1 \exp(ip_c y) - g(|A_2|^2 + 2|A_1|^2) A_2 \exp(-ip_c y)$. After separating terms modulated with $\exp(ip_c y)$ and $\exp(-ip_c y)$, which corresponds to decomposition (1.50), we obtain the structure of Eq. (1.73) with $h = 2g$.

$$\tilde{\gamma}_1 \partial_t \varphi = K_3 \hat{c}_\perp \cdot \nabla^2 \hat{c} + (K_1 - K_3)\hat{c}_\perp \cdot \nabla(\nabla \cdot \hat{c}) + \chi_a (\hat{c} \cdot \vec{H})(\hat{c}_\perp \cdot \vec{H}) + \frac{\Gamma q_c p_c}{2}(|\tilde{A}_1|^2 - |\tilde{A}_2|^2). \tag{1.140}$$

This form is similarly restricted in its usefulness as Eqs. (1.130,1.131).

The Rescaled Form

A rather simple normal-form equation can be obtained when only one roll direction is present[16] ($A_2 = 0$, say):

$$\partial_{\check{t}} \check{A}_1 = \Big[1 + (\partial_{\check{x}} - i\check{\varphi})^2 + \partial_{\check{y}}^2 - |\check{A}_1|^2 + i\check{\beta}_x \check{\varphi}_{,\check{x}} + i\check{\beta}_y \check{\varphi}_{,\check{y}} \Big] \check{A}_1, \tag{1.141}$$

$$\partial_{\check{t}} \check{\varphi} = \check{K}_{ij} \partial_i \partial_j \check{\varphi} - \varepsilon^{-1} \check{H}^2 \check{\varphi} + \varepsilon^{-1/2}\, \check{\Gamma} |\check{A}_1|^2, \tag{1.142}$$

with i, j running over the indices $\check{x}$ and $\check{y}$. The correspondence between the unscaled equations (1.73,1.138) and the normal form (1.141,1.142) is not as easily obtained as for normal rolls. First, rewrite Eqs. (1.73,1.138) in matrix notation:

$$\partial_t A_1 = \Big(\varepsilon + (\partial_{\vec{r}} - i\hat{z}\times\vec{q}_c\,\varphi)^T \mathbf{\Xi} (\partial_{\vec{r}} - i\hat{z}\times\vec{q}_c\,\varphi) + i\vec{\beta}^T \nabla\varphi - g|A_1|^2\Big) A_1 \tag{1.143}$$

$$\partial_t \varphi = \left(\nabla^T \mathbf{K} \nabla\right) \varphi - \chi_a H^2 \varphi + \frac{\Gamma q_c p_c}{2} |A_1|^2, \tag{1.144}$$

with

$$\mathbf{\Xi} = \begin{pmatrix} \xi_{xx}^2 & \xi_{xy}^2 \\ \xi_{xy}^2 & \xi_{xx}^2 \end{pmatrix}, \quad \mathbf{K} = \begin{pmatrix} K_3 & 0 \\ 0 & K_1 \end{pmatrix}, \quad \vec{\beta} = \begin{pmatrix} \beta_x \\ \beta_y \end{pmatrix}, \quad \hat{z}\times\vec{q}_c = \begin{pmatrix} -p_c \\ q_c \end{pmatrix} \tag{1.145}$$

Let the coordinates $\vec{r} = (x, y)^T$ and $\vec{\check{r}} = (\check{x}, \check{y})^T$ be related by

$$\vec{r} = \varepsilon^{-1/2} \mathbf{M}^{-1}\, \vec{\check{r}}, \quad \partial_{\vec{r}} = \varepsilon^{1/2} \mathbf{M}\, \partial_{\vec{\check{r}}}. \tag{1.146}$$

After dividing by ε the second term on the *r.h.s.* of Eq. (1.143) can be transformed like

[16] I have put the $\check{\varphi}$ together with the $\partial_{\check{x}}$ in the $\check{A}$ equation in order to make a clear distinction from Eq. (1.123)

$$\begin{aligned}
&\varepsilon^{-1}(\partial_{\vec{r}} - i\hat{z}\times\vec{q}_c\,\varphi)^T\,\boldsymbol{\Xi}(\partial_{\vec{r}} - i\hat{z}\times\vec{q}_c\,\varphi) && (1.147)\\
&\quad = (\mathbf{M}\partial_{\vec{\tilde{r}}} - i\hat{z}\times\vec{q}_c\,\varphi\varepsilon^{-1/2})^T\,\boldsymbol{\Xi}(\mathbf{M}\partial_{\vec{\tilde{r}}} - i\hat{z}\times\vec{q}_c\,\varphi\varepsilon^{-1/2}) && (1.148)\\
&\quad = (\partial_{\vec{\tilde{r}}} - i\mathbf{M}^{-1}\hat{z}\times\vec{q}_c\,\varphi\varepsilon^{-1/2})^T\,\mathbf{M}^T\boldsymbol{\Xi}\mathbf{M}(\partial_{\vec{\tilde{r}}} - i\mathbf{M}^{-1}\hat{z}\times\vec{q}_c\,\varphi\varepsilon^{-1/2}) && (1.149)\\
&\quad = \left(\partial_{\vec{\tilde{r}}} - \begin{pmatrix} i\breve{\varphi} \\ 0\end{pmatrix}\right)^T\left(\partial_{\vec{\tilde{r}}} - \begin{pmatrix} i\breve{\varphi} \\ 0\end{pmatrix}\right) && (1.150)
\end{aligned}$$

if $\mathbf{M}^{-1}$ has the form

$$\mathbf{M}^{-1} = \begin{pmatrix} a & b \\ q_c c & p_c c\end{pmatrix} \tag{1.151}$$

with $a, b, c \in \mathbb{R}$, and

$$\mathbf{M}^T\boldsymbol{\Xi}\mathbf{M} = 1. \tag{1.152}$$

The value of $\breve{\varphi}$ is given by

$$\breve{\varphi} = (-p_c\,a + q_c\,b)\varphi\varepsilon^{-1/2}. \tag{1.153}$$

Rewrite Eq. (1.152) as

$$\boldsymbol{\Xi} = (\mathbf{M}^{-1})^T\,\mathbf{M}^{-1} = \begin{pmatrix} a^2 + c^2\,{q_c}^2 & a\,b + c^2\,p_c\,q_c \\ a\,b + c^2\,p_c\,q_c & b^2 + c^2\,{p_c}^2\end{pmatrix}. \tag{1.154}$$

Notice that the signs of a and c may still be chosen freely (the relative sign of a and b is fixed). One of the solutions to Eq. (1.154) is

$$a = \frac{-p_c\,\xi_{xx}^2 + q_c\,\xi_{xy}^2}{N}, \tag{1.155}$$

$$b = \frac{-p_c\,\xi_{xy}^2 + q_c\,\xi_{yy}^2}{N}, \tag{1.156}$$

$$c = \frac{\sqrt{|\boldsymbol{\Xi}|}}{N}, \tag{1.157}$$

$$\text{with}\quad N = \sqrt{{p_c}^2\,\xi_{xx}^2 - 2\,p_c\,q_c\,\xi_{xy}^2 + {q_c}^2\,\xi_{yy}^2} \tag{1.158}$$

$$\text{and}\quad |\boldsymbol{\Xi}| = \det\boldsymbol{\Xi} = \xi_{xx}^2\,\xi_{yy}^2 - \xi_{xy}^4. \tag{1.159}$$

The numerator in the formula for c is always real. Otherwise $\boldsymbol{\Xi}$ would not be positive definite, which in turn would violate property number 3 in Section 1.2.

N is always real when the numerator of c is real. With these choices of the signs Eq. (1.153) becomes

$$\check{\varphi} = N\varphi\varepsilon^{-1/2}. \tag{1.160}$$

The pattern amplitude in the rescaled equations is $\check{A}_1 = (g/\varepsilon)^{1/2}A_1$. For the remaining coefficients of Eqs. (1.141,1.142) one gets

$$\begin{pmatrix}\check{\beta}_x \\ \check{\beta}_y\end{pmatrix} = N^{-1}\,\mathbf{M}^T\vec{\beta}, \quad (\check{K}_{ij}) = \frac{\tau}{\tilde{\gamma}_1}\mathbf{M}^T\mathbf{K}\mathbf{M}, \tag{1.161}$$

$$\check{\Gamma} = N\frac{\tau\Gamma q_c p_c}{2\tilde{\gamma}_1 g}, \quad \check{H}^2 = \frac{\tau\chi_a H^2}{\tilde{\gamma}_1}. \tag{1.162}$$

It is interesting to notice that by choosing the opposite sign for a, b, and c in Eqs (1.155–1.157), only $\check{\Gamma}$ would change sign. All other coefficients would remain unchanged. While a change of sign in Γ does strongly change the qualitative behavior of normal rolls, it is less significant for oblique rolls. For $\check{\beta}_x, \check{\beta}_y$ we get the explicit formulae

$$\check{\beta}_x = \frac{-\beta_x\,p_c + \beta_y\,q_c}{N^2}, \quad \check{\beta}_y = \frac{p_c\,(\beta_y\,\xi_{xx}^2 - \beta_x\,\xi_{xy}^2) + q_c\,(-\beta_y\,\xi_{xy}^2 + \beta_x\,\xi_{yy}^2)}{N^2\sqrt{|\Xi|}}. \tag{1.163}$$

When $\check{A}_1, \check{\varphi} = O(1)$, $\check{H}^2 = O(\varepsilon)$ in Eqs. (1.141,1.142) the $\check{\Gamma}$-term in Eq. (1.142) is easily seen to be uncompensated in the limit of small ε. In order to reobtain a uniform scaling in Eq. (1.142), $\check{A}_1 \sim \varepsilon^{1/4}$ ($A_1 \sim \varepsilon^{3/4}$) has to be assumed. In turn, the third order (Landau) term in Eq. (1.141) becomes negligible when $\varepsilon \to 0$. Hence, for small ε (and $H^2 = O(\varepsilon)$), we must expect a scenario where the nonlinear saturation of $\check{A}$ does not come directly from the Landau term, but indirectly via Eq. (1.142). If this is the case, $\check{\Gamma}$ can be set to unity by another rescaling of $\check{A}_1$. As long as the diffusive term in this equation is negligible, Eq. (1.142) does not fix a time scale. Then $\Delta t \sim \tau/\varepsilon$ is the only characteristic time of the system. The transition to the small ε behavior should occur when $\varepsilon^{-1/2}\check{\Gamma} = O(1)$, i.e. when $\varepsilon \approx \check{\Gamma}^2$. Two possible scenarios for the limit $\varepsilon \to 0$ will be described below. In both cases we assume $H^2 = 0$ for simplicity.

Rotating Rolls

In the first scenario the $\check{\Gamma}$-term balances nearly completely with the time derivative of $\check{\varphi}$. There is a steady increase of $\check{\varphi}$ (taking a positive $\check{\Gamma}$). Strictly speaking, we would soon leave the range of validity of the amplitude equations. But similar to normal rolls, the rotational invariance of the original system survives in the normal form (1.141,1.142) as a symmetry under $\check{\varphi} \to \check{\varphi} + \delta$, $\check{A}_1 \to \check{A}_1 \exp(i\delta\check{x})$, and the equations remain, to some extent, valid, as long as $\mathrm{Im}[(\partial_{\check{x}}\check{A}_1)/\check{A}_1]$ and φ do not differ too much. Due to the constant change of $\check{\varphi}$, the range of wave vectors $(k_{\check{x}}, k_{\check{y}})$ in the Fourier transform of $\check{A}_1$ for which the growth rate $1-(k_{\check{x}}-\check{\varphi})^2 - k_{\check{y}}^2$ is positive is constantly changing. For Fourier modes in this unstable range, these linear terms give the dominant contribution to their dynamics. In order to determine their absolute amplitude, however, nonlinear contributions have to be invoked. Here the Landau term in Eq. (1.141) may come into play again. Assume that the dominating modes can be found in a circle (in Fourier space) of radius κ centered around $(k_{\check{x}}, k_{\check{y}}) = (\varphi - 1, 0)$, the point where the Fourier modes just ceased to have the longest possible phase of growth. Through the cubic Landau term, these modes lead to an excitation of all modes in a circle of radius 3κ around the same point. The excitation is particularly strong in the direction of positive $k_{\check{x}}$, where the damping is weakest. Since $\check{\varphi}$ is steadily increasing, these modes will soon themselves be in the small circle and belong to the dominating modes of $\check{A}_1$. The average value of $\partial_{\check{t}}\check{\varphi}$ will adjust itself in such a way that the average of the resulting amplitude $|\check{A}_1|$ reaches an equilibrium. Other possible sources of initial excitations for the subsequent growth of Fourier modes are spatial modulations of φ and the noise (e.g. thermal), which would be present in every real physical system. In order for this mechanism to work, the other roll amplitude A_2 has to be suppressed nonlinearly by A_1. Since $|A_1|$ is just in equilibrium, one could think that the weak suppression through the term $-h|A_1|^2A_2$ in Eq. (1.73), which is the only difference in the linearized dynamics of A_1 and A_2, is sufficient (this term is by a factor $\sim \varepsilon^{1/2}$ smaller than the other terms). Numerical solutions of Eqs. (1.139,1.140) show that such a scenario is in fact possible. However, it seems that A_2 can be suppressed over long times only if ε is not too small.

We will look at the results of a simulation of Eqs. (1.139,1.140) demonstrating this mechanism in more detail (Fig. 1.2). It was done for a plane of extension[17]

$$F := 160 \times 160 = (95.98)^2\, |\Xi|^{1/2}\, \varepsilon^{-1}. \tag{1.164}$$

[17] The expression $|\Xi|^{1/2}\varepsilon^{-1}$ is an estimate of the area over which modulations of A_1 or A_2 are correlated. It is the two-dimensional counterpart to the correlation length.

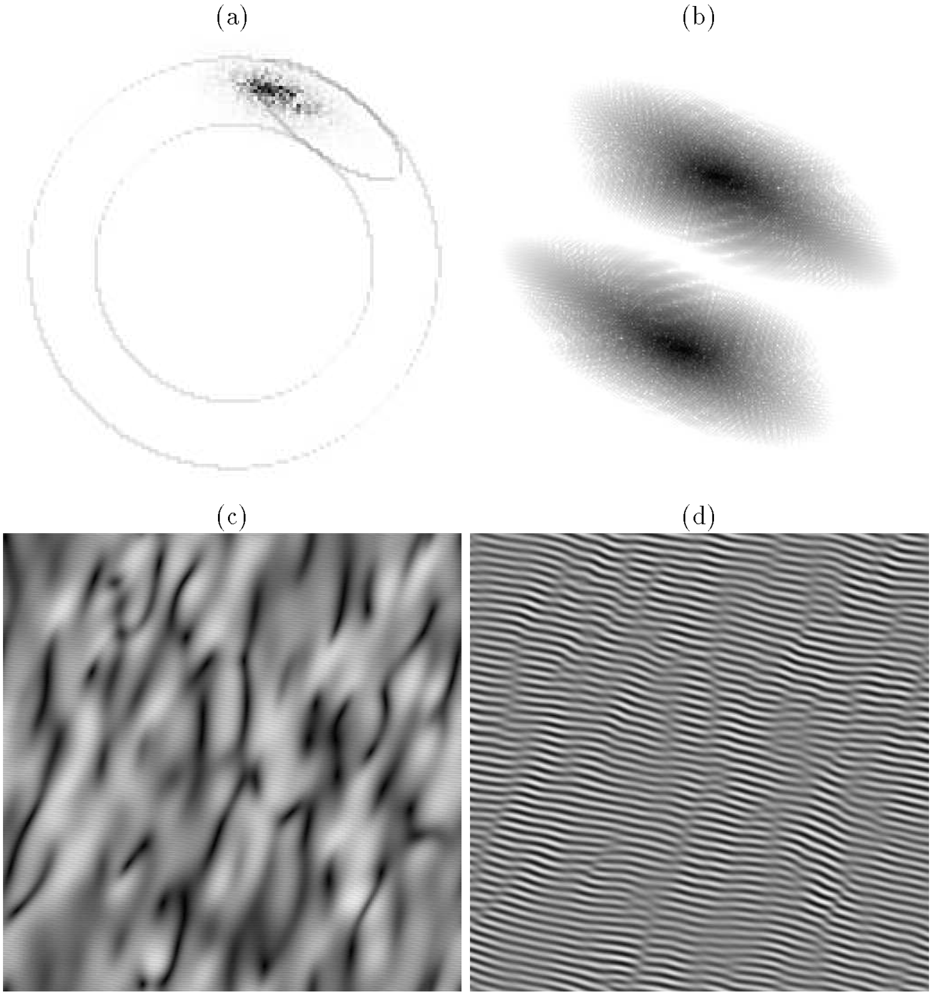

Figure 1.2: *Snapshot of $\tilde{A}_1$ in the rotating-roll state in simulations of Eqs. (1.139,1.140). The rolls are rotating counterclockwise. (a) is the spatial power spectrum of $\tilde{A}_1$, encoded in a linear gray scale. The region of unstable modes of $\tilde{A}_1$ corresponding to the momentary spatial average of φ and the annulus covered by this region during a full rotation are also sketched. (b) shows the power spectrum of* $\mathrm{Re}[\tilde{A}_1]$ *in a logarithmic gray scale. In both images black corresponds to the highest value, the point $k_x = k_y = 0$ is in the center of the images. Notice that, compared to (b), (a) is enlarged by a factor of two. (c) and (d) show* $|\tilde{A}_1|$ and $\mathrm{Re}[\tilde{A}_1]$ *in the full* 160×160 *plane.*

The coefficients were chosen as[18]

$$
\begin{gathered}
\varepsilon = 0.08, \quad \tau = 0.0761124, \quad p_c = 1.72626, \quad q_c = 0.74985, \\
\xi_{xx}^2 = 0.54347, \quad \xi_{yy}^2 = 0.14038, \quad \xi_{xy}^2 = 0.16389, \\
\beta_x = 0.30988, \quad \beta_y = 0.02329, \quad K_1 = 1.13762, \quad K_3 = 1.24826, \\
g = 5.0365, \quad h = 9.5758, \quad \Gamma = -20.317, \quad \tilde{\gamma}_1 = 1.
\end{gathered}
\tag{1.165}
$$

which leads to

$$
\begin{gathered}
N = 0.54736, \quad \check{\beta}_x = -0.64135, \quad \check{\beta}_y = 0.59918, \\
\check{\Gamma} = -0.10877, \quad \check{K}_{xx} = 1.03953, \quad \check{K}_{xy} = \check{K}_{yx} = 0.15187, \\
\check{K}_{yy} = 0.18229.
\end{gathered}
\tag{1.166}
$$

Figure 1.3(a) shows the evolution of the spatial mean value of the rescaled amplitude $|\check{A}_1|^2 = |A_1|^2 \times g/\varepsilon$. Its steady-state average $\langle|\check{A}_1|^2\rangle_{F,t} = 0.2836(11)$ is notably smaller than its value in saturation $|\check{A}_1|^2 = 1$. It can be seen in the spatial power spectrum of a steady-state snapshot of $\tilde{A}_1$, Fig. 1.2(a), that the range of active modes is small compared to the range of unstable modes. As explained above, the active modes are concentrated close to the lagging end of the unstable range. Fig. 1.3(c) shows how the director is steadily turning clockwise [with $\partial_t\langle\varphi\rangle\, N\varepsilon^{-3/2} = -0.1091$]. Since the director as well as the (average) wave vector perform a joined and steady rotation, we will call the scenario "rotating rolls". A special initial condition had to be prepared in order to reach this attractor. φ was initialized to $\varphi \equiv 0$ and $\tilde{A}_1$ to $\tilde{A}_1 = (\varepsilon/g)^{1/2}\exp(i(q_c x + p_c y)) +$ noise, while $\tilde{A}_2$ was initialized with noise only, but much weaker than $\tilde{A}_1$. In Fig. 1.3(b) it can be seen that the initial perturbations in $\tilde{A}_2$ decay; however, the decay is quite slow [$\tau\varepsilon^{-1}\ \partial_t \log|\tilde{A}_2| \approx -8\cdot 10^{-2}$ compared to $-h\varepsilon^{-1}|\check{A}_1|^2 = -0.54$], and strongly fluctuating on top of this [see Fig. 1.3(b)]. Clearly it is important for rotating rolls to be stable (i.e. an attractor) that the perturbations $\tilde{A}_2$ decay, but it is not at all obvious when this will be the case. A slightly broken R_y-symmetry, caused, for example, by rotating the physical system around an axis normal to the plane of the layer, would break the degeneracy of oblique rolls and help to stabilize the rotating-roll state. Certainly the rotating-roll scenario is appealing from a theoretical point of view. In the equation for $\partial_{\check{t}}\check{A}_1$, Eq. (1.141), most of the modes are either responding adiabatically to the excitations from the nonlinearity or are mostly controlled by the linear terms. The nonlinear saturation basically comes from the nonlinear term in the equation for $\partial_{\check{t}}\check{\varphi}$, Eq. (1.142), and the most important

[18]These values correspond to the experimental system described in Chapter 3 with the standard material parameters and $\omega\tau_0 = 0.73$.

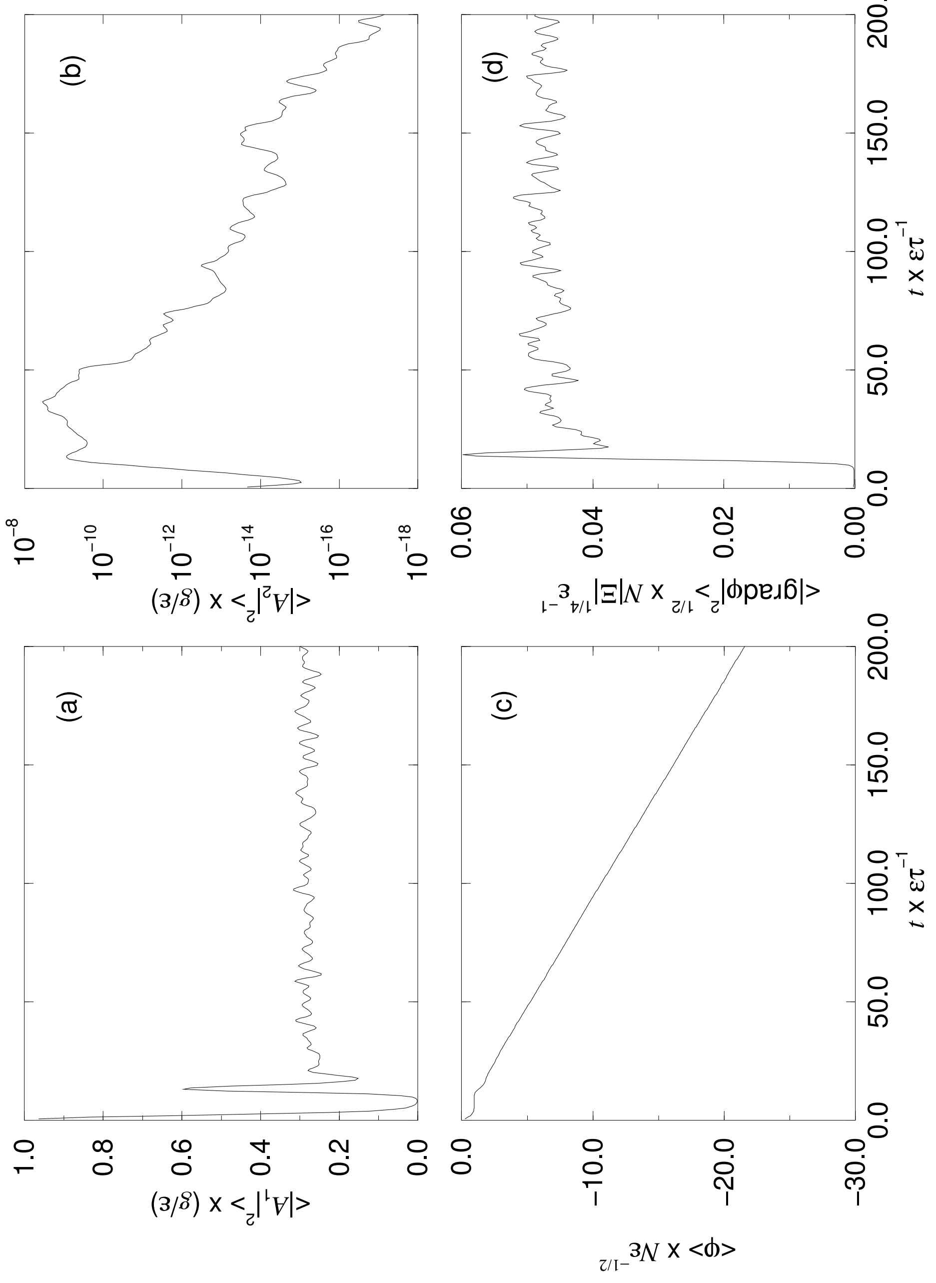

Figure 1.3: *Results of a simulation of a "rotating-roll" state. For explanations see text.*

contribution of this term seems to be its global average (which is constant in time in the limit of a steady state in an infinite system). Spatial fluctuations of $\check{\varphi}$ are rather small [compare Fig. 1.3(d) with Fig. 1.7(b)]. Rotating rolls do therefore naturally come very close to an ideal mean field approximation. Deviations from it may be treatable perturbatively, possibly in a Gaussian approximation for the distribution of $\check{A}$. This route has not yet been followed, basically because the rotating-roll scenario has not been found in experiments[19] yet.

Swinging Rolls

Another scenario involves both oblique-roll modes A_1 and A_2. Again, the director turns to the side as soon as one of the modes (A_1, say) dominates over the other. In contrast to the rotating-roll scenario, the amplitude A_2 is not so small that it could not participate in the dynamics. Instead of A_1 steadily adjusting its wave vector when φ changes, A_1 dies out (similar to what can be seen in the transient of Fig. 1.3(a)) and is replaced by A_2 instead. When $|A_2|^2 > |A_1|^2$, the director starts turning into the other direction and another half cycle begins. There is a permanent oscillation between A_1 and A_2. This will be called the "swinging-roll" scenario.

The argument made above to show that $|A_1| \sim \varepsilon^{3/4}$ as $\varepsilon \to 0$ is also valid if both amplitudes are allowed: It is still possible to rescale length, time, A_1, A_2, and φ in such a way that Eqs. (1.73,1.138) become[20]

$$\begin{aligned}\tau\partial_t A_{1/2} = \Big[& 1 + \xi_{xx}^2(\partial_x \pm ip_c\varphi)^2 + \xi_{yy}^2(\partial_y - iq_c\varphi)^2 \\ & \pm 2\xi_{xy}^2(\partial_x \pm ip_c\varphi)(\partial_y - iq_c\varphi) - g\varepsilon^{1/2}|A_{1/2}|^2 \\ & -h\varepsilon^{1/2}|A_{2/1}|^2 \pm i\beta_x\varphi_{,x} + i\beta_y\varphi_{,y} \Big] A_{1/2},\end{aligned} \tag{1.167}$$

$$\tilde{\gamma}_1\partial_t\varphi = K_1\partial_y^2\varphi + K_3\partial_x^2\varphi - \varepsilon^{-1}\tilde{\chi}_a H^2\varphi + \frac{\Gamma q_c p_c}{2}(|A_1|^2 - |A_2|^2). \tag{1.168}$$

When $H^2 = 0$ and $\varepsilon \to 0$, the terms of third order in $A_{1/2}$ in Eq. (1.167) become negligible and the rest independent of ε. If these equations have an attractor that exhibits the swinging-roll scenario, it will be so at arbitrarily low ε.

A numerical example for swinging rolls will be presented in detail. Again, the explicitly rotationally invariant equations [Eqs. (1.139,1.140)] have been used.

[19] The preparation of a rotating-roll state requires to select the same roll direction over the entire layer of the pattern-forming system. This is probably easier in not too large aspect ratio cells.

[20] No further use will be made of these equations. Therefore we abstain from introducing new variable names.

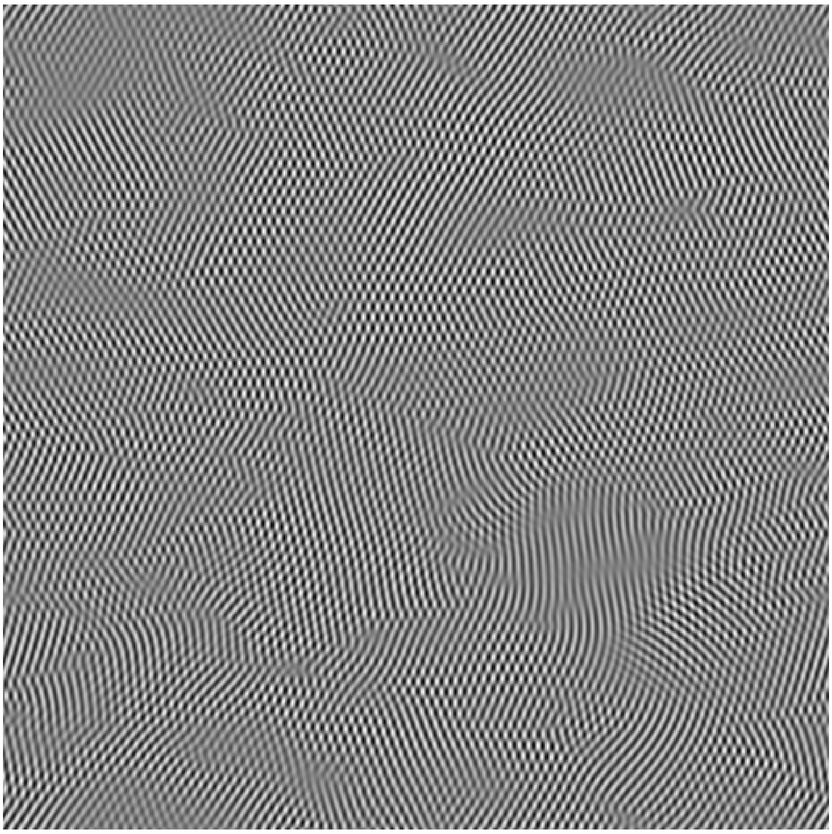

Figure 1.4: *Snapshots of* $\mathrm{Re}[\tilde{A}_1 + \tilde{A}_2]$ *in the swinging-roll state in simulations of Eqs. (1.139,1.140). The area of the image is the full* 320×320 *plane of integration.*

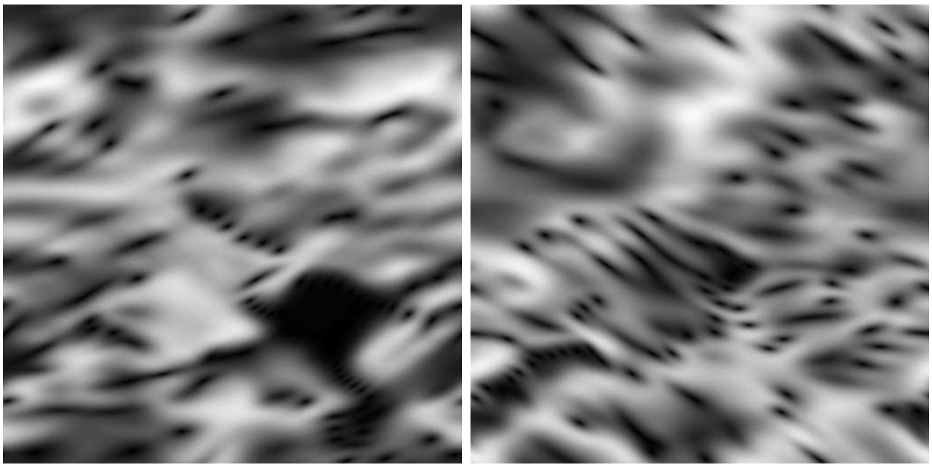

Figure 1.5: *Snapshots of* $|\tilde{A}_1|$ *(left) and* $|\tilde{A}_2|$ *(right) in the swinging-roll state in simulations of Eqs. (1.139,1.140). The largest values are white, black corresponds to* $\tilde{A}_{1/2} = 0$. *The area of each image is the full* 320×320 *plane of integration.*

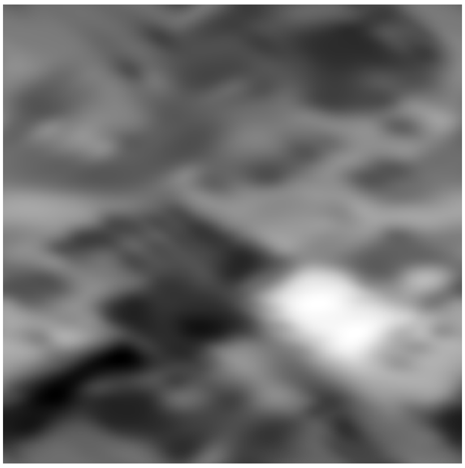

Figure 1.6: *Snapshots of the deformation of the director field* (φ) *in the swinging-roll state in simulations of Eqs. (1.139,1.140). The largest angle is white, the smallest black. The area of the image is the full* 320×320 *plane of integration.*

For swinging rolls the crossover to the $A_{1/2} \sim \varepsilon^{3/4}$ scaling region is a little lower than for rotating rolls, because φ cannot move as freely in the swinging-roll case as for rotating rolls. The simulation was done with the same coefficients as the rotating-roll example, except that $\varepsilon = 0.01$. Swinging rolls do also exist at higher ε, but then $\langle|\tilde{A}_1|^2+|\tilde{A}_2|^2\rangle \times \varepsilon/g$ saturates at some value ≈ 0.6. In our case we get $(|\tilde{A}_1|^2+|\tilde{A}_2|^2)\times\varepsilon/g = 0.383(3)$. The lower value of ε requires also a larger system size $F = 320 \times 320 = (67.9)^2\,|\Xi|^{1/2}\,\varepsilon^{-1}$. Figure 1.4 shows a snapshot of the modulation pattern $\mathrm{Re}[\tilde{A}_1 + \tilde{A}_2]$. In most of the picture the wave vectors of the rolls are still close to their critical value for $\varphi \equiv 0$ [i.e. $\vec{q}_{loc} \approx (q_c, \pm p_c)$], which was the initial condition for φ. Only in the lower right part of the image there is a region where rolls are oriented considerably different. In this region the state seems to behave rather according to the rotating-roll scenario. This can also be seen in the images showing $|A_1|$, $|A_2|$, and φ (Figs. 1.5,1.6). The drift underlying the oscillations of $\langle\varphi\rangle_F$ in Fig. 1.7(c) is also related to this region. Such localized transitions to rotating rolls seem to appear intermittently for the parameters used. The dependence of this effect on the system parameters and its influence on the long term stability of the swinging-roll state have not been investigated. Therefore it is also not possible to decide if rotating and swinging rolls are really two independent, concurrently existing attractors.

We will concentrate on the oscillations. The Fourier transform of the time series of $\langle\varphi\rangle$, Fig. 1.7(d), shows that the typical frequency of the oscillations is $\omega = 0.5\varepsilon/\tau$. The same frequency can also be seen in the temporal correlation functions[21] of A_1 and A_2 that are displayed in Fig. 1.8. There, however, it is superimposed with another, slowly decaying, non-oscillatory component.

In contrast to rotating rolls, the average director changes only very little for swinging rolls. They are therefore much better compatible with a broken isotropy introduced by $H^2 > 0$. In fact, swinging-roll like oscillations of oblique rolls have been observed for liquid crystal electroconvection with broken isotropy (page 6114 of [19]).

Transition to higher ε

For not so small ε the chaotic solutions of the oblique-roll amplitude equations are very complicated and not understood. Depending on ε (and other parameters), the details of the structure of the solutions change drastically. This shall be shown on the series of correlation functions displayed in Fig. 1.9. They were

[21] The temporal correlation function of the modulation pattern $\Psi = \mathrm{Re}[A_1 + A_2]$ is simply the sum of the correlation functions for A_1 and A_2. When comparing with experimental data it must be noticed that the correlation function can be substantially different when the modulation pattern also contains the contributions from higher spatial Fourier modes, as is typical for raw experimental images.

calculated for a different set of parameters,

$$\begin{gathered}\tau = 0.10997, \quad p_c = 1.09320, \quad q_c = 1.31622, \quad \xi_{xx}^2 = 0.45171, \\ \xi_{yy}^2 = 0.31581, \quad \xi_{xy}^2 = 0.16365, \quad \beta_x = 0.53548, \\ \beta_y = 0.01427, \quad K_1 = 1.22016, \quad K_3 = 1.22700, \quad g = 6.319, \\ h = 10.149, \quad \Gamma = -16.667, \quad \tilde{\gamma}_1 = 1,\end{gathered} \tag{1.169}$$

yielding

$$\begin{gathered}N = 0.78485, \quad \check{\beta}_x = -0.919816, \quad \check{\beta}_y = 0.623599, \\ \check{\Gamma} = -0.16377, \quad \check{K}_{xx} = 0.639161, \quad \check{K}_{xy} = \check{K}_{yx} = 0.0679276, \\ \check{K}_{yy} = 0.251683.\end{gathered} \tag{1.170}$$

Obviously the $A_{1/2} \sim \varepsilon^{3/2}$ scaling range has not yet been reached at the lowest value of ε used (simulations at lower ε have not been carried out because they would have lasted prohibitively long, at least when Eqs. (1.139,1.140) were used). Nevertheless, drastic structural changes in the correlation functions can be seen. In particular it is remarkable that the *rescaled* decay rate of the correlations does first increase (approaching lower ε) and then fall again. This result does not agree with the experiments reported in [20], where the rescaled decay rate is found to be constant over the range $\varepsilon = 0.025 \ldots 0.8$.

Of course, the highest value $\varepsilon = 0.64$ used in the simulations is far outside the range of validity of our equations. The simulation results only indicate that probably things *do* change for higher ε, but they cannot predict how.

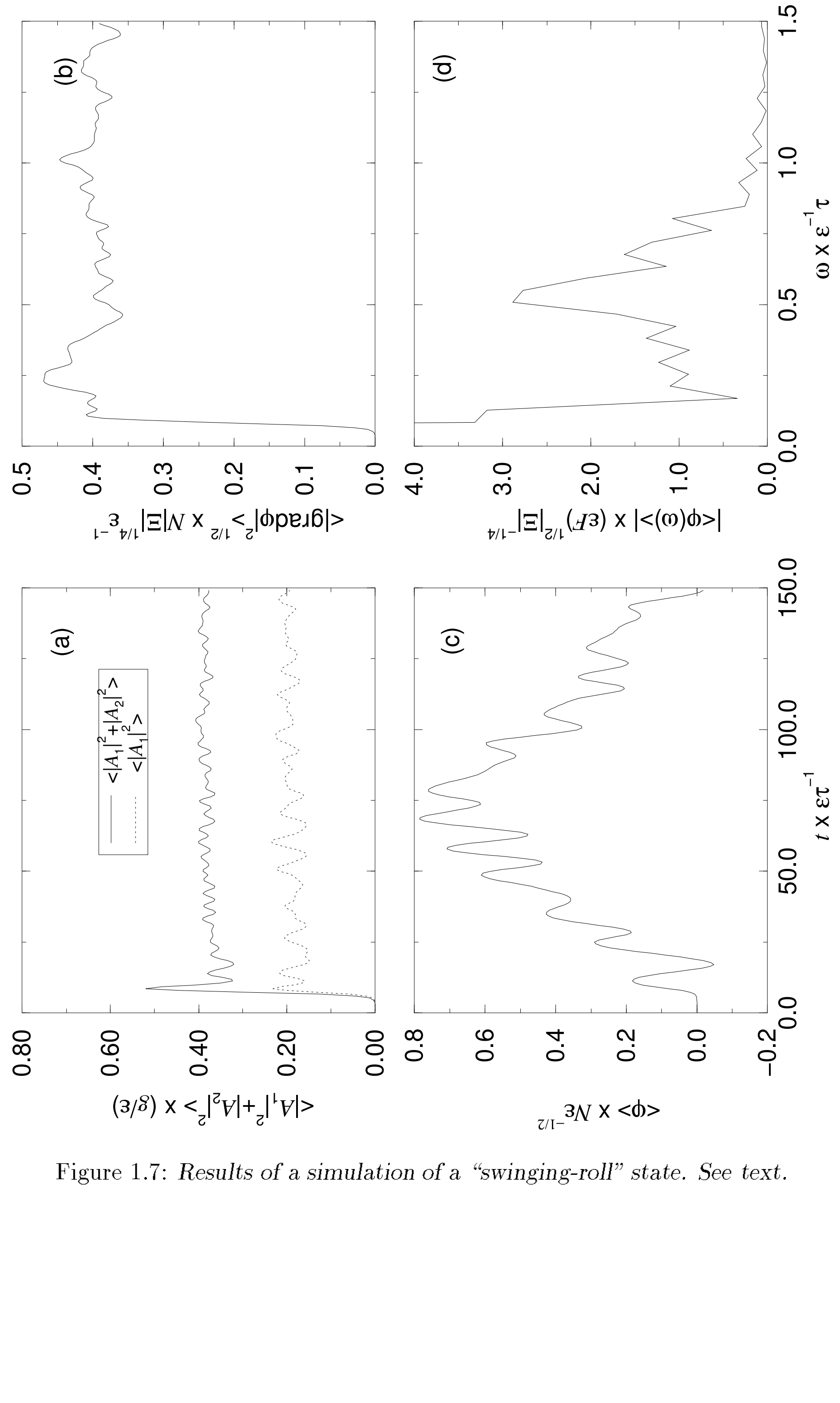

Figure 1.7: *Results of a simulation of a "swinging-roll" state. See text.*

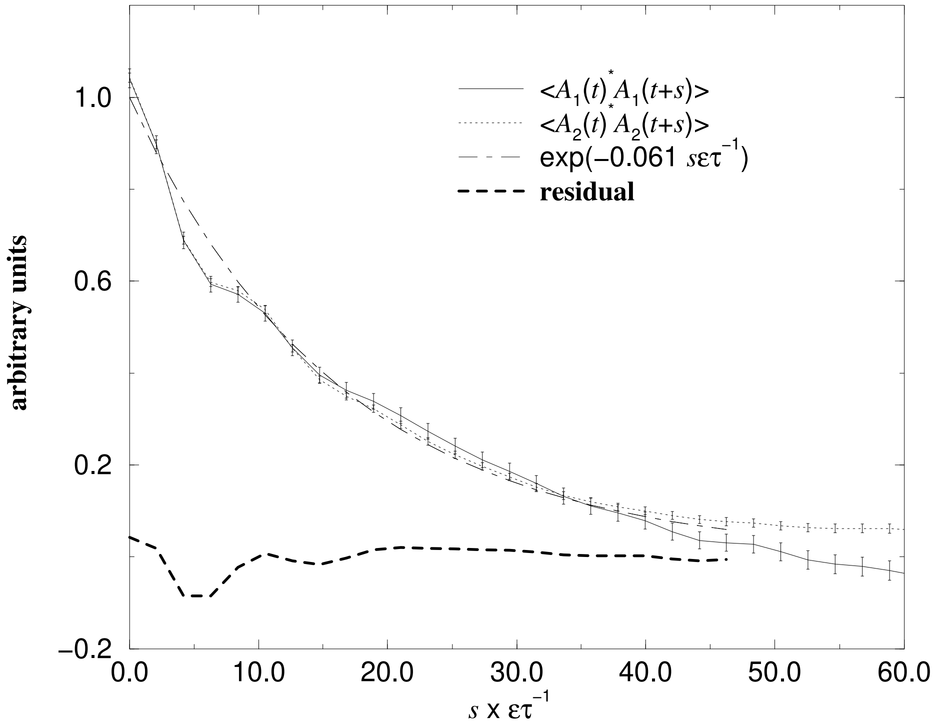

Figure 1.8: *Autocorrelation functions of A_1 and A_2 (or equivalently $\tilde{A}_1$ and $\tilde{A}_2$) in the swinging-roll state. The curve named "residual" is the average over both amplitudes of the differences between the autocorrelation function and the exponential fit.*

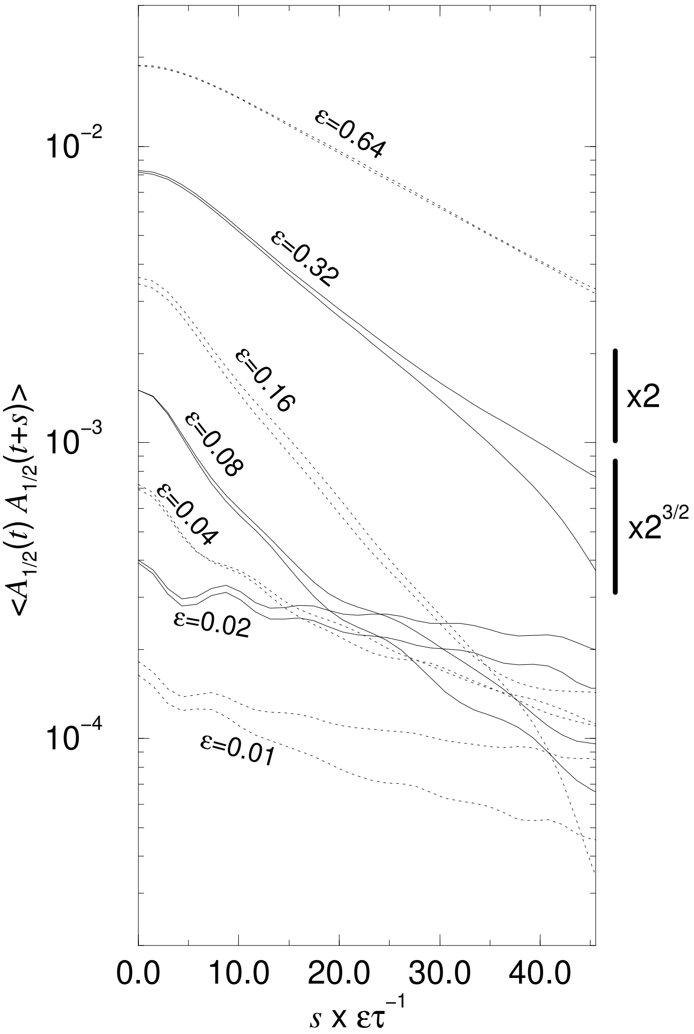

Figure 1.9: *The dependence of the correlation function of oblique rolls on ε. Instead of averaging the correlation functions of A_1 and A_2 they were plotted separately in order to give some impression of the statistical error. The thick bars on the side allow a comparison with the two predicted scaling laws $A_{1/2} \sim \varepsilon^{1/2}$ and $A_{1/2} \sim \varepsilon^{3/4}$. The former would correspond to a factor of 2 in the correlation function for successive values of ε, the latter to a factor $2^{3/2}$.*

Chapter 2

Stability of Roll Solutions

This chapter is concerned with the stability analysis of regular roll solutions of the amplitude equations. Due to its rather easy experimental and theoretical accessibility, the stability problem is traditionally an important test for the modeling of pattern forming systems. It is also of some interest in its own right, because beyond the stability limit the structure of the pattern often changes drastically; spatio-temporal chaos may appear. The limits of stability are often also the limits of understanding. A profound knowledge of the limits may allow us to cross them.

2.1 Normal-Roll Range

2.1.1 Existence and Stability with Respect to Homogeneous Perturbations

We begin with a discussion of the existence and linear stability of homogeneous time independent solutions of the form

$$A = A_0 e^{i(Qx+Py)}, \quad \varphi = \varphi_0, \quad A_0, P, Q, \varphi_0 \in \mathbb{R} \tag{2.1}$$

of Eqs. (1.123,1.127) (Notice that in this section all carets ˇ will be suppressed.). Such solutions do only exist if $g > 0$. The state Eq. (2.1) has to satisfy either the trivial condition $A_0 = \varphi_0 = 0$ or

$$A_0^2 = 1 - (P - \varphi_0)^2 - Q^2, \tag{2.2}$$

$$(H^2/\varepsilon + 2\Gamma A_0^2)\varphi_0 = 2\Gamma A_0^2 P. \tag{2.3}$$

Although it is convenient to do the analytic calculations in rescaled coordinates (used in Eqs. (1.123,1.127)) it is sometimes easier to interpret the results when the original ε dependence of the length scales is reintroduced. On the other hand, the formulas become difficult to read when they explicitly contain all coefficients of Eqs. (1.71,1.126). We will therefore express most final results in terms of the quantities

$$\eta := \frac{2|\Gamma|\varepsilon}{H^2}, \quad q := \eta^{1/2}Q, \quad p := \eta^{1/2}P, \quad \text{and} \quad s := \mathrm{sign}\Gamma. \tag{2.4}$$

Inserting (2.2) into (2.3) yields a cubic polynomial that fixes φ_0 as a function of $s\eta$, P and Q. For example, Eq. (2.2) requires $(P-\varphi_0)^2+Q^2<1$ for A_0 to be positive. At the limit $A_0^2=0$ Eq. (2.3) yields $\varphi_0=0$. This gives us the neutral curve where $A_0=0$ is marginally stable:

$$\eta_{\mathrm{NC}} = p^2+q^2 \quad \text{(neutral curve)}. \tag{2.5}$$

In its general form the polynomial has a unique real root φ_0 as long as

$$P^2 \geq \frac{4}{27}\eta^2(1+s/\eta-Q^2)^3. \tag{2.6}$$

The corresponding threshold can be written as

$$\eta_{\mathrm{SN}} = -s+\frac{3|p|^{2/3}}{2^{2/3}}+q^2 \quad \text{(saddle-node)}. \tag{2.7}$$

For $\Gamma<0$ ($s=-1$) Eqs. (2.2,2.3) have three solutions with different φ_0 if $\eta>\eta_{\mathrm{SN}}$. The solutions with the largest and the smallest value of φ are stable against homogeneous perturbations (there may be modulation instabilities), and the middle one is always unstable. We will call a (homogeneously) stable solution of Eqs. (2.2,2.3) a "normal roll" solution if $\Gamma P/\varphi_0>0$ or $P=\varphi_0=0$ and an "abnormal roll"[1] solution if $\Gamma P/\varphi_0\leq 0$ and $\varphi_0\neq 0$ (the latter only exist for $\Gamma<0$). With this definition, normal rolls correspond to the relative configuration of director, wave vector and the isotropy breaking "magnetic field", that is found in the limit of small η, where the additional degree of freedom φ can be treated perturbatively. There are two disconnected branches of abnormal rolls, one with $\varphi_0>P\geq 0$, the other with $\varphi_0<P\leq 0$. Only the first branch is shown in the stability diagrams displayed throughout this section. In Fig. (2.1), for example, it can be seen how abnormal rolls connect to normal rolls. Similar to branching

[1] The notion of "abnormal rolls" goes back to [45], who optically detected an unexpected symmetry breaking in electroconvection in homeotropically aligned nematic liquid crystals. Clear experimental evidence for this phenomenon was found in [37].

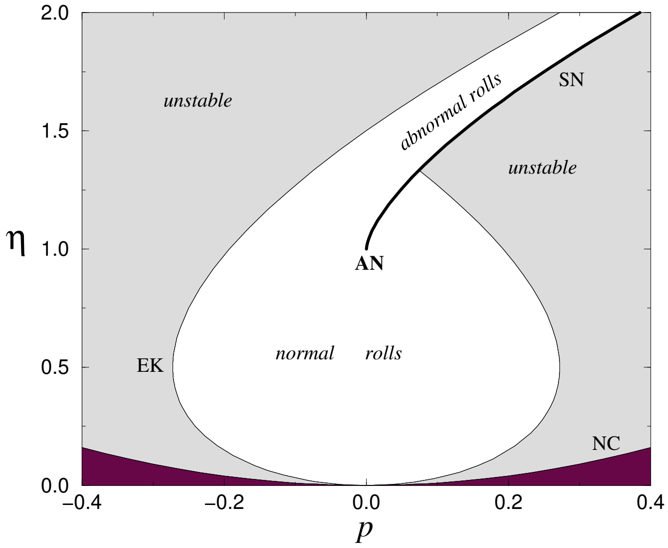

Figure 2.1: *Stability diagram for normal and abnormal rolls with* $\Gamma < 0$ *and* $\beta_y = -0.4$ *(or lower). The abbreviations stand for: EK – Eckhaus boundary; SN – saddle-node bifurcation line; AN – abnormal-roll branching point; NC – neutral curve.*

points of analytic functions in the complex plane, the configuration space for $\Gamma < 0$ has a branching point (co-dimension 2) at $p = 0$ and

$$\eta = \eta_{\mathrm{AN}} = 1 + q^2 \quad \text{(abnormal roll).} \tag{2.8}$$

In order to connect continuously one abnormal-roll branch with the other, one has to walk around the branching point in configuration space. In the figures, the role of the branch cut (known from function theory) is played by the saddle-node bifurcation line (SN).

If η is increased for fixed $P = 0$, the solution of Eqs. (2.2,2.3) goes through a pitchfork bifurcation from normal rolls to abnormal rolls at the branching point (AN), above which

$$\varphi_0 = \pm\sqrt{1 - \eta^{-1} - Q^2} \quad (P = 0). \tag{2.9}$$

For a moment we will go back to the unscaled variables used in Eqs. (1.71,1.126). In the present situation, with $P = 0$ (i.e. $A = const.$), Eq. (1.126) reduces to $0 = (-\chi_a H^2 - 2\Gamma|A|^2)\varphi$. This implies that for abnormal rolls ($\varphi \neq 0$) the amplitude in the original units $|A|^2 = -\chi_a H^2/(2\Gamma)$ becomes independent of ε.

When $\Gamma > 0$ ($s = 1$) the situation is very different. Then the value of A_0^2 corresponding to $\eta = \eta_{\rm SN}$ is positive only for $p^2 > 1/2$. For lower values, it has no physical meaning. At $p^2 = 1/2$ the saddle-node curve (2.7) defined by $\eta = \eta_{\rm SN}$ has a common tangent with the neutral curve (2.5), touching it from below (see Fig. 2.2). For the neutral curve, the point $p^2 = 1/2$ corresponds to a tri-critical point, where the type of bifurcation changes from a supercritical to a subcritical pitchfork. This transition naturally leads to a saddle-node bifurcation at higher p^2.

2.1.2 Instabilities with Respect to Long-Wavelength Modulations

In a next step we allow for modulated perturbations of the homogeneous state like $A = A_0 + \delta A, \varphi = \varphi_0 + \delta\varphi$, with[2]

[2]After a change of variables $A' := Ae^{-i(Qx+Py)}$, Eqs. (1.123,1.127), linearized around the state (2.1), become translation invariant, which justifies this ansatz for the linear modes.

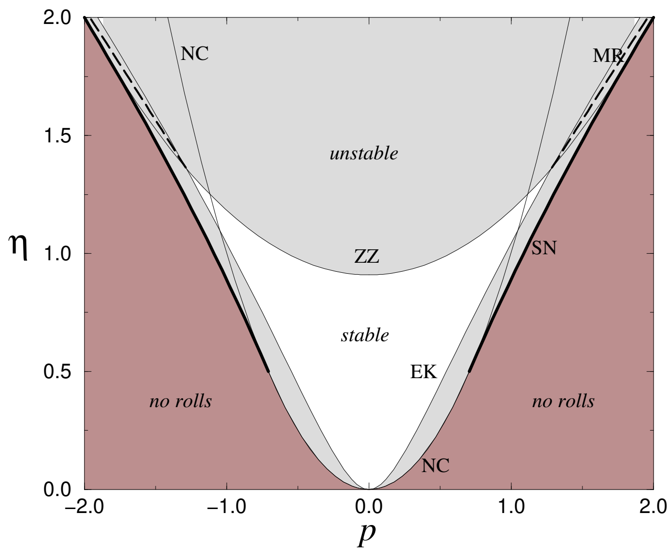

Figure 2.2: *Stability diagram for normal and abnormal rolls with $\Gamma = 1$ and $\beta_y = -2.1$. Same abbreviations as in Fig. 2.1. The absolute value of Γ is of relevance only for the "marginal re-stabilization" line (MR, dashed) that will be discussed in Section 2.1.3.*

$$\begin{aligned}\delta A &= (A^+ e^{st+i(k_x x+k_y y)} + A^- e^{s^* t - i(k_x x+k_y y)}) e^{i(Qx+Py)},\\ \delta\varphi &= (\tilde{\varphi} e^{st+i(k_x x+k_y y)} + \text{c.c.}).\end{aligned} \tag{2.10}$$

The Case $P, \varphi = 0$

The case $P = 0$, $\varphi_0 = 0$ must be treated separately. Then three inequalities have to be satisfied by stable solutions. The first, $H^2/\varepsilon + 2\Gamma(1-Q^2) > 0$, becomes important only when $\Gamma < 0$ and is then equivalent to $\eta < \eta_{\mathrm{AN}}$ (the pitchfork bifurcation at η_{AN} has already been discussed.) The second inequality, $H^2/\varepsilon + 2\Gamma(1-Q^2)(1+\beta_y) > 0$, may be relevant when $\Gamma\,(1+\beta_y) < 0$, and then leads to $\eta < \eta_{\mathrm{ZZ}}$ with

$$\eta_{\mathrm{ZZ}} = \frac{1}{|1+\beta_y|} + q^2 \quad \text{(zig-zag, } p = 0\text{)}. \tag{2.11}$$

Finally one has the usual Eckhaus condition $Q^2 < 1/3$, which can be rewritten as

$$\eta > \eta_{\mathrm{EK}} = 3q^2 \quad \text{(Eckhaus, } p = 0\text{)}. \tag{2.12}$$

If $Q = 0$ (in addition to $P, \varphi_0 = 0$) it is even possible to write down explicit formulas for the wave vector (k_x, k_y) and the growth rate s of the fastest-growing mode. Provided it can be shown that the fastest-growing mode has either $k_x = 0$ or $k_y = 0$ (which usually seems to be the case), they are also valid for $Q \neq 0$ [then competing with the well known Eckhaus mode, which grows like $\tau s = (3Q^2-1)^2/(4Q^2)$ at $k_y = 0$, $k_x = (1+Q^2)(3Q^2-1)/(4Q^2)$]. We will use the abbreviations

$$a := 2A_0^2\Gamma + H^2, \quad b := 2A_0^2\Gamma\beta_y, \tag{2.13}$$

where A_0^2 is simply given by $A_0^2 = 1 - Q^2$. In region III (see Fig. 2.3), which is bounded by

$$b < 0 \quad \text{and} \quad -\tau^{-1}|b| < a < |b| \tag{2.14}$$

(the upper bound for a corresponds to $\eta = \eta_{\mathrm{ZZ}}$), the most unstable mode has

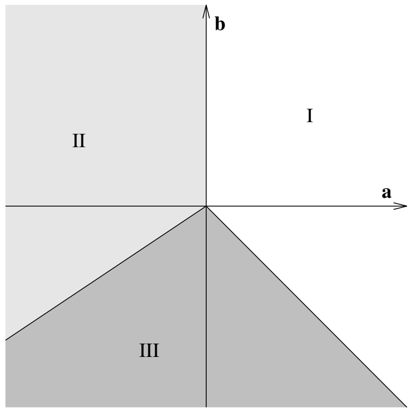

Figure 2.3: *The dominating instability mechanism for normal rolls at* $P, \varphi_0 = 0$. $a = 2A_0^2\Gamma + H^2$, $b = 2A_0^2\Gamma\beta_y$. *I: stable, II: homogeneous destabilization, III: finite wavelength instability.*

$$k_x = 0, \tag{2.15}$$

$$k_y^2 = \frac{\tau(1-\tau)a + 2\tau b + (1+\tau)\sqrt{\tau b[(1-\tau)a+b]}}{(1-\tau)^2}, \tag{2.16}$$

$$s = \frac{-(1-\tau)a - (1+\tau)b - 2\sqrt{\tau b[(1-\tau)a+b]}}{(1-\tau)^2}. \tag{2.17}$$

For $b < 0$, which is the relevant case, the expressions for k_y^2 and s can be analytically continued at $\tau = 1$. At the edges of region III the mode is continuously connected to the most unstable modes of regions II and I. They are, in region II, the instability of the director (with $s = -a > 0$) that leads to abnormal rolls, and in region I the translational mode ($s = 0$), both of which are homogeneous ($k_x, k_y = 0$) perturbations. The knowledge of the most unstable mode may help to understand the experimental results of [32], where the type of destabilization after a “jump” deep into the unstable range was examined.

The Case $Q, P, \varphi_0 \neq 0$

For fixed Q, P, φ_0 with $P \neq 0$ or $\varphi_0 \neq 0$ the growth rate of modulation instabilities in the limit of small k_x and k_y is proportional to $(k_x, k_y)\mathbf{M}(k_x, k_y)^{\mathbf{T}}$, where

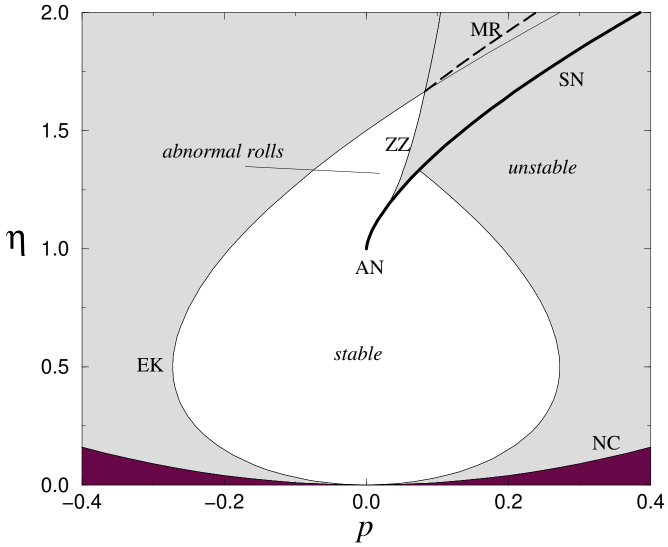

Figure 2.4: *Same as Fig. 2.1.* $\Gamma = -1$, $\beta_y = -0.1$. *MR – marginal re-stabilization.*

$$
\begin{aligned}
M_{xx} &= P(1-3Q^2) - (P-\varphi_0)^2(P+2\varphi_0), \\
M_{xy} = M_{yx} &= (P-\varphi_0)Q((1-\beta_y)\varphi_0 - 2P), \qquad (2.18) \\
M_{yy} &= (P+\beta_y\varphi_0)(1-3(P-\varphi_0)^2 - Q^2),
\end{aligned}
$$

and φ_0 is given by Eqs. (2.2,2.3).

Thus, at the boundary of the long-wavelength ($k_x, k_y \to 0$) stable range one has $\det \mathbf{M} = 0$ and the direction of the critical wave vector is given by the null space of $\mathbf{M}$. A close inspection shows that the long-wavelength stable range is given by $\det \mathbf{M} > 0$. However, if also $\beta_y \varphi_0 / P < -1$ rolls are usually unstable with respect to finite-wavelength modulations (see Section 2.1.3). The $\det M_{ij} = 0$ iso-planes in q, p, η-space are shown at the end of this section in Figs. 2.9, 2.10. From these figures it can be seen that in the general case no clear distinction between Eckhaus and zig-zag instability is possible.

The Case $Q = 0$

For $Q = 0$ the condition $\det M_{ij} > 0$ reduces to

$$0 < (P - (P-\varphi_0)^2(P+2\varphi_0))(P+\beta_y\varphi_0)(1-3(P-\varphi_0)^2). \qquad (2.19)$$

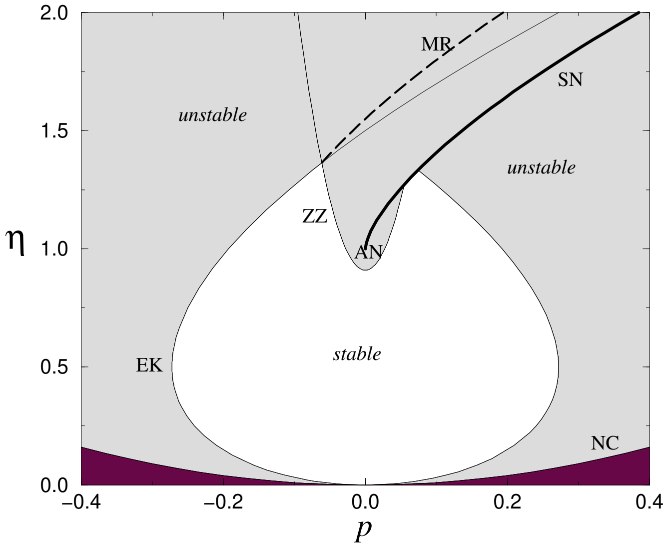

Figure 2.5: *Same as Fig. 2.1.* $\Gamma = -1$, $\beta_y = 0.1$.

The first factor changes sign exactly when $\eta = \eta_{\rm SN}$, and is only relevant for abnormal rolls[3]. This is one of many non-generic properties of the case $Q = 0$ (another non-generic feature is that (2.19) factorizes into three terms). For $\eta = \eta_{\rm SN}$ and $s = -1$, one has $\det M_{ij} = -Q^2(1-(P-\varphi_0)^2-Q^2)^2(1+\beta_y)^2/4/(P-\varphi_0)^2$, which is negative definite in Q, i.e. the system usually becomes unstable before reaching the saddle-node bifurcation.

The second factor changes sign when $\Gamma(1+\beta_y) < 0$ and

$$\eta = \eta_{ZZ} = \frac{1}{|1+\beta_y|} + \frac{(1+\beta_y)^2 p^2}{\beta_y^2} \quad \text{(zig-zag, q=0).} \tag{2.20}$$

If $\beta_y > 0$ (and $\Gamma < 0$) or $\beta_y < -1$ (and $\Gamma > 0$) rolls are unstable for $\eta < \eta_{\rm ZZ}$. When $\Gamma < 0$, the parabola given by Eq. (2.20) encloses the abnormal-roll bifurcation point at $\eta = 1$, $p = 0$ (see Fig. 2.5), and abnormal rolls are always unstable. For $-1 < \beta_y < 0$ ($\Gamma < 0$), the value of φ_0 corresponding to $\eta = \eta_{\rm ZZ}$ belongs to a homogeneously stable solution of Eqs. (2.2,2.3) only for abnormal

[3]There is also a change of sign at $P = 0$, $\varphi_0 = 0$ below $\eta_{\rm AN}$, but this is irrelevant because it is compensated by the second factor.

rolls with

$$p^2 > \frac{-\beta_y^3}{2(1+\beta_y)^3}. \tag{2.21}$$

The abnormal rolls are stable for $\eta > \eta_{\mathrm{ZZ}}$ (Fig. 2.4).

The last factor in (2.19) shall be interpreted as a generalization of the Eckhaus instability in the P-direction, which can also be found for the real Ginzburg-Landau equation (there giving $P^2 < 1/3$, see e.g. [36]). Including the η scaling, this reads

$$p_{\mathrm{EK}} = \frac{\eta^{1/2}(3 + 2\,s\,\eta)}{3^{3/2}} \quad \text{(Eckhaus, q=0)}. \tag{2.22}$$

Normal rolls are (Eckhaus) stable when $|p| < |p_{\mathrm{EK}}|$, abnormal rolls for $|p| > |p_{\mathrm{EK}}|$ (e.g. in Fig. 2.1). For $\Gamma < 0$ ($s = -1$) p_{EK} reaches a maximum $p_{\mathrm{EK}} = (2/27)^{1/2} \approx 0.272$ at $\eta = 1/2$. It has a simple zero at $\eta = 3/2$; for higher η only abnormal rolls can be stable. Notice also that for $\Gamma > 0$, as well as for $\Gamma < 0$, the Eckhaus curve remains above the saddle-node bifurcation line (see e.g. Fig. 2.2) for arbitrary large $|p|$.

The Eckhaus line and the zig-zag line (provided it exists) intersect[4] at

$$p^2 = \frac{-\left({\beta_y}^2\, s\right)}{2\left(1+\beta_y\right)^3}, \quad \eta = \frac{-3\,s}{2\,\left(1+\beta_y\right)}, \tag{2.23}$$

which closes the range of stable rolls (Busse-balloon).

The Case $H^2 = 0$

For the important case that $H^2 = 0$, i.e. $\eta = +\infty$, it can be summarized that homogeneous roll solutions are stable if

$$\Gamma > 0, \quad 1 + \beta_y > 0, \quad \text{and} \quad Q^2 < 1/3. \tag{2.24}$$

2.1.3 Marginal Re-stabilization

When the two last factors of (2.19) successively change their signs, stability against side band perturbations is regained. We will see below that in this case rolls remain unstable against finite wavelength perturbations. Only at a particular value of η and for $Q = 0$ all but one perturbations decay and the exceptional mode is marginally stable: Allowing for finite k_y, the general condition for stability can also be written as

[4] There are other intersections of the lines, but there the two lines belong to different branches of the solution.

$$0 < k_y^2[k_y^2 + 2\Gamma A_0^2(1+\beta_y) + H^2][k_y^2 + 2A_0^2 - 4(P-\varphi_0)^2] + \qquad (2.25)$$
$$8k_yk_xQ(\varphi_0 - P)[k_y^2 + \Gamma A_0^2(1+\beta_y) + H^2)] + O(k_x^2).$$

In several numerical tests the term $O(k_x^2)$ was found to be positive definite. The first two square brackets in the first addend correspond to the zig-zag and Eckhaus instability respectively. After crossing both, the zig-zag- and the Eckhaus line (e.g. starting from $p=0$, $\eta=0$), both factors are negative at $k_y=0$. For values of k_y^2 between $-(2A_0^2 - 4(P-\varphi_0)^2)$ and $-(2\Gamma A_0^2(1+\beta_y)+H^2)$ however (in this order or reversed), the total expression is negative at $k_x=0$. Hence the rolls are unstable. The exceptional situation described above occurs when $2A_0^2 - 4(P-\varphi_0)^2 = 2\Gamma A_0^2(1+\beta_y)+H^2)$ or, equivalently,

$$p_{\mathrm{MR}}^2 = \frac{\eta\,(-2\,\eta - 3\,s + \beta_y\,\Gamma\,s)^2\,(-1+\Gamma+\beta_y\,\Gamma + \Gamma\,s/\eta)}{(-3+\Gamma+\beta_y\,\Gamma)^3}, \qquad (2.26)$$

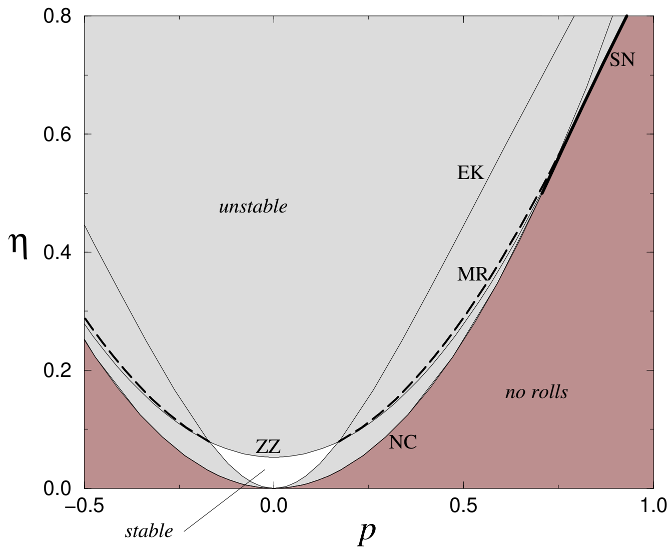

Figure 2.6: *Same as Fig. 2.1.* $\Gamma = 1$, $\beta_y = -20$. *Notice that the MR-line (as well as the ZZ-line) continues on the homogeneously unstable branch of solutions of Eqs. (2.2,2.3) (which is not shown) after reaching the SN-line.*

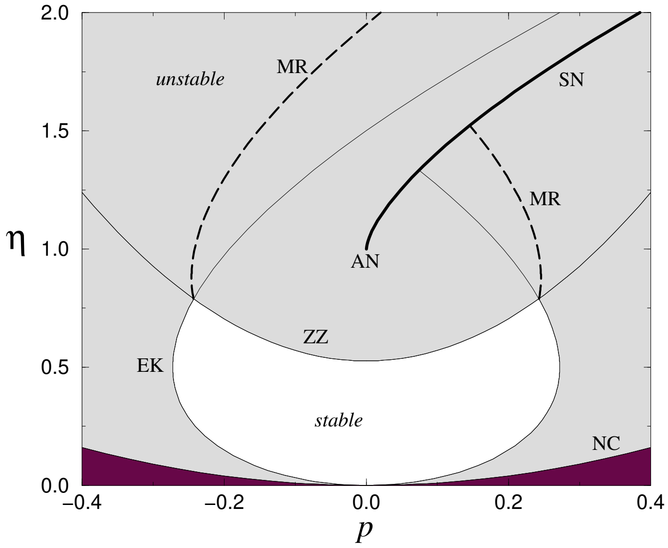

Figure 2.7: *Same as Fig. 2.1.* $\Gamma = -1$, $\beta_y = .9$.

where η must be higher than the intersection point (2.23). In fact, the curve defined by Eq. (2.26) goes right through that point. The marginally stable mode has the wave vector $k_x = 0$,

$$k_y^2 = \frac{2\,\Gamma\ (2 + 2\,\beta_y + 3\,s/\eta)}{-3 + \Gamma + \beta_y\,\Gamma}. \tag{2.27}$$

From (2.25) it is also clear that this marginal re-stabilization does not occur when $Q \neq 0$. Then an appropriate choice of k_x in the second addend always makes the total expression negative.

2.1.4 The Unfolding under Perturbation of the Amplitude Equations

As mentioned before, the intersection of zig-zag and Eckhaus line for $Q = 0$ is non-generic. The physical reason for this is not clear. To understand the relation to the generic case, consider an important perturbed version of system (1.123,1.127), which is obtained by replacing Eq. (1.123) by

$$\tau \partial_t A = \left[1 + \partial_x^2 + \partial_y^2 - 2ic_1\varphi\partial_y - c_2\varphi^2 - |A|^2 + i\beta_y\varphi_{,y}\,\right] A. \tag{2.28}$$

It represents the generalization of Eqs. (1.123,1.127) to the case that the rotational symmetry, as described by substitution rule (1.70), is broken, but φ remains an active mode[5]. By setting $c_1 = 1$ and $c_2 = 1$ the isotropic equations are reobtained.

When $c_1 = 1$, $c_2 \neq 1$, the determinant corresponding to (2.19) still factorizes and two intersecting lines are obtained as before. This only leads to a deformation of the stability diagram.

With $c_1 \neq 1$ the intersection point unfolds by a reconnection of zig-zag and Eckhaus lines. There are two topologically distinct ways to do so. In the first the lower parts of zig-zag and Eckhaus line (with respect to η) are connected to form a smooth line, such that the range of stable modes remains closed. This is what happens for $c_1 > 1$. Then the topology is the same as for a section through the stable range of the rotationally invariant system at fixed $q \neq 0$ (see Figs. 2.9, 2.10). The line (or plane) obtained by reconnecting the upper pieces indicates the upper limit of the long-wavelength unstable range. Presumably an instability at finite wavelength remains, as explained above for the marginal re-stabilization. The marginal re-stabilization itself can be shown to disappear for $c_1 > 1$.

In contrast, when $c_1 < 1$ the marginal re-stabilization line evolves into a band of fully stable solutions[6], which connects which the original stable range through the gap that opens when zig-zag and Eckhaus line reconnect in the second of the two possible ways (see Fig. 2.8). Due to the antithetical effect of $c_1 < 1$ and $q \neq 0$ it must be expected that the re-stabilized band becomes a channel of finite width in q when continued into the full q, p, η-space.

Although an analytic description of this scenario is possible for the system (2.28,1.127) at $Q = 0$, the results are very complicated and shall not be presented here. It is worth noticing that, corresponding to the singular character of the perturbation, the distortions of the stability bounds in the vicinity of the intersection points are of the order $\sqrt{|c_1 - 1|}$, and, in fact, very sensitive to the value of c_1.

Equations (2.28,1.127) with $c_1, c_2 \neq 0$ are not general enough to unfold the other peculiarity mentioned above for $Q = 0$: The term corresponding to the first factor in (2.19) still vanishes only on the saddle-node bifurcation line. It

[5] With $c_1 = c_2 = 256/(27\pi^2) \approx 0.961$ the amplitude equations for the dielectric regime of electroconvection of planarly aligned nematic liquid crystals in the limit of thick cells are obtained [26].

[6] Possibly this band has been observed experimentally: In electroconvection with homeotropically anchored nematics under a strong isotropy breaking magnetic field the authors of [20] report "reentrant normal rolls": Modulations of roll patterns (or rather the observed contrast of the rolls) setting in above some value of the driving voltage can be removed by further increasing the voltage. Close to the re-stabilization the modulation wavelength is considerably shorter than at the onset of instability (Figure 9 in [20]). However, the modulations are superimposed with an unexplained structure ("Bamboo-Chevron").

does not lead to an additional instability.

This stability analysis has basically been restricted to long-wavelength perturbations. It cannot be excluded that, within the long-wavelength stable range, finite wavelength instabilities occur. They may even be oscillatory.

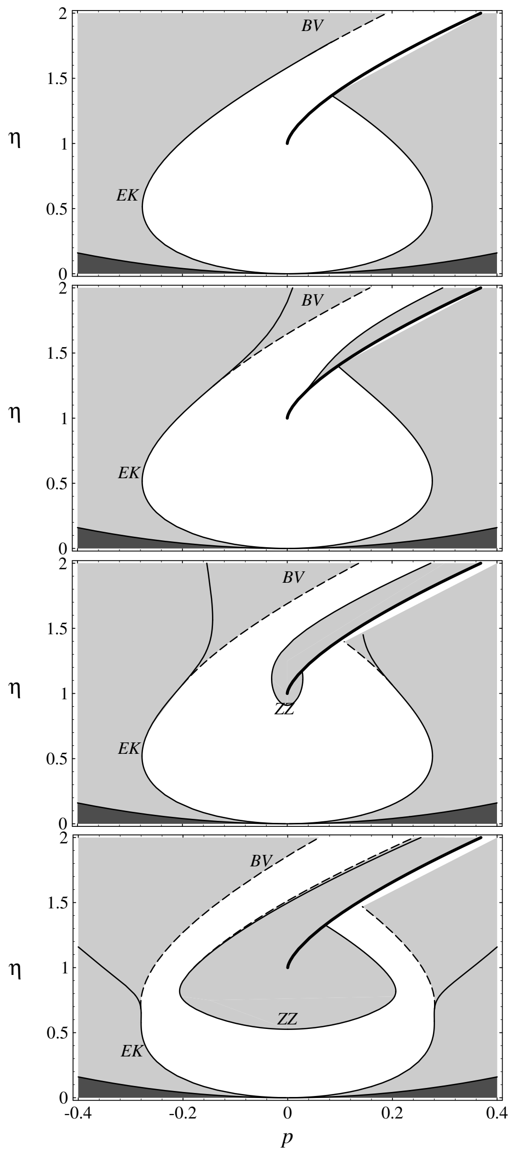

Figure 2.8: *Stability diagrams for the anisotropic system (2.28,1.127) with* $c_1 = 0.96$, $c_2 = 1$. *The values for* β_y *are the same as for the preceding figures (top to bottom:* $\beta_y = -0.4, -0.1, 0.1, 0.9$*) but* $\Gamma = -1/4$*, which brings the re-stabilized stripe closer to the saddle-node bifurcation line. Dashed lines are finite-wavelength stability bounds. BV indicates the close relation of this line to the "bimodal varicose", which was observed in thermoconvection in liquid crystals [40], and found numerically [37] to be part of a stability range with a topology very similar to the figures above.*

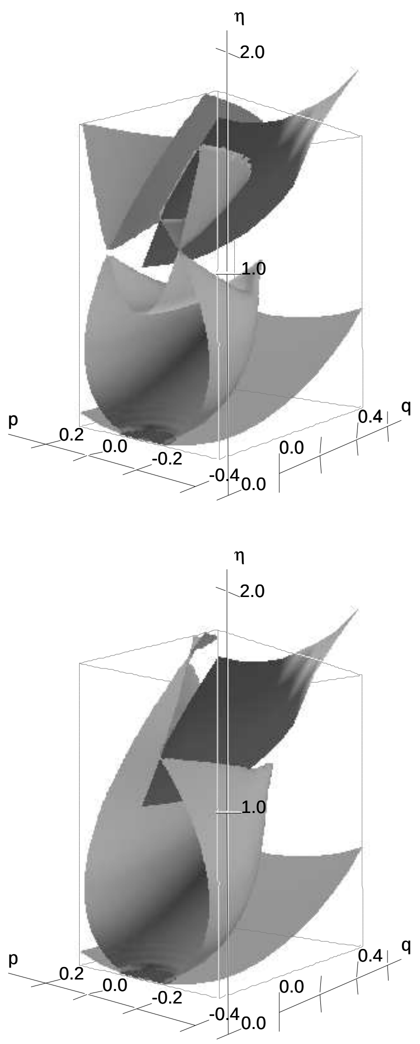

Figure 2.9: $\det M_{ij} = 0$ *iso-planes, corresponding to the limits of stability of normal rolls in* q, p, η*-space for* $\beta_y > 0$ *(top) and* $\beta_y < 0$ *(bottom). For better "in-sight" only the segment* $q > 0$ *is shown. The planes continue symmetrically into the* $q < 0$ *half space. (...)*

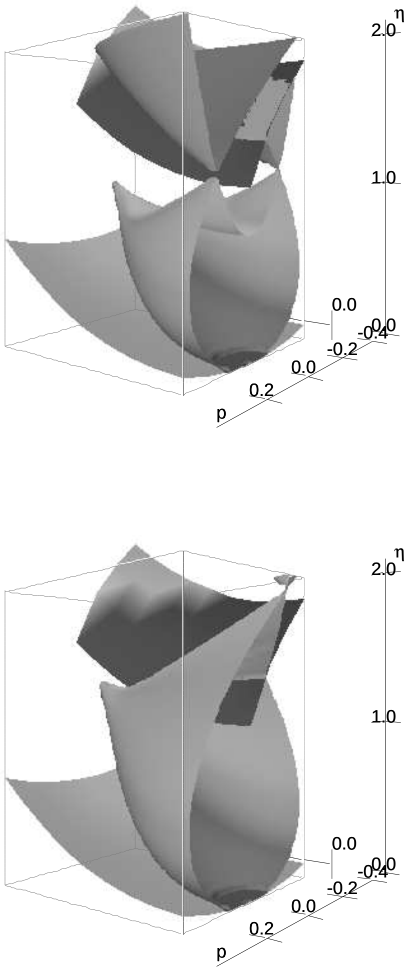

Figure 2.10: *(...) Here a different perspective. The neutral curve (transparent plane at the bottom) and the saddle-node instability plane (dark plane in the upper half of the box) are also shown. Notice that the edges of the planes at the front of the boxes correspond to the lines in Figs. 2.7 and 2.4.*

2.2 Oblique-Roll Range

2.2.1 Homogeneous Solutions

We will now try to get some insight into the set of stable homogeneous roll solutions to Eqs. (1.73,1.138). Assume solutions of the form

$$A_1 = a_1 \exp(i(Q_1 x + P_1 y)), \quad A_2 = a_2 \exp(i(Q_2 x + P_2 y)), \quad \text{and} \quad \varphi = \varphi_0, \tag{2.29}$$

with real $a_{1/2}, \varphi_0, P_{1/2}, Q_{1/2}$. After a translation in space we can assume without loss of generality that $a_{1/2} > 0$. When inserted into Eq. (1.73) we get

$$\begin{aligned} 0 &= \sigma_1 \, a_1 - g \, {a_1}^3 - h \, {a_2}^2 \, a_1 , \\ 0 &= \sigma_2 \, a_2 - g \, {a_2}^3 - h \, {a_1}^2 \, a_2 , \end{aligned} \tag{2.30}$$

where $\sigma_{1/2} = \sigma_{1/2}(P_{1/2}, Q_{1/2}, \varphi_0)$ is summarizing all terms linear in $a_{1/2}$ (excluding the time derivative). For simplicity we will treat σ_1 and σ_2 as if they were free parameters. In order to avoid complications, assume also $g, h > 0$. Equation (1.138) becomes

$$0 = -\bar{H}^2 \, \varphi_0 + \bar{\Gamma} \, \left({a_1}^2 - {a_2}^2\right) \tag{2.31}$$

where the abbreviations $\bar{H}^2 := \tilde{\chi}_a H^2$ and $\bar{\Gamma} := \Gamma q_c p_c / 2$ have been introduced.

Equations (2.30,2.31) have the nontrivial solutions

$$\varphi_0 = \pm \frac{\bar{\Gamma} \, \sigma_{1/2}}{g \, \bar{H}^2}, \quad a_{1/2} = \sqrt{\frac{\sigma_{1/2}}{g}}, \quad a_{2/1} = 0 \quad \text{and} \tag{2.32}$$

$$\varphi_0 = \frac{\bar{\Gamma} \, (\sigma_1 - \sigma_2)}{(g - h) \, \bar{H}^2}, \quad a_1 = \sqrt{\frac{g \, \sigma_1 - h \, \sigma_2}{g^2 - h^2}}, \quad a_2 = \sqrt{\frac{g \, \sigma_2 - h \, \sigma_1}{g^2 - h^2}}. \tag{2.33}$$

In order for the unimodal solutions (2.32) to exist, we need $\sigma_{1/2} > 0$. The bimodal solution (2.33) exists only if $g/h < \sigma_1/\sigma_2 < h/g$, when $g > h$ or if $h/g < \sigma_1/\sigma_2 < g/h$ when $g < h$ (Fig. 2.11).

Since $\sigma_{1/2}$ is really a function of φ_0, one has to solve the first equations of (2.33) and (2.32) in order to get the full set of fixed points. From Eq. (1.73) $\sigma_{1/2}$ is a quadratic polynomial in φ_0, hence solution (2.32) gives up to two fixed points ($\times 2$ for the interchange of 1 and 2). These solutions will be discussed in detail in Section 2.2.3. Solution (2.33) yields at most one fixed point, because the quadratic terms in φ_0 of σ_1 and σ_2 are identical, leading to a linear equation for φ.

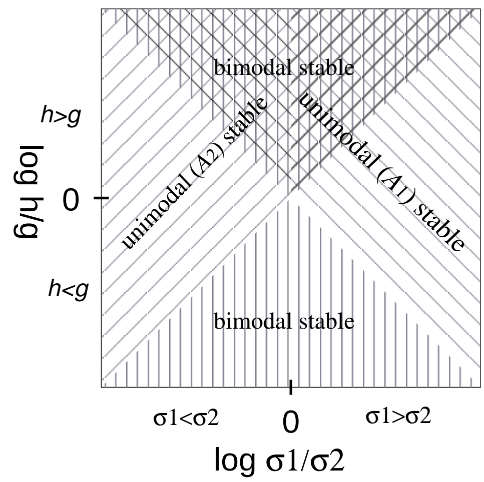

Figure 2.11: *Stability of steady oblique-roll states. For bimodal solutions the range of existence is identical with their range of (possible) stability. Notice that the conditions for stability are only necessary. In particular the bimodal solutions with $h > g$ are unstable for strongly broken isotropy (large $\bar{H}^2$). The boundaries of the areas are given by $h/g = \sigma_1/\sigma_2$ and $h/g = \sigma_2/\sigma_1$.*

2.2.2 Homogeneous Destabilizations

For a linear stability analysis, the functions $\sigma_{1/2}(\varphi, P_{1/2}, Q_{1/2})$ have to be expanded to first order in φ. We write

$$\sigma'_{1/2} := \frac{\partial}{\partial\varphi}\sigma_{1/2}(\varphi, P_{1/2}, Q_{1/2})\Big|_{\varphi=\varphi_0}. \tag{2.34}$$

From Eqs. (1.73,1.138) the growth rate s of the (homogeneous) linear modes is given by the zeros of the determinant

$$\begin{vmatrix} -3\,{a_1}^2\,g - {a_2}^2\,h + \sigma_1 - s\,\tau & -2\,a_1\,a_2\,h & a_1\,\sigma'_1 \\ -2\,a_1\,a_2\,h & -3\,{a_2}^2\,g - {a_1}^2\,h + \sigma_2 - s\,\tau & a_2\,\sigma'_2 \\ 2\,a_1\,\bar{\Gamma} & -2\,a_2\,\bar{\Gamma} & -\bar{H}^2 - \tilde{\gamma}_1\,s \end{vmatrix} \tag{2.35}$$

Non-oscillatory Instabilities

For unimodal solutions (2.32) all steady-state modes are found to be stable when

$$\sigma'_{1/2}\,\bar{\Gamma} < g\,\bar{H}^2 \quad \text{and} \quad \frac{h}{g} > \frac{\sigma_{2/1}}{\sigma_{1/2}}, \tag{2.36}$$

and for bimodal solutions (2.33) when[7]

$$(\sigma'_1 - \sigma'_2)\;\bar{\Gamma} < (g-h)\;\bar{H}^2 \quad \text{and} \begin{cases} \dfrac{h}{g} > \dfrac{\sigma_1}{\sigma_2} > \dfrac{g}{h} & \text{for } h > g\;, \\ \dfrac{h}{g} < \dfrac{\sigma_1}{\sigma_2} < \dfrac{g}{h} & \text{for } h < g\;. \end{cases} \tag{2.37}$$

As far as no assumption about the form of the linear growth rate was made, the range of validity of these results is even a little wider than just Eqs. (1.73,1.138). When applied to Eqs. (1.73,1.138), there is another restriction for the unimodal case: The excited mode $A_1 = a_1 \exp(i(Q_1 x + P_1 y))$ (say), has to compete with all mode of A_2. In particular with the one with the highest possible σ_2, which is $\sigma_2 = \varepsilon$. This is also the upper limit for $\sigma_1(P_1, Q_1, \varphi_0)$. The bounds (2.36) can therefore be supplemented *a priori* by a condition $\sigma_{2/1} \geq \sigma_{1/2}$, which restricts unimodal solutions to $h \geq g$.

[7] In the case of a transition from an unstable Hopf mode (see below) to an unstable steady state mode, the transition point is different.

For bimodal solutions, notice that in the limit of strongly broken isotropy ($\bar{H}^2 \to \infty$) the first part of condition (2.37) is violated when $h > g$. Bimodal solutions with $h > g$ are *stabilized* by the additional degree of freedom φ. It may however be difficult to prepare such a state experimentally, because it competes with the more robust unimodal solutions, and because the quantities σ_1' and σ_2' are difficult to control. The second part of the condition for bimodal solutions (2.37) already appeared in the condition for their existence.

Oscillatory Instabilities

For the bimodal state a Hopf bifurcation is also conceivable. The problem becomes quite simple when $\sigma_1 = \sigma_2 =: \sigma$ is assumed. When $h \approx g$, this is roughly satisfied for most solutions (see Fig. 2.11). Write the determinant (2.35) as a polynomial in s:

$$c_3 s^3 + c_2 s^2 + c_1 s + c_0 \tag{2.38}$$

At a Hopf bifurcation the polynomial has one real zero s_1 and two imaginary zeros $s_2 = i\omega$, $s_3 = -i\omega$. It is easily seen (e.g. [27], page 67) that this leads to

$$c_3\, c_0 = c_2\, c_1 \tag{2.39}$$

$$\text{and} \quad c_1 = \omega^2 > 0\,. \tag{2.40}$$

From the explicit form of the polynomial (2.38) it can be seen that Eq. (2.39) holds when

$$g = \frac{(\sigma_1' - \sigma_2')\,\bar{\Gamma}\,\tau}{2\,\left(2\,\tilde{\gamma}_1\,\sigma + \bar{H}^2\,\tau\right)} \tag{2.41}$$

$$\text{or} \quad \sigma = \sigma_{\text{Hopf}} := \frac{(h+g)\;\bar{H}^2\,\tau}{2\,(h-g)\;\tilde{\gamma}_1}. \tag{2.42}$$

The Hopf frequency is given by

$$0 < \omega^2 = \frac{2\,\sigma\;\left(2\,g\,\tilde{\gamma}_1\,\sigma - 2\,\tilde{\gamma}_1\,h\,\sigma - \sigma_1'\,\bar{\Gamma}\,\tau + \sigma_2'\,\bar{\Gamma}\,\tau + 2\,g\,\bar{H}^2\,\tau\right)}{\tilde{\gamma}_1\;(g+h)\;\tau^2}. \tag{2.43}$$

Insertion of Eq. (2.41) in (2.43) yields

$$0 < \omega^2 = \frac{-4\,\sigma^2}{\tau^2}, \tag{2.44}$$

which is obviously false. Hence Eq. (2.41) does not define a Hopf instability.

Equation (2.42) can only be satisfied for $h > g$. Elimination of σ from (2.43) by Eq. (2.42) leads to

$$0 < \omega^2 = \frac{\bar{H}^2 \left((\sigma_1' - \sigma_2') \bar{\Gamma} - (g-h) \bar{H}^2 \right)}{\tilde{\gamma}_1^2 (g-h)}. \tag{2.45}$$

For $h > g$ the expression is positive exactly as long as the rolls are not unstable by the first condition in (2.37). A numerical test reveals that Hopf stability requires to be on the

$$\sigma < \sigma_{\mathrm{Hopf}} \tag{2.46}$$

side of the critical point (2.42). In contrast to the homogeneous bifurcation we do here observe a *destabilization* by the additional degree of freedom φ. The oscillatory mode associated with this Hopf bifurcation is probably related to the swinging-roll scenario described in Section 1.4.2 for $\bar{H}^2 = 0$. For example, in the fully symmetric case $\sigma_1' = -\sigma_2'$ the critical mode is $(\delta a_1, \delta a_2, \delta\varphi) = \mathrm{Re}[(i, -i, c)\exp(i\omega t)]$ with some real number c. This is easily seen to be a linearized form of the time evolution that has been described for swinging rolls on page 50.

2.2.3 Unimodal Solutions and their Stability

For unimodal states the form of the solution will now be discussed in more detail. Some results about modulation instabilities will also be given.

Consider Eq. (1.142) with $H^2 \neq 0$. For large H^2 and small ε the equation trivially leads to $\check{\varphi}_0 = 0$. In order for the isotropy breaking term to be balanced, H^2 must scale like $\varepsilon^{1/2}$ (recall that for normal rolls $H^2 \sim \varepsilon^{-1}$ was found). With this scaling the last two terms dominate Eq. (1.142), and φ can be eliminated from Eqs. (1.141,1.142) adiabatically, i.e. under neglect of the space and time derivatives in Eq. (1.142). Without loss of generality we assume $\check{\Gamma} > 0$ and introduce the abbreviation

$$\hat{H}^2 := \frac{\varepsilon^{-1/2}\check{H}^2}{\check{\Gamma}} = \frac{2\chi_a \varepsilon^{-1/2} H^2 g}{N\Gamma q_c p_c} \tag{2.47}$$

and the new dependent variable

$$B := \frac{\check{A}_1}{|\hat{H}|}. \tag{2.48}$$

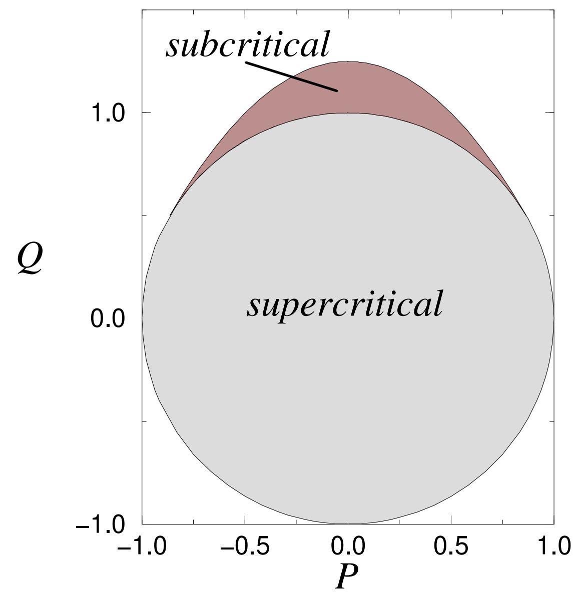

Figure 2.12: *Allowed wave vector range of unimodal oblique rolls ($\hat{H}^2 = 1$).*

Equation (1.141) then becomes

$$\partial_{\check{t}} B = \partial^2_{\check{x}} B - 2i|B|^2 \partial_{\check{x}} B + \partial^2_{\check{y}} B + B\left(1 + i\check{\beta}_x \partial_{\check{x}}|B|^2 + i\check{\beta}_y \partial_{\check{y}}|B|^2 - \hat{H}^2|B|^2 - |B|^4\right). \tag{2.49}$$

The amplitude of homogeneous roll solutions $B = B_0 \exp(i(Q\check{x} + P\check{y}))$ is given by

$$B_0^2 = \frac{-\hat{H}^2 + 2\,Q \pm \sqrt{4 + \hat{H}^4 - 4\,P^2 - 4\,\hat{H}^2\,Q}}{2}. \tag{2.50}$$

When $\hat{H}^2 > 2$ only the branch with '+' at the square root exists and is confined to the unit circle $Q^2 + P^2 \leq 1$. If $\hat{H}^2 < 2$ and $P^2 < 1 - \hat{H}^4/4$, the range of the '+'-branch is extended to reach up to $Q = (4 + \hat{H}^4 - 4P^2)/(4\hat{H}^2)$ (see Fig. 2.12), where $\hat{H}^2 B_0^2 = 1 - P^2 - \hat{H}^4/4$. From there the solution bends back to $Q = (1 - P^2)^{1/2}$ over the unstable '−'-branch (Fig. 2.13). The amplitude is maximal ($\check{A}_1 = 1$) at $P = 0$, $Q = \hat{H}^{-2}$, which is close to the upper limit of existence $Q = (4 + \hat{H}^4)/(4\hat{H}^2)$ of the solution when $H^2 \to 0$.

Expressed in the original, unscaled units the relation $Q \sim \hat{H}^{-2}$ becomes

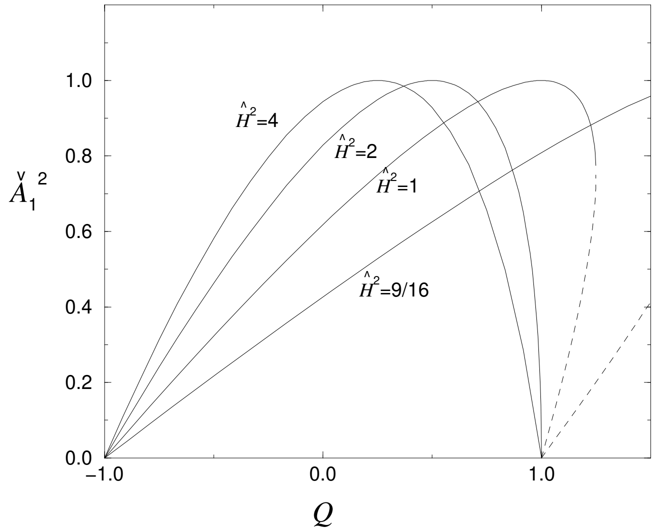

Figure 2.13: *Amplitude of unimodal oblique rolls, for different values of* $\hat{H}^2$, $P = 0$ *as given by Eq. (2.50).*

$|\vec{q} - \vec{q}_c|\varepsilon^{-1/2} \sim \varepsilon^{1/2}H^{-2}$. An experiment aimed at keeping the roll amplitude maximal (and hopefully the rolls stable) would have to scale $H^2 \sim \varepsilon$. We are thus back at the previous scaling for H^2.

Recall that $\breve{A}_1^2 = (g/\varepsilon)A_1^2$. Combined with (2.32) this leads to $\hat{H}^2 B_0^2 = \breve{A}_1^2 = \sigma_1/\varepsilon$. Since ε is the largest possible value of σ_2, according to Eq. (2.36) zig rolls ($\breve{A}_1$) are stable against zag rolls only if

$$\hat{H}^2 B_0^2 > \frac{g}{h}. \tag{2.51}$$

Modulation Instabilities

The linear stability analysis of Eq. (2.49) does not provide many technical difficulties. For vanishing growth rates the determinant characterizing the stability against perturbations of the form

$$\delta B = \left(b_1 e^{st+i(k_x x + k_y y)} + b_2 e^{s^* t - i(k_x x + k_y y)} \right) e^{i(Qx+Py)} \tag{2.52}$$

of the linearized problem contains only terms of second and fourth order in k_x, k_y (combining the powers of both). Physically it is clear that in the limit

$|(k_x, k_y)| \to \infty$ the system is stable. Hence all instabilities are of the long-wavelength type, and it is sufficient to check whether the growth rate s is negative definite at second order in k_x, k_y. At this order, the sign of the growth rate is the same as the sign of $(k_x, k_y)\mathbf{M}(k_x, k_y)^T$, with

$$\begin{aligned} M_{xx} &= (1 - P^2 + Q^2) - 2\left(\hat{H}^2 - \check{\beta}_x Q\right) B_0{}^2 + \left(-1 - 2\check{\beta}_x\right) B_0{}^4, \\ M_{xy} = M_{yx} &= 2PQ + \left(-2P + \check{\beta}_x P + \check{\beta}_y Q\right) B_0{}^2 - \check{\beta}_y B_0{}^4, \\ M_{yy} &= (1 + P^2 - Q^2) - 2\left(\hat{H}^2 - \check{\beta}_y P - 2Q\right) B_0{}^2 - 3 B_0{}^4. \end{aligned} \tag{2.53}$$

For $Q, P = 0$ one gets the concise result that (2.50) is stable if

$$4\check{\beta}_x > \check{\beta}_y^2 \left(1 - \hat{H}^2\left(4 + \hat{H}^4\right)^{-1/2}\right) - \hat{H}^2\left(\hat{H}^2 + \left(4 + \hat{H}^4\right)^{1/2}\right), \tag{2.54}$$

in particular $4\check{\beta}_x > \check{\beta}_y^2$ for small $\hat{H}^2$.

In the special case $\check{\beta}_x = -1$ and $\check{\beta}_y, P = 0$, the limits of stability for Q are given by

$$-\frac{1}{\sqrt{3}} + \frac{2}{3\hat{H}^2} < Q < \begin{cases} \dfrac{4 + \hat{H}^4}{4\hat{H}^2} & \text{for } \hat{H}^2 < \dfrac{2}{3^{1/2}}, \\ \dfrac{1}{\sqrt{3}} + \dfrac{2}{3\hat{H}^2} & \text{for } \hat{H}^2 > \dfrac{2}{3^{1/2}}. \end{cases} \tag{2.55}$$

When $\hat{H}^2 < 2/3^{1/2}$ the upper bound for Q is identical with the limit of existence of the unperturbed solution, a behavior which seems to be generic, starting below some finite $\hat{H}^2$ or when $\hat{H}^2 \to 0$, as numerical tests indicate. The lower bound may in general stay negative, converge to a finite positive value, or even come arbitrarily close to the upper bound, as $\hat{H}^2 \to 0$. The transition between the first two cases is described by condition (2.54).

In conclusion, by carefully adjusting ε and H^2 (with $H^2 \sim \varepsilon$) it is in principle possible to have stable unimodal rolls for arbitrary low $\hat{H}^2$ at least when $4\check{\beta}_x > \check{\beta}_y^2$ and $g < h$. However, these rolls will not appear spontaneously because they require a wave vector with $Q > 1$, i.e. in the subcritical range. For fixed Q and P (e.g. $Q, P = 0$) the stability bounds scale like $H^2 \sim \varepsilon^{1/2}$.

Chapter 3

Electroconvection — A Model System

The present work was motivated by recent experimental investigations of electroconvection in nematic liquid crystals [46, 45, 47, 42, 33, 20]. In this chapter we will apply some theoretical results of the previous chapters to a model of the experimental system.

3.1 What are Nematic Liquid Crystals?

Nematic liquid crystals differ from usual liquids by the fact that the molecules they consist of (usually lengthy organic compounds) are locally oriented along a preferred direction $\vec{n} \in \mathbb{R}^3$ ($|\vec{n}| = 1$, $\vec{n}$ and $-\vec{n}$ are equivalent).

Like the velocity field, the temperature field, *etc.*, the director field $\vec{n}$ is a dynamical variable of the liquid crystal (see e.g. [3, 8, 11, 25]).

3.2 Electroconvection in Homeotropic Geometry

The electroconvection experiments are usually done with a cell consisting of two parallel glass plates (typically $\sim 50\mu m$ apart), which are coated to

1. become conductive, such that an electrical voltage V can be applied between the two plates,

2. enforce a specific orientation of the director at the glass plates.

In most experiments the director is anchored at the plates in such a way that it aligns parallel to them in a specified direction ("planar" alignment). Here we are concerned with the "homeotropic" geometry. In this case the director is forced to align normal to the boundary. With no voltage applied, such a cell filled with a liquid crystal has symmetry properties as required in the list on page 10 (x- and y-coordinate are parallel to the layer, the z-coordinate is normal to it).

In order to produce the symmetry-breaking ground state and the roll pattern, an AC voltage is applied. The period of the AC frequency $2\pi/\omega$ is much smaller (typically $\omega/(2\pi) = 100 - 1000\,\mathrm{Hz}$) than the time scale of the dynamics of the pattern ($\approx 1 - 100\,\mathrm{s}$). The applied voltage does therefore preserve time translational symmetry and R_y to a good approximation.

The liquid crystal material is chosen in such a way that an orientation of the director vertical to the electric field (i.e. parallel to the plates) is energetically preferred (negative dielectric anisotropy). On the other hand the director has an inherent "elasticity". In order to minimize the elastic energy, its orientation in the bulk of the liquid should be the same as at the boundaries, i.e. normal to the plates (Fig. 3.1).

If the electric voltage is sufficiently high to overcome the elastic forces, the director bends away from the z-direction towards an arbitrary direction within the x-y-plane. In the resulting Freedericksz state the rotational symmetry in the plane of the layer is broken spontaneously. It is easily verified (Fig. 3.1) that the Freedericksz state has the correct symmetry to serve as the ground state of Section 1.1. Roughly speaking, the amplitude of the Goldstone mode φ introduced in Section 1.1 is given by $\tan(\varphi) = n_y/n_x$ ($\vec{n} = (n_x, n_y, n_z)$).

When the conductivity $\sigma_{\|}$ of the liquid crystal along the director axis is higher than the conductivity $\sigma_{\perp}$ vertical to it (positive anisotropy of conductivity), electroconvection may set in after a further increase of the voltage. The mechanism that reinforces director field modulations and leads to electroconvection [15] can be sketched like this:

1. Assume an initial director modulation.

2. Due to the anisotropy of the conductivity the current density induced by the electric field becomes inhomogeneous.

3. This leads to an accumulation of charges (the charge relaxation times of the liquid crystals used is large, $\sim 10^{-3}s$).

4. The electric field acting on the charges leads to bulk forces and a flow field...

5. ...which deforms the director field through viscous effects.

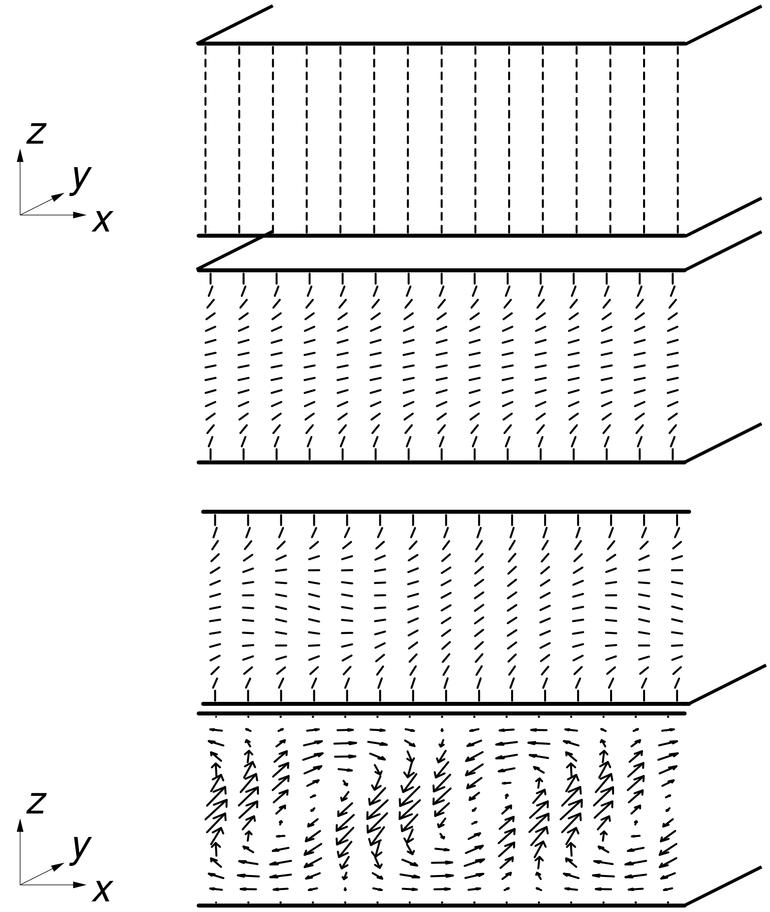

Figure 3.1: *The upper three figures show how the director field evolves in the different stages that lead to the convection pattern. Top: no voltage (the director field being completely determined by the boundary conditions) — second: after the Freedericksz transition (here towards the x-direction) — third: after the onset of convection. The bottom figure shows the flow field associated with the convection pattern. The figures are based on a numerical solution of the nematohydrodynamic equations (courtesy to A. Hertrich [16]).*

These modulations correspond to the roll pattern which, in the amplitude formalism, is quantified by its complex amplitude A. Both oblique-roll and normal-roll patterns are possible.

Actually there are two different kinds of convection rolls. They are distinguished by their internal symmetry (see e.g. [25]). The so-called "conductive" rolls (or Williams domains) appear at low driving frequencies, and the "dielectric" rolls at high frequencies. The transition occurs at the "cutoff" frequency, which is typically at $\omega\tau_0 \sim 2$ (see below for τ_0). All results presented here relate to the conductive regime. For the dielectric regime with planar alignment the coefficients have been calculated analytically in [26] (there the anisotropic boundary conditions play the role of the isotropy breaking magnetic field, see Section 4.6).

3.3 Numerical Method

The equations describing the dynamics of the liquid crystal [11] are so complicated that even a numerical solution provides difficulties. The calculation of the coefficients of the amplitude equations was done with an adaptation of a code developed by W. Decker [12] and A. Hertrich [16]. Parts of the code were automatically generated from the constituting equations. It is an implementation of the Galerkin method using a basis of trigonometric and Chandrasekhar functions to model the z-dependences of the different fields. A basis of three to four components per field (`moz=6,8` in Bayreuth's nomenclature) showed to be accurate to about 10% (see Table 3.2 below).

3.4 Coefficients Calculated for MBBA

One of the best characterized liquid crystal substances that show the effect of electroconvection is MBBA[1]. The same set of material constants as in [16] was used (which is the set named "MBBA I" in [5], for the definition of the constants see e.g. [11]): At $25°\,C$,

$$\begin{gathered}
k_{11} = 6.66\,10^{-12}N, \quad k_{22} = 4.2\,10^{-12}N, \quad k_{33} = 8.61\,10^{-12}N, \\
\alpha_1 = -18.1\,10^{-3}\,\mathrm{kg\,m^{-1}\,s^{-1}}, \quad \alpha_2 = -110.4\,10^{-3}\,\mathrm{kg\,m^{-1}\,s^{-1}}, \\
\alpha_3 = -1.1\,10^{-3}\,\mathrm{kg\,m^{-1}\,s^{-1}}, \quad \alpha_4 = 82.6\,10^{-3}\,\mathrm{kg\,m^{-1}\,s^{-1}}, \\
\alpha_5 = 77.9\,10^{-3}\,\mathrm{kg\,m^{-1}\,s^{-1}}, \quad \alpha_6 = -33.6\,10^{-3}\,\mathrm{kg\,m^{-1}\,s^{-1}}, \\
\varepsilon_{\|} = 4.72, \quad \varepsilon_{\perp} = 5.25.
\end{gathered} \tag{3.1}$$

[1] *4-methoxybenzylidene4'-n-butyl-aniline*

Number of Galerkin modes	moz	$\sigma_\parallel/\sigma_\perp$	V_c^2 [$\mathrm{V_{eff}}^2$]	q_c	p_c	$\lvert\vec{q}_c\rvert$	p_c/q_c
				dimensionless			
1	2	1.43	56.7	1.63	0.75	1.79	0.46
2	4	1.43	56.3	1.39	0.96	1.69	0.69
1	2	1.30	84.	1.80	0.46	1.86	0.26
2	4	1.30	88.9	1.74	0.64	1.86	0.36

Table 3.1: *Sensitivity of threshold and critical mode to the anisotropy of conductivity. Apart from $\sigma_\parallel$, the material parameters $\sigma_\perp = 2.3\,10^{-7}\Omega^{-1}\,\mathrm{m}^{-1}$, $\varepsilon_\parallel = 4.21$, $\varepsilon_\perp = 4.70$ and the magnetic field $H = 1.45\sqrt{k_{33}/k_{11}}$ (see footnote 2) were adjusted according to the values given in [20]. Calculated and experimental values are for $\omega\tau_0 \to 0$. The upper two rows in the table are for the experimental value of $\sigma_\parallel$, the lower two for a slightly different one. In our units the measured [20] values are $V_c^2 \approx 85\mathrm{V}_{\mathrm{eff}}^2$, $q_c \approx 2.6$, and $p_c/q_c \approx 0.28$. Notice that $\lvert\vec{q}_c\rvert$ is rather stable under variations of $\sigma_\parallel$ and the number of Galerkin modes. The reason for the large difference between theory and experiment for this value must be found elsewhere.*

A large part of the conductivity of MBBA is due to contamination (or dopants) and is difficult to control. A typical value is $\sigma_\perp = 1.0\,10^{-8}\Omega^{-1}\,\mathrm{m}^{-1}$. Therefore the modulation frequency of the driving voltage is usually expressed in terms of the charge relaxation time $\tau_0 = \varepsilon_0\varepsilon_\perp/\ \sigma_\perp$. Then the conductivity is eliminated to a good approximation form the nematohydrodynamic equations, provided the ratio $\sigma_\parallel/\sigma_\perp$ is kept fixed. The conductivity ratio $\sigma_\parallel/\sigma_\perp \approx 1.5$ itself does not change so much, but even small variations of it have a strong influence on the critical voltage and the wave vector at onset (see Table 3.1). For the calculation of the coefficients it was adjusted to $\sigma_\parallel/\sigma_\perp = 1.575$ in order to fit the numerical values of the critical wave vector to those measured in [47].

Convenient numerical values for the coefficients are obtained by measuring length in units of d/π (d is the thickness of the fluid layer), time in director relaxation times $\tau_d = \gamma_1 d^2/k_{11}\pi^2$ and magnetic fields in splay (!) Freédericksz fields[2] $H_f^2 = k_{11}\pi^2/\chi_a d^2$. In these units the coefficient $\tilde{\chi}_a$, that appears in the amplitude equations, becomes $\tilde{\chi}_a = 1$ (provided we choose $\tilde{\gamma}_1 = 1$ as it was done in Section 1.2). The control parameter ε is defined by $\varepsilon = (V^2 - V_c^2)/V_c^2$, V_c being the voltage at which convection sets in.

The dimensions of the amplitude A depend on the normalization chosen for the convective mode. For this reason, only the ratios h/g and Γ/g, that are independent of the normalization, will be shown.

[2] The bend Freedericksz field, which is the one relevant for the homeotropic alignment is then given by $H = \sqrt{k_{33}/k_{11}}$.

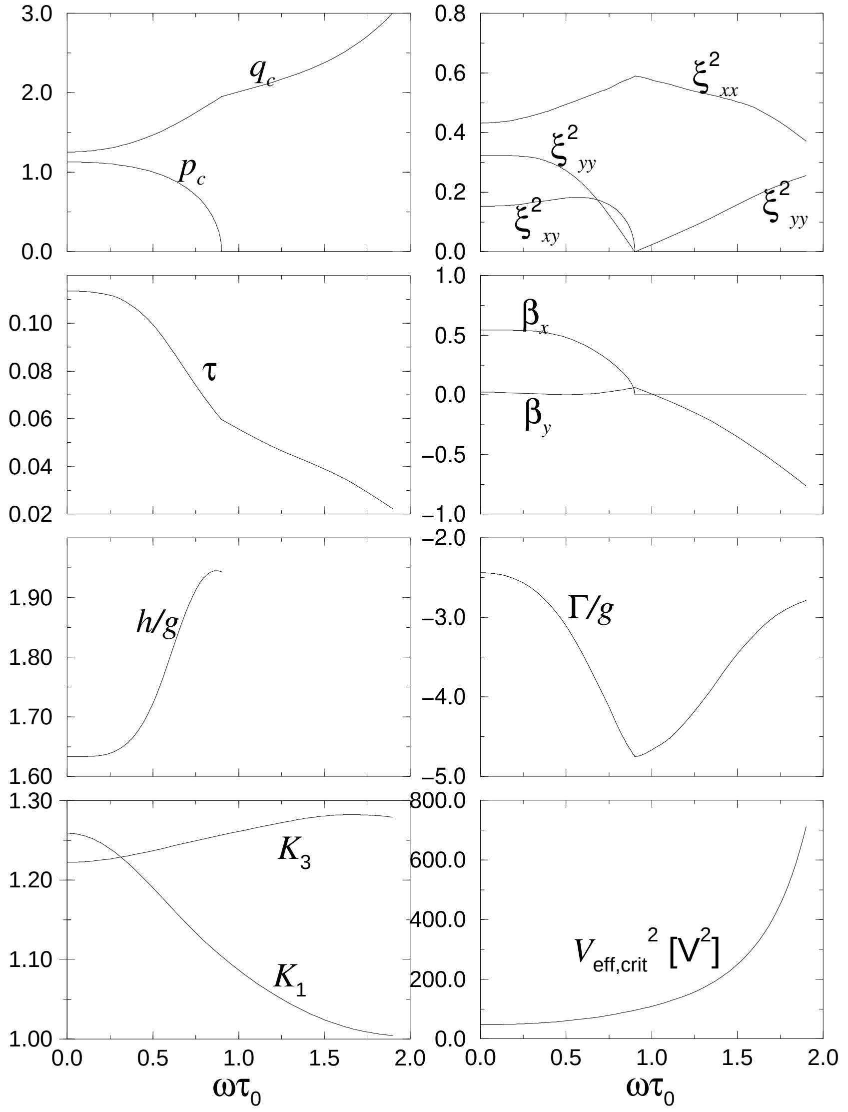

Figure 3.2: *Calculated coefficients for MBBA as a function of the frequency of the applied ac field. As a reference the bottom right graph shows the voltage at which convection sets in.*

In Fig. 3.2 the obtained numerical values for the coefficients are displayed. For small frequencies one has oblique rolls ($p_c \neq 0$), at high frequencies normal rolls ($p_c = 0$). The transition occurs at the "Lifshitz point" $\omega_{\rm Lif}\tau_0 = 0.90$.

The ratio h/g shown in Fig. 3.2 does *not* converge to 2 when $\omega \longrightarrow \omega_{\rm Lif}$ as was claimed in footnote 15 on page 42. This can be traced back to a minor shortcoming of the numerical code used: The velocity field $\vec{v}$ of the liquid crystal is expressed in terms of velocity potentials $F(x, y, z)$ and $G(x, y, z)$ as

$$\vec{v} = (\partial_x\partial_z, \partial_y\partial_z, -\partial_x^2 - \partial_y^2)F + (\partial_y, -\partial_x, 0)G. \tag{3.2}$$

Obviously a flow like $\vec{v} = (v_x(z), 0, 0)$ cannot be generated by bounded potentials. But such a flow should appear as a second order effect in the convection amplitude and is relevant for the coefficients[3] g and h. The contribution from this flow is missing, and leads to an error in the calculated values for g and h. In fact, the absolute errors are equal for both values, hence the relative error is twice as large for g as for h. This is the reason for the discrepancy between the calculated and the expected value of h/g as $\omega \longrightarrow \omega_{\rm Lif}$. From the numerical value $h_{\rm num}/g_{\rm num} = 1.95$ it can be calculated that the error in $g_{\rm num}$ at $\omega = \omega_{\rm Lif}$ is only $\approx 5\%$[4].

As a straightforward qualitative test, we compare simulations of the "rotationally invariant" equations for oblique rolls (1.139,1.140) at $\omega\tau_0 = 0.73$ and normal rolls (1.130,1.131) at $\omega\tau_0 = 1.75$ with corresponding experimental images [44], which were Fourier filtered to select only modulations with the critical wave vector, while higher spatial harmonics are being suppressed (Fig. 3.3). In order to obtain a good fit to the wavelength the thickness $d = 28.5\,\mu$m was used instead of the nominal value $d = 20\,\mu$m given in [44] (d was not measured directly). This only rescales length. No other parameter was fitted. The experimental normal rolls did not move, while they did in the simulations; a fact that remains unexplained. Comparing the images for oblique rolls, it appears that in the competition between rotating rolls and swinging rolls (Sec. 1.4) the rotating-roll scenario is more relevant in the simulations than in the experiment. With a different form of the rotationally invariant equations (the "Swift-Hohenberg" equations in [49]) this discrepancy was found to be smaller. Apparently the competition between rotating and swinging rolls is quite delicate for MBBA.

---

[3]For ground states with $(x, y, z, t) \to (x, y, -z, t)$ symmetry this problem does not seem to appear.

[4]There is another component of the flow which differs from the missing one only by an additional slow modulation in the y-direction and contributes to $h_{\rm num}$ by $h_{\rm num} - 2g_{\rm num}$. This allows to calculate (and in principle also to correct) the errors in $g_{\rm num}$ and $h_{\rm num}$ at $\omega = \omega_{\rm Lif}$

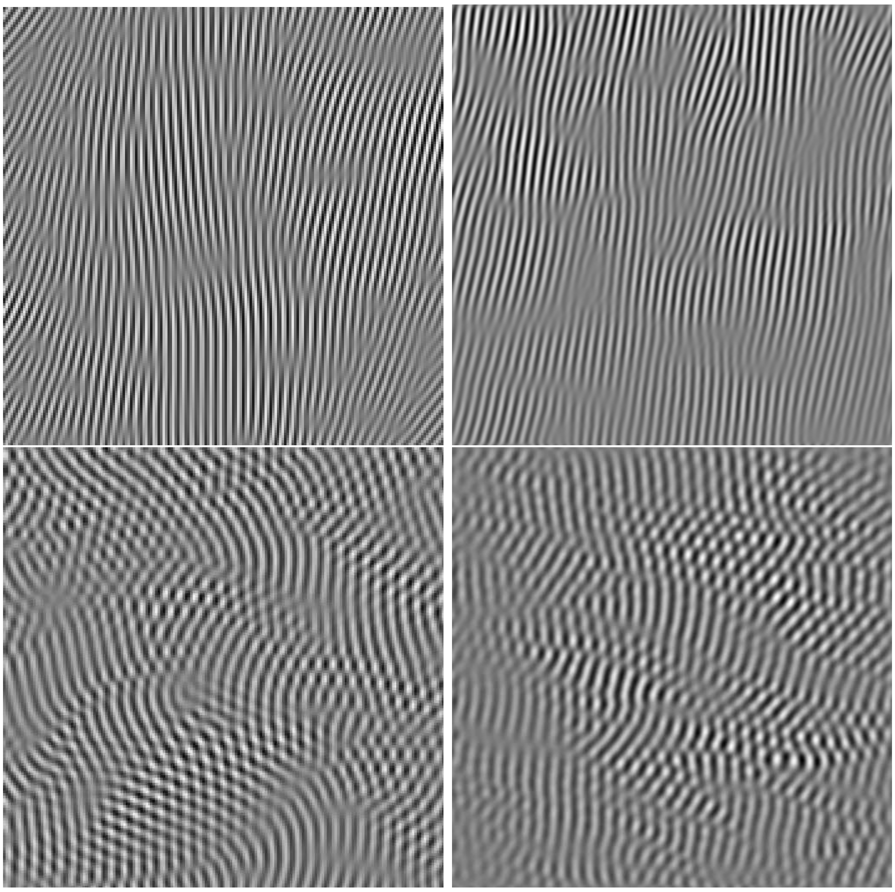

Figure 3.3: *Simulations of Eqs. (1.130,1.131) and (1.139,1.140) (left) vs. experiment [46, 44] (right) for normal (top) and oblique (bottom) rolls. See text for details.*

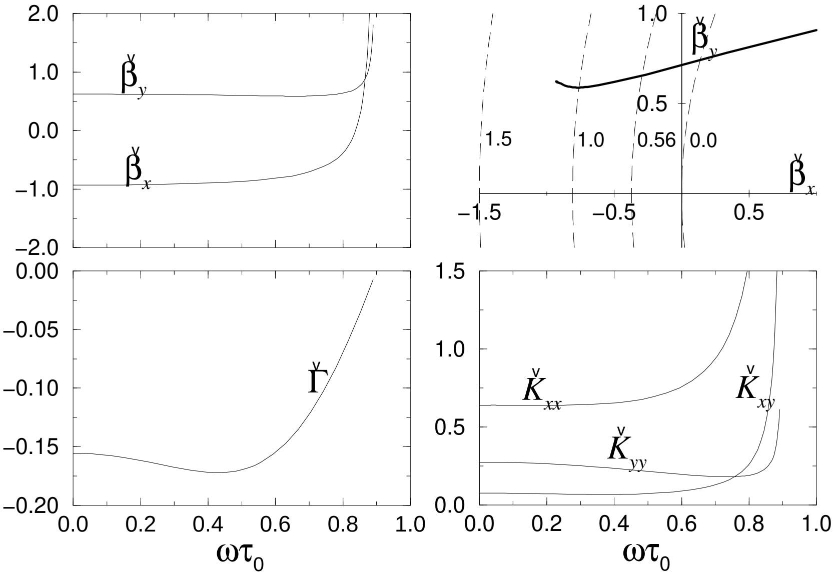

Figure 3.4: *Rescaled coefficients for oblique rolls. The upper right graph shows the same values as the upper left graph, but in the* $\check{\beta}_x$*-*$\check{\beta}_y$*-plane, in order to allow a direct comparison with the stability result (2.54). The dashed lines are the stability boundaries (at* $P, Q = 0$*) for the rescaled magnetic fields* $\check{H}^2 = 0.0$, $0.56(= 9/16)$, 1.0, *and* 1.5 *as indicated. The stable range is to the right of the lines.*

3.5 Comparison with Numerics and Experiment

From the numerically found coefficients we may now calculate the corresponding coefficient in the rescaled equations and compare the analytic stability bounds with those found in direct numerical calculations and experiments.

Oblique Rolls

The rescaled coefficients for oblique rolls are shown in Figure 3.4. It can be seen that over most of the frequency range unimodal oblique rolls do first become unstable against modulation instabilities at finite $\check{H}^2$. Shortly before the Lifshitz point (above $\omega\tau_0 = 0.85$), however, oblique rolls at the critical wave vector are stable with respect to modulations at arbitrary low $\check{H}^2$ (or $\varepsilon \to \infty$), according to our description. Instead, there is an instability with respect to a growth of the second oblique-roll mode. This becomes the first instability for $\omega\tau_0 > 0.78$ (Fig. 3.5).

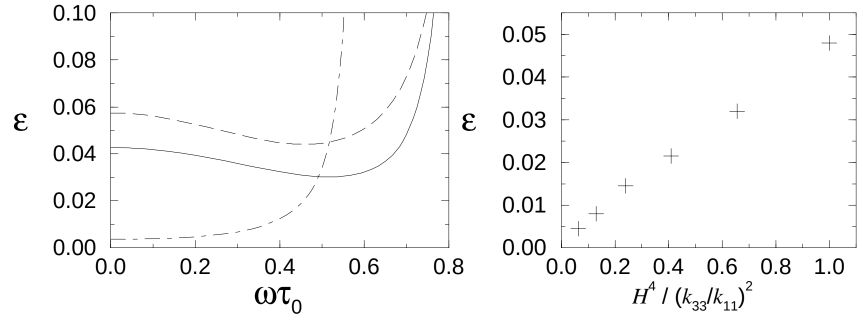

Figure 3.5: *Threshold of instabilities for oblique rolls.* Left panel: $H = 0.5\sqrt{k_{33}/k_{11}}$. *Threshold for modulation instabilities using Eq. (2.11) (solid), threshold for the instability of zig against zag according to Eq. (2.51) (dashed). The dashed line intersects with the solid line at* $\omega\tau_0 = 0.78$, $\varepsilon = 0.15$ *(not shown) which implies a change of the relevant instability mechanism. The dash-dotted line also corresponds to Eq. (2.11), but is based on coefficients that were calculated with only one Galerkin mode per field* (`moz=2`)*, where, for example,* $\Gamma/g \approx -11$. *It it is very similar to the corresponding curve of [16], where the same truncation was used.* Right panel: *The threshold values for modulation instabilities at* $\omega\tau_0 \to 0$ *as read off from the series of figures in [16], page 44. As it was found in Section 2.2.3 of this work, they scale like* $\varepsilon \sim H^4$

These results allow a comparison with the fully numerical work of [16]. As can be seen in Fig. 3.5, the numerical data (Fig. 3.14 of [16]) show an $\varepsilon_{\text{instab}} \sim H^4$ scaling in agreement with the finding of Section 2.2.3. The actual values are different, which is probably due to truncation errors in the Galerkin approximation (see caption of Fig. 3.5). In particular the increase of stability close to the Lifshitz point is also found in [16].

An important difference is that the numerical [16] bound for modulation instabilities connects continuously to the zig-zag instability line of normal rolls at $\omega = \omega_{\text{Lif}}$, $\varepsilon = 0$, a point that cannot be described by our equations. It is not unexpected that the theory fails in the vicinity of the Lifshitz point where oblique rolls turn into normal rolls: Because of the small coefficient ξ_{yy}^2, higher order terms become relevant [5]. Work to clarify the situation at the Lifshitz point is currently in progress.

Normal Rolls

For normal rolls, the comparison with direct numerical stability calculations based on the code of Hertrich and Decker was done more extensively (Fig 3.6).

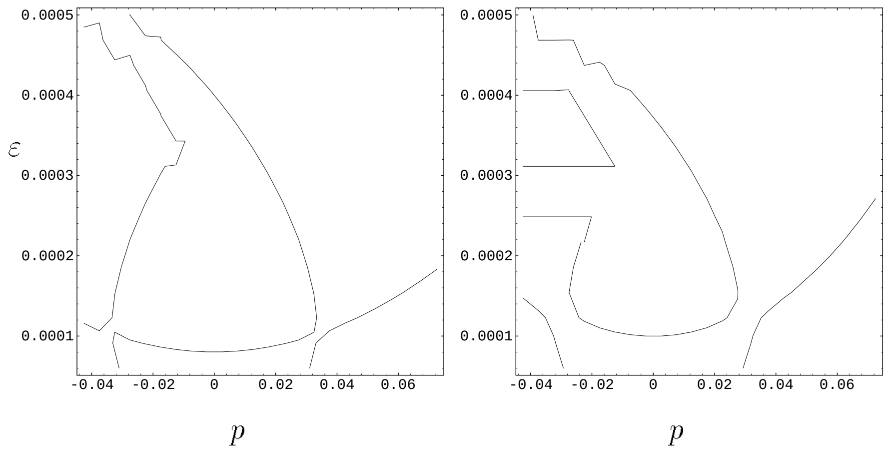

Figure 3.6: *Comparison of analytic and numeric stability analysis. There are no free parameters. For performance reasons both graphs are based on calculations with only one Galerkin mode per field. Material parameters as in [16] were used. The driving frequency* $\omega\tau_0 = 0.8$ *is slightly above the Lifshitz point* $\omega_{\rm Lif}\tau_0 = 0.70$ *(for this mode truncation). Therefore* $\breve{\beta}_y = 2.24$ *is quite high, which leads to the low zig-zag line. Only the lines where the maximum growth rate of long-wavelength modulations vanishes have been plotted.* Left panel: *analytic result. In order to make the connection to Sec. 2.1, compare with Fig. 2.7, page 69.* Right panel: *numerical result. The horizontal lines at* $\varepsilon \approx 3 \cdot 10^{-4}$ *are due to numerical difficulties at the abnormal-roll bifurcation point. Similarly, the artifacts in the upper part of the graphs originate from the vicinity of the saddle-node bifurcation.*

Number of Galerkin modes	`moz`	$\varepsilon_{\mathrm{AN}}$ direct numerical result	$\varepsilon_{\mathrm{AN}}$ result using Eq. (2.8)
1	2	0.0689	0.0676
2	4	0.1402	0.1408
3	6	0.1469	0.1522
4	8	0.1268	0.1315

Table 3.2: *Test of numerical accuracy, comparing the direct numerical method to calculate the abnormal-roll instability point ($\omega\tau_0 = 1.3$, $H = \sqrt{k_{33}/k_{11}}$, $\sigma_{\|}/\sigma_{\perp} = 1.5$) with the results using the amplitude equations. It should be emphasized that the second method is much less time consuming.*

Although the code used for the direct stability calculations is to a large part identical with the code used for calculating the coefficients, this comparison still allows to verify if

- the amplitude equations were set up in a proper form,
- the formulas for calculating the coefficients are right,
- the stability analysis for normal rolls was correct.

The calculations were done for small H^2, such that the instabilities occur at very low values of ε, because otherwise the zig-zag and the Eckhaus line would not so clearly be seen to intersect. Instead, there would be splitting and reconnection of the instability lines as described in Section 2.1.4. A remainder of this behavior can still be seen in the numerical stability diagram. Obviously this corresponds to the topology for $c_1 < 1$ (see Section 2.1.4). For stronger magnetic fields and larger ε the zig-zag line reduces to the small "bubble" around the abnormal-roll bifurcation point. Such a bubble was previously found numerically for homeotropic alignment (Fig. 3.17 of [16]) as well as for planar alignment (e.g. Fig. 5.17 in [12]). For the abnormal-roll bifurcation, the convergence as $\varepsilon, H^2 \to 0$ is much better. As an example, see Table 3.2.

Figure 3.7 shows the rescaled coefficients (1.125) for normal rolls. At high frequencies the value of $\check{\beta}_y$ approaches -1. This is the value for which the dynamics of A can be derived from a potential when φ is given (Section 1.4.1), and the zig-zag instability curve (2.11) vanishes. In fact, to the numerical accuracy, the convergence is exponential as ω increases. The relation $\check{\beta}_y \approx -1$ has also been found in the dielectric regime of planarly aligned electroconvection, where it becomes exact when the back-flow associated with director modulations is ignored [26]. But it is not completely clear how this observation leads to a more general explanation that would also apply to the present case.

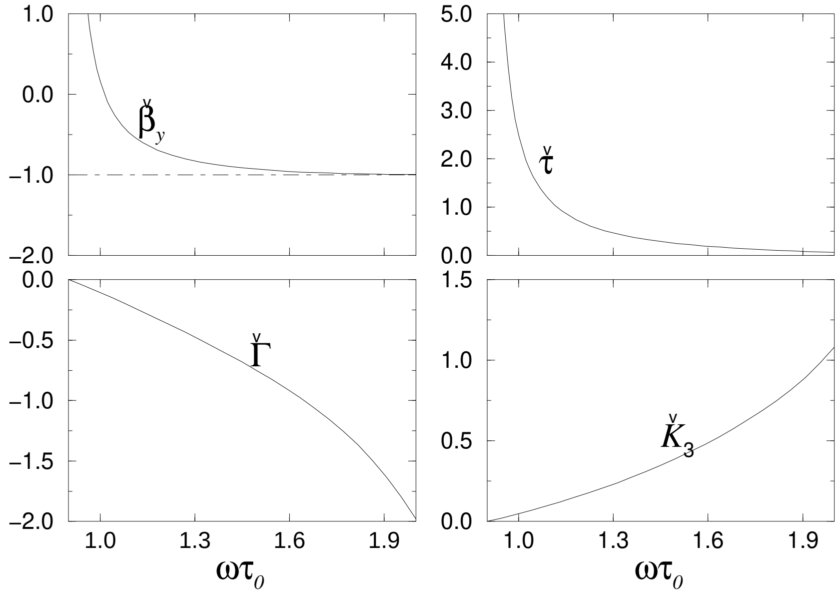

Figure 3.7: *Rescaled coefficients for normal rolls. The dot-dashed line in the graph of* $\check{\beta}_y$ *is a guide to the eye.*

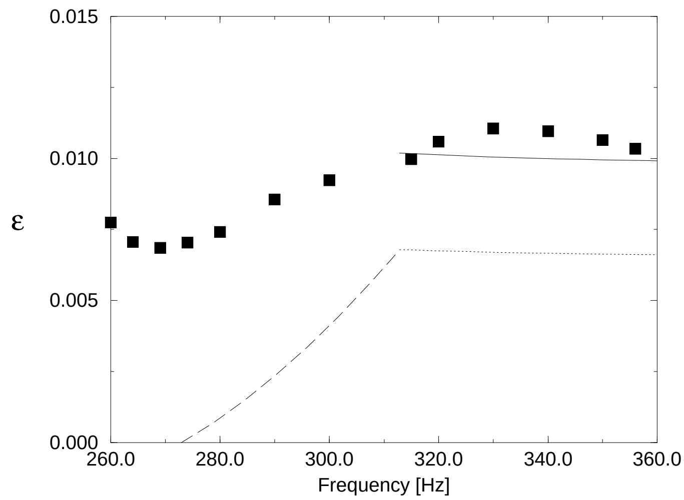

Figure 3.8: *Experimental values of* ε *at which the roll pattern destabilizes and defects appear (squares).* $H = 0.2 \times \sqrt{k_{33}/k_{11}}$. *Theoretical lines included are: back-bent Eckhaus instability (solid), abnormal-roll bifurcation (dotted), zig-zag instability (dashed). Always at* $Q, P = 0$. *(To connect to Sec. 2.1, notice that decreasing frequencies correspond to increasing* $\check{\beta}_y$ *which in turn corresponds to the sequence of stability diagrams for* $\check{\Gamma} < 0$ *that are scattered throughout Sec. 2.1.)*

The only available experimental results on the stability at low magnetic fields and low ε are the measurements of P. Tóth ([54], page 54). For a comparison with theory, the coefficients were calculated with $\sigma_{\|}/\sigma_{\perp} = 1.47602$ to fit the oblique-roll critical wave vector. The frequency scale (i.e. τ_0) was chosen to match the Lifshitz point. No other fitting was done. As can be seen in Fig. 3.8, the order of magnitude of the measured instability points agrees well with the theory. Nevertheless, discrepancies are too large to allow a clear identification of the relevant instability mechanism. In particular it would be interesting to clarify whether the instability observed at high frequencies is an abnormal-roll bifurcation or of the Eckhaus type.

3.6 Mean-Flow Effects

There is one flaw to the applicability of the present theory to homeotropically aligned electroconvection: The growth rate of the Goldstone mode $\sigma_G(q,p)$ is non-analytic at $(q,p) = 0$. The reason is that there is an additional marginally stable mode associated with a homogeneous change of pressure $\mathcal{P}$ in the liquid crystal or, equivalently [9], with the gauge symmetry of the velocity potential $G = G(x,y,z)$ that generates the vertical-vorticity component of the fluid flow $\vec{v} = (\partial_y, -\partial_x, 0)G$. In the context of convection patterns the effect is called "mean flow" (see e.g. [52, 9, 23]), while in nematohydrodynamics it might rather be referred to as "backflow". Though it is a small effect for the lowest-order amplitude equations considered here, it involves some interesting physics and deserves a detailed discussion.

Phenomenology

For simplicity, consider a situation below the threshold of convection. As a model, we write down a coupled system of equations for the modulated Goldstone mode $\varphi(x,y)$ and an order parameter $B(x,y)$ that describes the amplitude of some component $B(x,y)G_0(z)$ of the mean-flow potential $G(x,y,z)$. The flow profile $G_0(z)$ can be found by methods as described in [23, 22]. Keeping consistence with symmetry in mind,

$$0 = (b_1\partial_x^2 + b_2\partial_y^2)B + (c_1\partial_x^2 + c_2\partial_y^2)\varphi \tag{3.3}$$

$$\tilde{\gamma}_1\partial_t\varphi = (c_3\partial_x^2 + c_4\partial_y^2)B + (K_3\partial_x^2 + K_1\partial_y^2)\varphi. \tag{3.4}$$

Equations (3.3,3.4) contain no explicit time derivative of B, because the flow described by B is strongly damped by the horizontal boundaries. Obviously, modulations with wave vector (q, p) have a growth rate $\sigma = \sigma(q, p)$ given by

$$\tilde{\gamma}_1 \sigma = -(K_3 q^2 + K_1 p^2) + \frac{(c_1 q^2 + c_2 p^2)(c_3 q^2 + c_4 p^2)}{(b_1 q^2 + b_2 p^2)}. \tag{3.5}$$

This model indicates what kind of nonanalyticities have to be expected for σ: For fixed (q, p) a Taylor expansion of $\sigma(lq, lp)$ with respect to a book-keeping parameter l is possible, but an expansion of the form $\sigma(q, p) = \sum_{i,j} \sigma_{i,j}\, q^i\, p^j$ fails. In particular, even though B is a "slaved" variable, it cannot be eliminated from Eqs. (3.3,3.4) such that a single partial differential equation remains.

Numerically the nonanalyticity seems to be small: With typical experimental parameters the equation $\sigma(q, 0) + \sigma(0, p) = \sigma(q, p)$ is satisfied to about 0.1% as $q, p \to 0$. In fact, below it will be shown that, in order to exhibit the nonanalyticity, the code would have to include temporal modulations with frequencies higher than the driving frequency ω or flexoelectric effects, both of which have been discarded in the code as small corrections.

A heuristic argument indicates that c_1 and c_2 are small: Let φ be weakly modulated with a wave vector $(q, 0)$ with some small $q \neq 0$. According to Eq. (3.3), $B = (c_1/b_1)\,\varphi$. By the definition of B, this implies a flow component $\vec{v} = (0, v_y, 0)$ with v_y proportional to $\partial_x \varphi$. Considering the modulation in φ to be just a Fourier component of a more complex modulation, we conclude that every (small and slow) modulation of φ along the x-axis leads to a flow proportional to $\partial_x \varphi$ along the y-direction (there can be an additional, globally constant flow, i.e. $0 \neq \partial_x B = const.$, superimposed to this). Now, notice that, by fixing φ at some points in the convection cell, there may be steady state ("equilibrium") solutions to Eqs. (3.3,3.4), that have $\partial_y \varphi = 0$ and constant, small, non-vanishing $\partial_x \varphi$ over a large area, which generates a constant, steady flow. Obviously this would be impossible for a system in thermodynamic equilibrium. In fact, in the "microscopic" nematohydrodynamic equations, terms corresponding to those containing c_1 and c_2 in Eq. (3.3) do not occur. Instead of φ, its time derivative $\partial_t \varphi$ excites the flow, which is then symmetric under time-reversal and a reversible (i.e. non-dissipative) coupling. The effects that lead to the excitation of the flow by a constant director gradient (not only its viscous damping) have to be essentially irreversible. But the structure of the Freedericksz state, and therefore of the Goldstone mode, is basically determined by non-dissipative effects, which suggests that c_1 and c_2 are small.

Perturbative Calculation of the Growth Rate

To make this argument rigorous, $\sigma(lq, lp)$ will be calculated directly from the eigenvalue problem for the linear operator L up to second order in l. The resulting form of the growth rate does then justify Eqs. (3.3,3.4). In contrast to

Sections 1.1 and 1.3, the eigenvalue problem is now of the generalized form

$$0 = \Lambda \partial_t V + LV, \tag{3.6}$$

where Λ and L are linear, spatial, partial differential operators, and the null space of $L_{0,0}$ (see page 26 for this notation) is two-dimensional. It contains the rotational Goldstone mode W_G and the mode associated with a homogeneous change of pressure[5] $W_{\mathcal{P}}$. The adjoined subspace of $L_{0,0}$ is spanned by W_G^+ and $W_{\mathcal{P}}^+$, where $\langle W_G^+ | (\Lambda\partial_t + L) \cdot \rangle$ projects onto the balance equation for the angular momentum acting on the nematic molecules [41, 17] and $\langle W_{\mathcal{P}}^+ | (\Lambda\partial_t + L) \cdot \rangle$ selects the continuity (mass conservation) equation, both integrated over z. Only the crucial steps of the calculation will be discussed. $\sigma(lq, lp)$, $L_{lq,lp}$, the similarly defined operator $\Lambda_{lq,lp}$ and the "z-profile" $W(z) = V(x = 0, y = 0, z, t = 0)$ [6] of the eigenvector are expanded in powers of l. The "local" form of Eq. (3.6),

$$0 = \Lambda_{lq,lp} \sigma W + L_{lq,lp} W, \tag{3.7}$$

is solved order by order. Expansion coefficients are denoted by a superscript index, e.g.

$$\sigma(q,p) = \sigma^{(0)} + \sigma^{(1)} l + \sigma^{(2)} l^2 + \dots \tag{3.8}$$

It is easily seen by symmetry arguments that $\sigma^{(0)} = \sigma^{(1)} = 0$ for any $W^{(0)} = a_{\mathcal{P}}^{(0)} W_{\mathcal{P}} + a_G^{(0)} W_G$. The solvability condition for $W^{(2)}$ at order l^2 does itself lead to a generalized eigenvalue problem for $\sigma^{(2)}$:

$$0 = \begin{pmatrix} \langle W_{\mathcal{P}}^+ | \mathcal{L} W_{\mathcal{P}} \rangle & \langle W_{\mathcal{P}}^+ | \mathcal{L} W_G \rangle \\ \langle W_G^+ | \mathcal{L} W_{\mathcal{P}} \rangle & \langle W_G^+ | \mathcal{L} W_G \rangle \end{pmatrix} \begin{pmatrix} a_{\mathcal{P}}^{(0)} \\ a_G^{(0)} \end{pmatrix} =: M_{ij} a_j^{(0)}, \tag{3.9}$$

where

$$\mathcal{L} = \Lambda^{(0)} \sigma^{(2)} + L^{(2)} - L^{(1)} \tilde{L}^{(0)^{-1}} L^{(1)} \tag{3.10}$$

and $\tilde{L}^{(0)^{-1}}$ is the left pseudoinverse of $L^{(0)}$. The eigenvector $(a_{\mathcal{P}}^{(0)}, a_G^{(0)})$ fixes the composition of $W^{(0)}$, which was left undetermined at zeroth and first order.

Notice that, since $L^{(0)}$ does not depend on q or p, all entries of M_{ij} are quadratic polynomials in q and p. Assuming incompressibility, $\Lambda^{(0)}\sigma^{(2)}$ contributes only to the entry M_{GG} of M_{ij}. When either $M_{G\mathcal{P}}$ or $M_{\mathcal{P}G}$ vanishes,

[5] A discussion in terms of the pressure mode has some technical advantages over the introduction of velocity potentials.

[6] Here t is the "slow" time of pattern dynamics. The oscillations of the state that are related to the oscillations of the electric driving field are separated from this slow time dependence by a Floquet analysis and are contained in W.

$\sigma^{(2)}$ is polynomial in q and p. From the simple form of the continuity equation $\nabla\vec{v} = 0$ it follows immediately that the entry $M_{\mathcal{P}G}$ is determined only by the indirect term $L^{(1)}\tilde{L}^{(0)^{-1}}L^{(1)}$ (in the language of Section 1.1 this is the contribution of R), and that this contribution is nonzero only if a flow is excited at first order in the modulation of the rotational Goldstone mode. Before discussing possible mechanisms for this, some consequences of the approximation $M_{\mathcal{P}G} = 0$ shall be analyzed.

At lowest order in the amplitude equation $M_{\mathcal{P}G} = 0$ leads to considerable simplifications. The coefficients c_1 and c_2 in Eq. (3.3) vanish and the growth rate of modulations in φ takes the simple form $\sigma = -K_3q^2 - K_1p^2 + h.o.t.$. Above the threshold of convection, the nonlinear excitation of the mean-flow mode B is at lowest order given by adding a term of the form $\partial_x\partial_y|A|^2$ to the r.h.s. of Eq. (3.3) [23]. It is easily seen that this contribution is small compared to the direct excitation of φ by the term $(\Gamma/4)(-iq_cA^*(\partial_y - iq_c\varphi)A + \text{c.c.})$. Hence, when $M_{\mathcal{P}G} = 0$, all effects pertaining to mean flow can be discarded at lowest order. But, as will be shown now, $\sigma(q,p)$ still has nonanalytic contributions at higher orders.

Generally speaking, at order l^k in the expansion of Eq. (3.7), $W^{(k)}$ is determined only up to a contribution $a_{\mathcal{P}}^{(k)}W_{\mathcal{P}} + a_G^{(k)}W_G$. The coefficients $a_i^{(k)}$ are given by the solvability condition for $W^{(k+2)}$ at order $k+2$. When $k > 0$ this solvability condition assumes the form of an inhomogeneous linear system

$$M_{ij}a_j^{(k)} + I_i + \left\langle W_i^+ \middle| \Lambda^{(0)}\sigma^{(k+2)}W_G \right\rangle a_G^{(0)} = 0, \tag{3.11}$$

where I_i is some complicated expression. Since M_{ij} itself has a nontrivial kernel, there is also a solvability condition for Eq. (3.11), which in turn is satisfied by setting

$$\sigma^{(k+2)} = -\frac{a_i^+ I_i}{a_i^+ \left\langle W_i^+ \middle| \Lambda^{(0)}W_G \right\rangle a_G^{(0)}}. \tag{3.12}$$

The a_i^+ are given by $a_i^+M_{ij} = 0$, i.e. $a_{\mathcal{P}}^+/a_G^+ = -\left\langle W_G^+ \middle| \mathcal{L}W_{\mathcal{P}} \right\rangle / \left\langle W_{\mathcal{P}}^+ \middle| \mathcal{L}W_{\mathcal{P}} \right\rangle$. Because of this nontrivial adjoined eigenvector, $\sigma^{(k+2)}$ is in general a rational expression in q, p, even if I_i is polynomial. As a result, $\sigma(q,p)$ is always nonanalytic. The final conclusion remains valid when the assumption of incompressibility is relaxed. This effectively leads to a continuity equation of the form $c\partial_t\mathcal{P} + \nabla\vec{v} = 0$ (with some constant c) and therefore to another (formally) slow mode, but the general structure of the perturbation scheme remains unchanged.

Physical Mechanisms

In order to discuss possible mechanisms to excite mean flow by gradients of φ, a closer look at the nematohydrodynamic equations is necessary. The formulation of Pleiner and Brand with the notation of [41] will be used. For concreteness we come back to the geometry described above: The homogeneous ground state is perturbed by modulations of φ with a small wave vector $(q, 0)$. We are looking for an excitation of v_y at linear order in φ and q.

The fluid flow is given by the Navier-Stokes equation

$$\rho(\partial_t + v_j \nabla_j)v_i + \nabla_j \sigma_{ij} = \rho_e E_i + P_j \nabla_j E_i. \tag{3.13}$$

As usual, ρ denotes the mass density, ρ_e the charge density, P_j electric polarization, E_i the electric field and σ_{ij} the stress tensor. Indices run over x, y, z. Excitation of flow by the electric terms on the r.h.s. would imply a contribution to E_y which is constant along y. The corresponding linear increase of the electric potential is incompatible with the equal-potential horizontal boundary conditions that are imposed by the conductive coating of the glass plates. The term $\nabla_z \sigma_{yz}$ may lead to some flow, but it is averaged out when the continuity equation is integrated over z, and does therefore not contribute to $M_{\mathcal{P}G}$.

Only the contribution $\nabla_x \sigma_{yx}$ remains. Since this term already contains an explicit linear dependence on p, the stress σ_{yx} must be a contribution that is present also for a homogeneous excitation of φ. This contribution is simply given by a rotation of the stress tensor of the ground state, which is the Freedericksz state with the director turned into the x-direction in our case. A rotation leads to off-diagonal elements like σ_{xy} only if the stress of the Freedericksz state is anisotropic, i.e. $\sigma_{xx} - \sigma_{yy} \neq 0$.

Some details of the Freedericksz state are needed for a further discussion. Since the applied electric voltage is modulated in time, the deformation of the director field does not only have the static component which is shown in Fig. 3.1 and is of order unity but also a modulated component with an amplitude of order $1/(\omega\tau_d) \approx 10^{-4} - 10^{-2}$, where τ_d is the director relaxation time and ω the electric driving frequency. The modulation has a component quadratic in the applied voltage (i.e. with frequency 2ω), which stems from the dielectric anisotropy, and a linear component (modulated with ω) from flexoelectric effects. These oscillations of the director do in turn drive an oscillatory shear flow in x-direction. Because of the inhomogeneity of the conductivity and of the dielectric tensor along z, there is also an accumulation of charges in the bulk of the liquid, which is modulated with frequency ω.

The general form of the stress tensor is

$$\sigma_{ij} = \tilde{p}\delta_{ij} + \Phi_{lj}\nabla_i n_l - \frac{1}{2}\lambda_{kji}\delta^{\perp}_{kl}h_l - \nu_{ijkl}\nabla_l v_k, \tag{3.14}$$

where $\tilde{p}$ is a generalized pressure, Φ_{lj} is the Ericksen tensor and contains elastic and (static) flexoelectric effects, h_l is a variant of de Gennes "molecular field", which tends to align the nematic director parallel to itself, and contains elastic, dielectric, and (static) flexoelectric contributions. Here it is used to describe the reversible coupling between director rotation and shear flow, mediated by λ_{kji}. Furthermore, ν_{ijkl} is the dissipative viscosity tensor, δ_{ij} the Kronecker symbol and $\delta^{\perp}_{kl} := \delta_{kl} - n_k n_l$ the projector onto the plane normal to the nematic director. By symmetry, there is no contribution from the first two terms on the r.h.s. of Eq. (3.14) to $\sigma_{xx} - \sigma_{yy}$ for the Freedericksz state.

To see the effect of the other two terms, it is useful to consider the equation of motion for the director, which does here take the form

$$\partial_t n_k = \frac{1}{2}\lambda_{klm}\nabla_l v_m - \frac{1}{\gamma_1}\delta^{\perp}_{kl} h_l + \zeta^E_{klm}\nabla_l E_m. \tag{3.15}$$

γ_1 is, as usual, the rotational viscosity. The term containing ζ^E_{klm} describes the dynamic flexoelectric effect [6], a dissipative coupling which is not included in older formulations of nematohydrodynamics. Apparently, little is known about the magnitude of this effect.

Using Eq. (3.15), $\delta^{\perp}_{kl} h_l$ is eliminated from the third term on the r.h.s. of Eq. (3.14):

$$-\frac{1}{2}\lambda_{kji}\delta^{\perp}_{kl} h_l = \frac{\gamma_1}{2}\left(\lambda_{kji}\partial_t n_k - \frac{1}{2}\lambda_{kji}\lambda_{klm}\nabla_l v_m - \lambda_{kji}\zeta^E_{klm}\nabla_l E_m\right). \tag{3.16}$$

Now, observe that the director can be written as $\vec{n} = (\sin\theta, 0, \cos\theta)$. Apart from material constants, the tensors λ_{kji}, ζ^E_{klm}, and ν_{ijkl} depend only on $\vec{n}$ or, respectively, on θ. Therefore the first term in the parenthesis in Eq. (3.16) can be written as the time derivative of the bounded function $\int^{\theta(t)}(\lambda_{xji}n_z - \lambda_{zji}n_x)\,d\theta'$ and does, on the average, not contribute to σ_{ij}.

Furthermore, notice that, by symmetry and the incompressibility of the liquid crystal, the only non-vanishing component of $\nabla_l v_m$ is $\nabla_z v_x$, and the only way to excite this shear flow is through the term $\nabla_z \sigma_{xz}$ in the Navier-Stokes equation (3.13). In experiments the viscous relaxation time is usually small compared to $1/\omega$, and the quasistatic approximation $\nabla_z\sigma_{xz} = 0$ is justified to calculate $\nabla_z v_x$. Again, the first two terms on the r.h.s. of Eq. (3.14) do not contribute. With the substitution (3.16) it can be seen that there are two contributions to $\nabla_z v_x$: the first is from the term $\lambda_{kji}\partial_t n_k$ in (3.16), the second from the dynamic flexoelectric term. The first component leads to a shear flow that can be written in the form $\nabla_z v_x = f(\theta)\partial_t\theta$, with some function $f(\theta)$. Its contribution to $\sigma_{xx} - \sigma_{yy}$ through the viscous term in Eq. (3.14) and the term

$-(1/2)\lambda_{kji}\lambda_{klm}\nabla_l v_m$ in (3.16) can again be written as a complete time derivative of a bounded function, and it does not contribute to the temporal average of $\sigma_{xx} - \sigma_{yy}$.

We are left with the contribution of the second component of $\nabla_z v_x$ to $\sigma_{xx} - \sigma_{yy}$ and the contribution of the last term in (3.16), both of which involve the dynamic flexoelectric effect. Modulations of $\vec{n}$ in λ_{kji}, ζ^E_{klm}, and ν_{ijkl} contain components $O(\omega\tau_d)^{-1}$ from the static flexoelectric effect which have the correct frequency and spatial symmetry to generate a constant contribution to $\int \sigma_{xx}\, dz$ when multiplied with $\nabla_l E_m$. There is no particular phase shift between the two factors because the static flexoelectric effect has contributions proportional to E_z while the dynamic flexoelectric effect is a pure $\nabla_z E_z$ effect, and E_z and $\nabla_z E_z$ are shifted in phase because of the finite charge relaxation time τ_0. When $\omega\tau_0 = O(1)$ the resulting stress can therefore be estimated as $(\omega\tau_d)^{-1} \times$ static flexoelectric effect $\times$ dynamic flexoelectric effect. Though there is also some contribution to σ_{yy} through the viscous term, it differs from the contribution to σ_{xx}, since e.g. $\lambda_{iyy} \sim n_y = 0$ while $\lambda_{ixx} \neq 0$ (see [41]).

As a conclusion, the nonanalytic contribution due to mean flow enters the amplitude formalism in principle already at lowest nontrivial order. Presumably this contributions is small. A large part of it may be related to the dynamic flexoelectric effect, which could be of interest from the experimental point of view. When the amplitude formalism for homeotropic electroconvection is extended to higher orders, mean flow is always involved. According to recent results for a similar system [38], its relevance can be substantial. These conclusions are already valid for a dynamical description of the Freedericksz state without convection.

Chapter 4

Dynamic Solutions: Chevron Patterns

4.1 Introduction

This chapter falls somewhat outside the previous line of argumentation. Instead of making a careful transition from a stable homogeneous roll solution towards more disordered states, as suggested in the beginning of Chapter 2, we will now jump far into the chaotic regime of the normal-roll amplitude equations. The stability analysis was concerned with values of the control parameter $\eta = 2|\Gamma|\varepsilon/H^2 = O(1)$. The so-called "chevron" patterns discussed in this chapter typically appear at values $h^2 := \eta^{-1} = 0.02 \dots 0.2$ in simulations of Eqs. (1.123,1.127) (Fig. 4.1, Fig. 4.4). They are by far not the only possible structure that these equations can generate (Fig. 4.2). Nevertheless work has focused on these structures, because apparently they help resolve the problem of explaining an experimental observation which has been known for over 25 years, chevron patterns occurring in the dielectric regime of electroconvection (EC) in layers of planarly aligned nematic liquid crystals [15, 35, 13, 21, 3, 8, 11]:

Increasing the ac voltage applied across the layer (above the "cutoff frequency") one first observes a (nearly) periodic pattern of (narrow) convection rolls with wave vector parallel to the director orientation which was imposed by surface treatment of the plates forming the upper and lower boundaries of the layer. Then defects (dislocations) in the roll pattern start to appear, their density increasing as the voltage rises. Initially they move irregularly and their distribution is homogeneous. Defects carry a topological charge which is +1 or −1 depending on whether a roll "ends" or "begins" at that point. After a further increase of the voltage one observes the transition to chevron patterns,

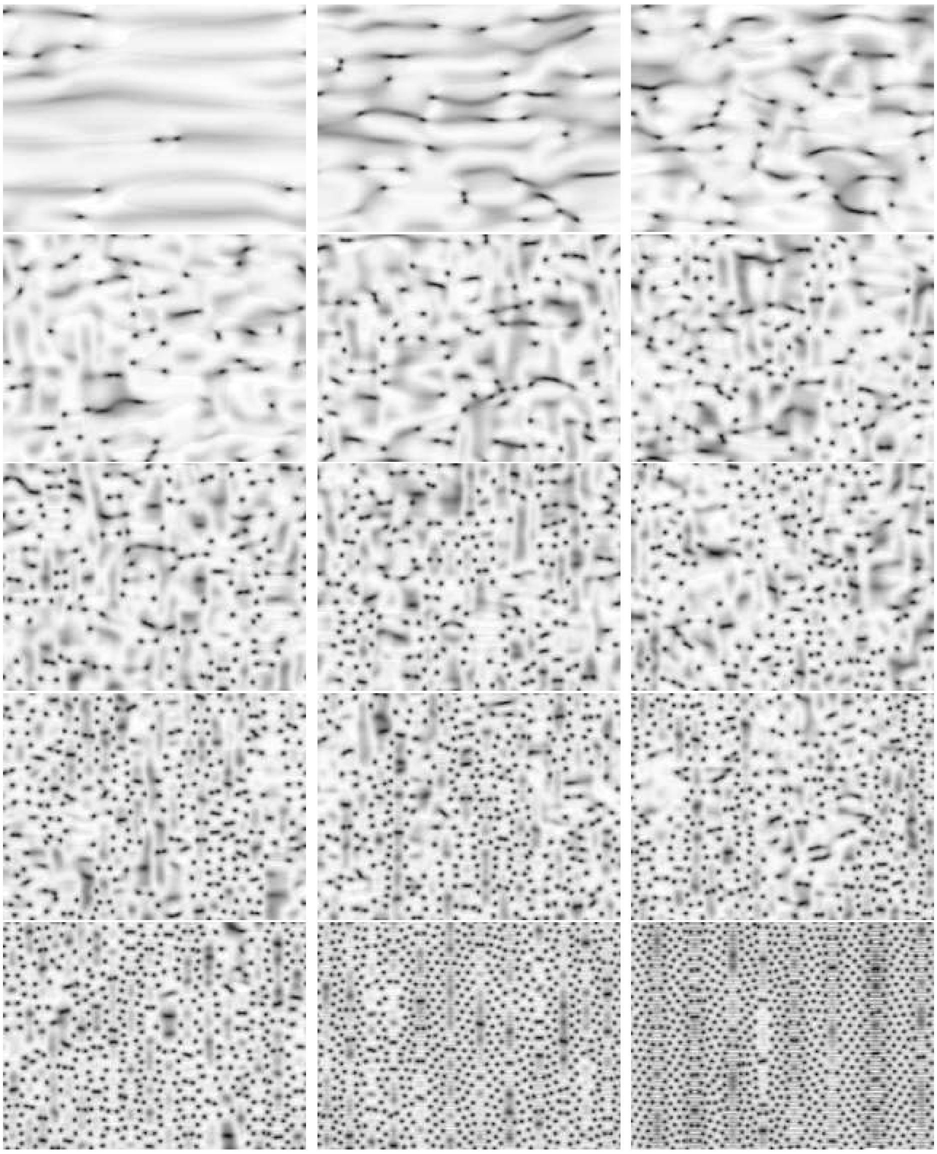

Figure 4.1: $|A|$ *in the steady state of simulations of Eqs. (1.123,1.127). The same parameters as in Figure 4.4 were used, but (from upper left to lower right)* $h^2 = 0.85$, *0.75, 0.55; 0.45, 0.35, 0.25; 0.21, 0.17, 0.15; 0.11, 0.09, 0.07; 0.05, 0.01, 0.002*

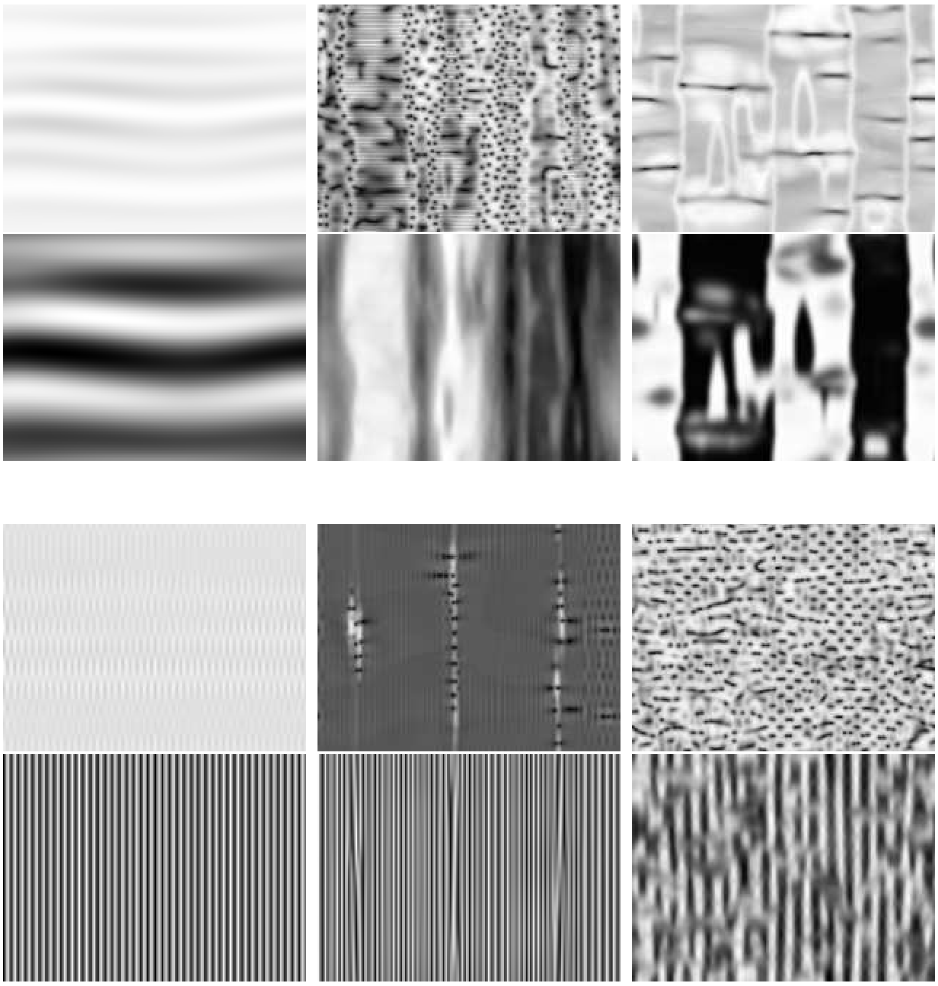

Figure 4.2: *Other structures appearing in simulations of the normal rolls equations Eqs. (1.123,1.127). $|A|$ (upper) and φ (lower) encoded in a gray scale. First row, left to right: spatio-temporally oscillating director modulations ($\beta_y = 1.07$, $\Gamma = -0.0304$, $K_3 = 0.0564$, $\tau = 2.19$, $h^2 = 0.9$); chevron standing oscillations ($\beta_y = 1.07$, $\Gamma = -0.0608$, $K_3 = 0.0564$, $\tau = 8.77$, $h^2 = 0.05$); abnormal-roll domains (possibly transient, $\beta_y = -0.502$, $\Gamma = -0.221$, $K_3 = 0.103$, $\tau = 1.14$, $h^2 = 0.6$). Second row: 2-d steady state director and phase modulations ($\beta_y = 1.07$, $\Gamma = -0.0608$, $K_3 = 0.0$, $\tau = 4.39$, $h^2 = 0.12$), the same with some defects, yet no motion ($h^2 = 0.08$); defect lattice ($\beta_y = 1.07$, $\Gamma = -0.122$, $K_3 = 0.0564$, $\tau = 4.39$, $h^2 = 0.16$).*

with defects of equal charge ordering along periodically arranged domains oriented parallel to the original roll direction. Simultaneously with the onset of the ordering process the increase of the number of defects with voltage becomes noticeably faster [50]. Between the chains the convection rolls are rotated away from their original orientation alternatingly to the left and to the right, which gives the whole structure a "herringbone"-like appearance.

Chevrons have recently also been observed in homeotropic EC [54], the system described in the previous chapter. Other systems where chevrons were observed are dielectric EC under oblique boundary conditions [19], EC in nematic polymers [55] and sometimes also in the conductive regime of EC in planarly aligned ordinary nematics [18].

4.2 Formal Setting

Writing the complex amplitude A as $A = |A|e^{i\theta}$ defines the phase modulations θ of the underlying stripe pattern up to multiples of 2π. This degeneracy plays no role as long as only the phase gradient

$$\nabla\theta = \mathrm{Im}\left\{\frac{\nabla A}{A}\right\} \tag{4.1}$$

is considered (and $A \neq 0$). $\nabla\theta$ is the deviation of the local wave vector from the most unstable wave vector at $\varphi = 0$ (up to the rescaling done in Eq. (1.123)). The wave vector of the roll pattern and the director $\hat{c}$ are parallel if $P := \partial_y\theta = \varphi$.

A topological defect in the stripe pattern corresponds to a simple zero of the complex amplitude A. Its topological charge is $\int d\vec{r}\cdot\nabla\theta/2\pi$, where the path of integration is a small loop encircling the defect in the positive sense.

We define defect densities

$$n_\pm(\vec{r}) = \sum_j \delta(\vec{r} - \vec{r}_{\pm,j}), \tag{4.2}$$

where the sum is over all positively or negatively charged defects at the positions $\vec{r}_{\pm,j}$, respectively, and $\delta(\cdot)$ is the Dirac δ function. The total defect density is $n := n_+ + n_-$ and the topological charge density is $\rho := n_+ - n_-$. One has

$$\int_{\partial\Omega} \nabla\theta(\vec{r})d\vec{r} = 2\pi\int_\Omega \rho(\vec{r})d\Omega \tag{4.3}$$

for any area Ω.

From an abstract point of view one can define chevrons as a periodic modulation of ρ, with a wave vector parallel to the x axis [21]. Hence we will only look at modulations of the defect chaotic state in the x direction and average all equations along y, which will be indicated by an overbar $\overline{\cdot} := L_y^{-1} \int \cdot \, dy$ (in this chapter we will always use the more convenient periodic boundary conditions for a plane with large spatial extensions $L_x, L_y \gg 1$). In particular one finds a topological condition

$$\partial_x \overline{P} = 2\pi\overline{\rho}, \tag{4.4}$$

by differentiating both sides of Eq. (4.3) for a rectangular area $\Omega = [0, \xi] \times [0, L_y]$ with respect to ξ. Obviously $\overline{P}$ can only change through defect motion. With fixed and (locally) constant φ, where Eq. (1.123) reduces to the simple Ginzburg-Landau equation, defects always move such that the (local) wavenumber approaches the value of highest growth rate [4], which includes the condition $P = \varphi$.

4.3 Linear Model

A simple model for the coarse-grained dynamics of the defect-chaotic state helps to understand chevron formation as a linear modulation instability of homogeneous defect chaos.

Led by symmetry considerations similar to Section 1.2 one can set up a model equation for the conservation of topological charge

$$\partial_t \overline{\rho} + \partial_x \left[-D \partial_x \overline{\rho} + \sigma (\overline{P} - \overline{\varphi}) \right] = 0. \tag{4.5}$$

The diffusion coefficient D and the "conductivity" σ are phenomenological constants. We do not calculate them here and assume both to be positive. This means that diffusion of defects acts to minimize topological charge imbalance and systematic drift acts to reduce $|\overline{P} - \overline{\varphi}|$. To get a corresponding equation for φ we average Eq. (1.127) over y.

$$\partial_t \overline{\varphi} = (K_3 \partial_x^2 + 2\Gamma h^2)\overline{\varphi} + 2\Gamma |A|^2_{\text{eff}} (\overline{P} - \overline{\varphi}). \tag{4.6}$$

The form of the last term follows from isotropy for small $\overline{P} - \overline{\varphi}$, $|A|^2_{\text{eff}}$ is a suitable constant. Equations (4.4,4.5,4.6) describe dynamics for small deviations from $\overline{\rho} = 0$ on length scales much larger than $n^{-1/2}$.

Using this model one can calculate the stability of homogeneous defect-chaotic solutions against periodic modulations of $\overline{P}$ and $\overline{\varphi}$ in x direction. After applying ∂_x on Eq. (4.6) and eliminating $\overline{P}$ through (4.4), Eqs. (4.5,4.6) take the form of a linearized reaction diffusion system for $\overline{\rho}$ and $\partial_x \overline{\varphi}$. Accordingly one gets a homogeneous Hopf bifurcation or a steady state, spatially periodic (diffusive) Turing instability or a simple non oscillatory, homogeneous bifurcation as the first instability (see e.g. [48]).

For

$$K_3/D > 1 \quad \text{and} \quad 1 < -\Gamma|A|^2_{\text{eff}}/\pi\sigma, \tag{4.7}$$

or

$$K_3/D < 1 \quad \text{and} \quad (D/K_3)^{1/2} + (K_3/D)^{1/2} < 2(-\Gamma|A|^2_{\text{eff}}/\pi\sigma)^{1/2} \tag{4.8}$$

one has the Hopf bifurcation at

$$h^2_{\text{Hopf}} = |A|^2_{\text{eff}} + \pi\sigma/\Gamma \tag{4.9}$$

with the Hopf frequency given by

$$\omega^2_{\text{Hopf}} = 4\pi\sigma(-\Gamma|A|^2_{\text{eff}} - \pi\sigma). \tag{4.10}$$

If

$$(D/K_3)^{1/2} + (K_3/D)^{1/2} > 2(-\Gamma|A|^2_{\text{eff}}/\pi\sigma)^{1/2} \quad \text{and} \quad K_3/D < -\Gamma|A|^2_{\text{eff}}/\pi\sigma \tag{4.11}$$

the chevron ("Turing") pattern with critical wavenumber

$$k^2_{\text{c}} = (-4\pi\Gamma|A|^2_{\text{eff}}\sigma/DK_3)^{1/2} - 2\pi\sigma/D \tag{4.12}$$

appears first at

$$h^2_{\text{c}} = \left(|A|_{\text{eff}} - (\pi K_3\sigma)^{1/2}(-D\Gamma)^{-1/2}\right)^2. \tag{4.13}$$

See also Fig. 4.3.

None of the two instabilities occurs in the remaining case where $K_3/D > -\Gamma|A|^2_{\text{eff}}/\pi\sigma$ and $1 > -\Gamma|A|^2_{\text{eff}}/\pi\sigma$. At $h^2 = 0$ the mode of homogeneous rotation (Goldstone mode) invokes an instability.

According to this model a crucial effect is the diffusive contribution in Eq. (4.5). It invokes a wave vector mismatch $(P - \varphi)$ for modulated P and φ which would otherwise be leveled out by defect motion. Due to this mismatch the repulsive "torque" on φ by the roll pattern (described by the term containing Γ in Eq. (4.6)) can then drive chevron formation. It should be noted that no particular assumption about the interaction of single defects was made. By inspection one finds that the model is robust against additional terms in Eq. (4.5), as long as modulations of P are weakened compared to modulations of φ. For example, a consistent truncation in powers of k should include a fourth-order derivative of $\overline{p}$ in Eq. (4.5), a term that has here been omitted for the sake of simplicity.

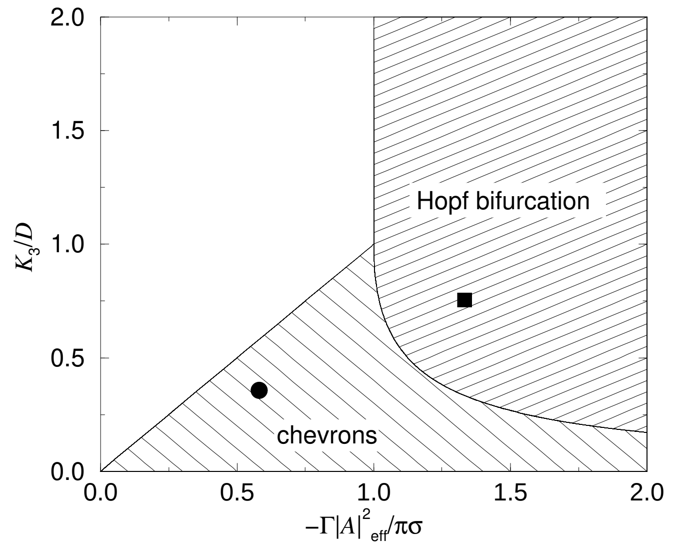

Figure 4.3: *Regions in parameter space where chevron instability and Hopf bifurcation respectively are the first to occur when h^2 is decreased. The circle and the square correspond to the two parameter sets analyzed in Section 4.5.*

4.4 Nonlinear Model

In the final, saturated chevron pattern the defect density n becomes strongly modulated with half the period of the chevron pattern. The defects accumulate along "chains". This can be understood with ideas similar to those describing a p-n junction in a semiconductor. In the regions along the chains a high density of positively or negatively charged defects is enforced by the strong bend $(\partial_x \varphi)$ of the director. This corresponds to doping the p and n regions of the semiconductor with charge carriers. The density of the oppositely charged species is strongly suppressed due to high recombination probability. As in the depletion layer of the p-n junction, in the region between the chains the *total* density of defects n is reduced compared to the "chain" region.

The coupling between ρ and n may also provide an important contribution to the nonlinear saturation of the chevron mode. Assume that defects are homogeneously created at a constant rate n_0/τ_n, while they are annihilated at a rate proportional to $n_+ n_-$, such that for the homogeneous defect chaos one has a time-averaged defect density $\langle n \rangle_t = 2n_0$ (in this section we only consider quantities averaged over y and drop the overbars). Ignoring correlations in the nonlinear terms we obtain

$$\partial_x j_\pm + \partial_t n_\pm = \frac{1}{\tau_n n_0}(n_0^2 - n_+ n_-), \tag{4.14}$$

where $j_\pm$ are the defect currents. Since $n_0^2 - n_+ n_- = n_0^2 - n^2/4 + \rho^2/4$, an excitation of the chevron mode (i.e. ρ) increases the equilibrium number of defects. One should expect that with increased defect density n the conductivity σ becomes higher (e.g. $\sigma = mn$ with some mobility constant m). This weakens the relative importance of the diffusive term in Eq. (4.5) so that the chevron mode saturates. In order to get a quantitative estimate of this effect we calculate the weakly nonlinear [10] steady state solution of Eqs. (4.6,4.14), assuming currents of the form

$$j_\pm = -D\partial_x n_\pm \pm m\, n_\pm (P - \varphi), \tag{4.15}$$

and allowing a modulation of $|A|^2_{\text{eff}}$ by substituting

$$|A|^2_{\text{eff}} \to |A|^2_{\text{eff}}\,(1 - c_1 n - c_2\rho^2 - c_3(P-\varphi)^2) \tag{4.16}$$

in Eq. (4.6).

For periodic solutions with wave number k one obtains, up to a phaseshift,

$$P = \sqrt{\frac{(h_c^2 - h^2)}{G}}\sin kx + O(h_c^2 - h^2)^{3/2}, \tag{4.17}$$

$$\varphi = (1 + \frac{Dk^2}{4\pi n_0 m})P + O(h_c^2 - h^2)^{3/2}, \tag{4.18}$$

$$\rho = \frac{k}{2\pi}\sqrt{\frac{(h_c^2 - h^2)}{G}}\cos kx + O(h_c^2 - h^2)^{3/2}, \tag{4.19}$$

$$n = 2n_0 + \frac{k^2(h_c^2 - h^2)}{16\pi^2 n_0 G}\cos^2 kx + O(h_c^2 - h^2)^2, \tag{4.20}$$

with

$$\begin{aligned} G = {} & Dk^4 |A|^2_{\text{eff}}\,(64\pi^2 m^2 n_0^2 (Dk^2 + 4\pi m n_0)^2)^{-1} \times \\ & [2\pi m^3 n_0 + \\ & \quad c_1(Dk^2 m^2 n_0 + 4\pi m^3 n_0^2) + \\ & \quad c_2(4Dk^2 m^2 n_0^2 + 16\pi m^3 n_0^3) + \\ & \quad c_3(12\pi D^2 k^2 m n_0 + 3D^3 k^4) \quad]. \end{aligned} \tag{4.21}$$

Here $h_c^2 = h_c^2(k)$ is the value of h^2 where modulations with wave number k become unstable.

Note the following points: The result is independent of τ_n. However, this degeneracy can be removed, e.g. by introducing cross diffusion terms $-D_2\partial_x n_{\mp}$ in Eq. (4.15). Another consequence of the particular form of Eqs. (4.14,4.15) is the simple relation

$$\tilde{n}_{2k,0} = \frac{|\tilde{\rho}_{k,0}|^2}{4n_0} \tag{4.22}$$

between the Fourier modes of ρ and n [we define the Fourier transform $\tilde{f}$ of a function f by $f(x,y) = \sum_{k,l} \tilde{f}_{k,l} \exp i(kx + ly)$]. To lowest order one has $n - 2n_0 \sim \cos^2 kx$, so that right between the chains there is no net effect of the pattern on the value of n. Both results should allow a simple comparison with experimental chevrons.

4.5 Comparison with Simulations

As pointed out in the introduction, chevron patterns are easily generated by simulations of our "microscopic equations" (1.123,1.127). Figures 4.4 and 4.9 show snapshots of the steady state for different sets of parameters.

For the semi-quantitative test of this model a pseudo-spectral algorithm on a 128×128 grid with spatial extensions $L_x = 159.63$, $L_y = 60.125$ and periodic boundary conditions was used.

The set of parameters in (1.123,1.127) was chosen in such a way that the chevron bifurcation sets in with a small wave number. Moreover it was made sure that the oscillatory mode is absent. These conditions are satisfied by keeping

$$\begin{aligned} \tau &= 1.53558, & \beta_y &= 1.07013, \\ K_3 &= 0.180594, & \Gamma &= -0.0304092 \end{aligned} \tag{4.23}$$

fixed, and using h^2 as a control parameter. Recall that the chevron amplitude increases by *lowering* h^2. The condition of small k_c implies also $h_c^2(k_c)$ to be small and consequently the supercritical range is rather small, too.

The most basic assumption of the model is that, to linear order, the dynamics of $\overline{P}$ and $\overline{\varphi}$ may be isolated from the remaining degrees of freedom and can be described by a set of linear PDEs, even though the full dynamics of A is strongly nonlinear. The coupling to the other degrees of freedom should be describable by adding noise. Close to the chevron instability, where one of the branches of eigenvectors of these linear PDEs is strongly excited by the noise, there should be a strong correlation between the Fourier modes of P and φ. Figure 4.5

shows the correlation coefficient $r(k) = \mathrm{Re}\langle \tilde{P}_{k,0}\tilde{\varphi}^*_{k,0}\rangle_t/(\langle|\tilde{P}_{k,0}|^2\rangle_t\langle|\tilde{\varphi}_{k,0}|^2\rangle_t)^{1/2}$ for $h^2 = 0.025$. Clearly there is essentially perfect correlation for $k < 0.24$. The sharp drop of $r(k)$ at $k \approx 0.3$ may be partly due to a change of the relative sign of $P_{k,0}$ and $\varphi_{k,0}$ in the linear mode.

In order to test the usefulness of the particular form (4.5,4.6) of the PDEs, methods were developed to "measure" σ and D in simulations. To find σ, the Fourier mode $\tilde{\varphi}_{0,0}$ of φ is fixed at some finite value φ_0, while all other modes evolve according to Eq. (1.127). This has been implemented by resetting $\tilde{\varphi}_{0,0}$ to φ_0 after each time step. The simulation is run until a steady state is reached. Then φ_0 is set equal to zero. Figure 4.6 shows the average value of P as a function of the time Δt after switching φ_0 to 0. Within the accuracy obtained, the decay is exponential. The relaxation rate of the global average of P equals $2\pi\sigma$.

Similarly, in order to measure D, a single pair of long-wavelength Fourier modes $\tilde{\varphi}_{k_0,0}$, $\tilde{\varphi}_{-k_0,0}$ of φ is fixed at a finite value φ_0. D/σ can then be calculated from the steady state average of $\tilde{P}_{k_0,0}$ by setting $\partial_t\overline{\rho} = 0$ in Eq. (4.5). The values for σ and D obtained for different values of φ_0 and k_0 were consistent. As simple estimates for $|A|^2_{\mathrm{eff}}$ and n_0 the spatial and temporal averages of $|A|^2$ and $n/2$ were used.

The numerically calculated coefficients at $h^2 = 0.025$ are

$$\begin{aligned} |A|^2_{\mathrm{eff}} &= 0.7996(4), & n_0 &= 0.00509(10), \\ D/\sigma &= 38.0(1.3), & \sigma &= 0.01330(73). \end{aligned} \tag{4.24}$$

Error estimates contain only stochastic contributions. From the linear model one then calculates the threshold $h_c^2 = 0.037(5)$ and the critical wavenumber $k_c = 0.214(5)$.

Critical slowing down and strong noise make a precise determination of the threshold in simulations difficult. Since we expect h_c^2 to be close to zero, where the Goldstone mode becomes unstable, the straightforward method of extrapolating the supercritical modulation amplitude to zero cannot be applied. Instead we look at the subcritical excitation of linear modes by noise. Without nonlinear interaction one expects a relation of the type $\left\langle|\tilde{\rho}_{k,0}|^2\right\rangle_t^{-1} \sim -s_k(h^2)$, where $s_k(h^2)$ is the growth rate of the linear mode at wave number k. Figure 4.7 shows some numerical results for $\left\langle|\tilde{\rho}_{k,0}|^2\right\rangle_t^{-1}$ at various values of k. The dotted line is a linear fit to $k = 0.19680$, which implies a threshold value of $h^2_{\mathrm{c,num}} \approx 0.01$. At $h^2_{\mathrm{c,num}}$, however, the $k = 0.19680$ mode itself is already strongly suppressed by nonlinear interaction with other modes. Possibly the discrepancy between h_c

and $h_{\mathrm{c,num}}$ is to a large part an effect of the combination of nonlinear interaction and strong noise. For further discussion see the next section. Figure 4.9 shows the fully excited chevron pattern at $h^2 = 0.005$.

Two aspects of the nonlinear model were tested. Firstly, Eq. (4.22) is found to be well satisfied, as long as only one mode is active. In Fig. 4.8 the distribution of pairs $(|\tilde{n}_{2k,0}|, |\tilde{\rho}_{k,0}|^2)$ and the theoretical line for $k = 0.19680$ and $h^2 = 0.025$ are shown. While $|\tilde{\rho}_{k,0}|^2$ is large the other modes are suppressed nonlinearly and the single mode approximation made in Eq. (4.22) is legitimate, whereas when $|\tilde{\rho}_{k,0}|^2$ is small the influence of competing modes becomes noticeable.

Secondly, the prediction of Eqs. (4.17,4.19,4.21) for the chevron amplitude was tested. Due to the intricate situation at threshold our simple result cannot give more than an order of magnitude estimate. The solid line plotted in Fig. 4.7 shows the prediction of formula (4.19). It was calculated using coefficients as for the linear model with $k = k_c$, $m = \sigma/2n_0 = 1.31(8)$ and $c_1, c_2, c_3 = 0$ without any fitting. It is easily seen that in our case the terms containing c_1, c_2, c_3 give only small corrections as long as $c_1, c_2, c_3 = O(1)$.

The Hopf bifurcation predicted by our model can actually be found in simulations of Eqs. (1.123,1.127). For example, at $\tau = 2.19369$, $\beta_y = 1.07013$, $K_3 = 0.338614$, $\Gamma = -0.0608184$ and $h^2 = 0.1$ one gets $|A|^2_{\mathrm{eff}} = 0.7409(5)$, $\sigma = 0.01075(36)$ and $D/\sigma = 44.4(2.2)$. From this the Hopf threshold is found to be $h^2_{\mathrm{Hopf}} = 0.186(19)$. The frequency of the $k = 0$ eigenmode is $\omega^2 = -4\pi\Gamma|A|^2_{\mathrm{eff}}\sigma - [\Gamma(|A|^2_{\mathrm{eff}} - h^2) - \pi\sigma]^2 = (0.0282(7))^2$ which is in good agreement with the maximum of the Fourier transform of the simulated time series of $\tilde{\varphi}_{0,0}$ shown in Fig. 4.10.

4.6 Discussion

As mentioned before the most striking case of experimental chevron formation occurs in the dielectric regime of electroconvection in planarly oriented nematics. At first glance one would not expect this system to fall into the class described by the theory, Eqs. (1.123,1.127), because here the horizontal orientation of the nematic director $\hat{n}$, which would represent the isotropy breaking degree of freedom, is fixed by the boundaries which have been prepared to align the director in one direction. However, in the dielectric regime the wavelength of the convection pattern is essentially independent of, and usually much smaller than the thickness of the layer d [25]. Then the boundaries can be reduced to a perturbative effect that may be described by the term $H^2\varphi$ in Eq. (1.127) [26].

It is not easy to verify the validity of our model for planar dielectric EC. The most important prediction is the relation between the local wave vector and the director. A straightforward polarimetric measurement of the director making use of the birefringence of the material, however, is not possible, since the polarization axis of light passing the probe follows the director essentially adiabatically. The polarization axis is therefore determined by the boundaries. Only recently a special optical setup made it possible to directly visualize the modulations of the director [1].

Defects in experimental chevrons can align much better along chains than has been found in the simulations. This is presumably because higher-order terms and non-adiabatic effects that couple the defect cores to the underlying roll structure are not included in the amplitude equations. When experimental chevron patterns are strongly excited it is usually observed that defects start to move along the chains, alternatingly 'up' and 'down', i.e. there is a correlation between $\partial_x \varphi$ and the y component of the velocity of a defect (ignoring its charge). This cannot be observed in simulations of Eqs. (1.123,1.127). In fact, it is forbidden by the accidental symmetry $\varphi \to -\varphi$, $A \to A^*$ of Eqs. (1.123,1.127). Inclusion of higher order terms would break this symmetry. In contrast, the invariance under $\varphi \to -\varphi$, $y \to -y$, which follows from inversion symmetry, remains.

It should be emphasized that chevrons cannot appear directly from the homogeneous (basic) state via a stationary supercritical bifurcation. Although this is consistent with most experiments there is some evidence that at sufficiently high frequencies chevrons can be observed directly at onset of the dielectric instability [21]. This would mean that either the primary bifurcation becomes subcritical, which is not expected from theory, or there is a ("hidden") bifurcation leading to an inhomogeneous state already below the dielectric instability. According to some older measurements the possibility of a first transition to a state with "wide domains" (with width $\sim d$) appears to exist [43, 31, 2, 55], but this phenomenon has not been clarified. In any case this cannot be the general explanation.

Chevron-like structures have also been found in simulations of the anisotropic version of the well-known complex Ginzburg-Landau equation [56]. The mechanism operative here is presently under investigation.

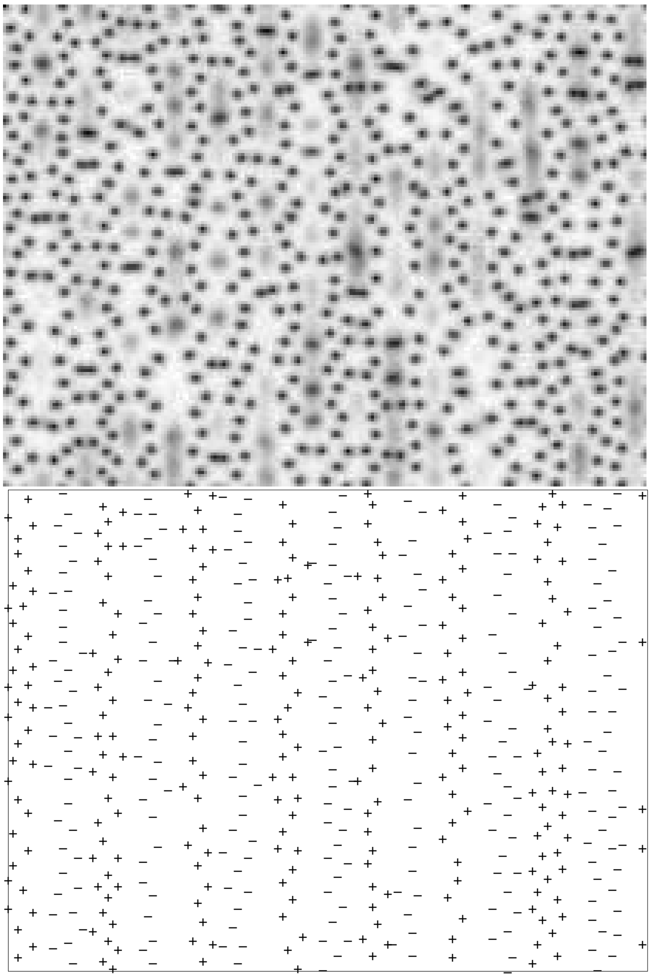

Figure 4.4: *Snapshot of a simulation of Eqs. (1.123,1.127) with* $\tau = 4.38738$, $\beta_y = 1.07013$, $K_3 = 0.0564357$, $\Gamma = -0.0304092$, $h^2 = 0.03$ *in a rectangle of size* 159.631×120.25. *The upper image shows* $|A|$ *encoded in a grey scale, the lower one shows the positions and polarity of defects as detected by the algorithm used throughout this work.*

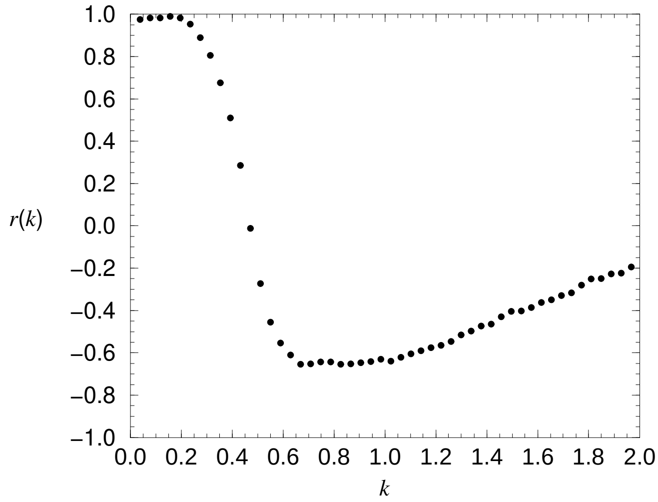

Figure 4.5: *Correlation between Fourier modes (see text).*

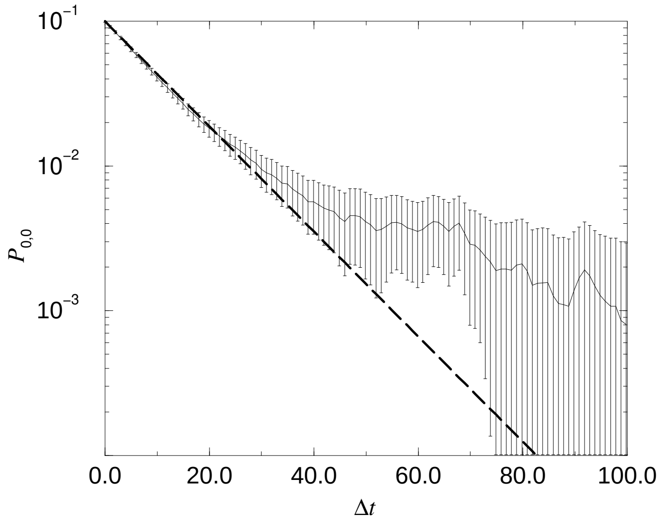

Figure 4.6: *Relaxation of* $\tilde{P}_{0,0}$ *after a jump in* $\tilde{\varphi}_{0,0}$ *from* $\varphi_0 = 0.1$ *to* 0*, averaged over 59 runs. The dashed line is a least square fit.*

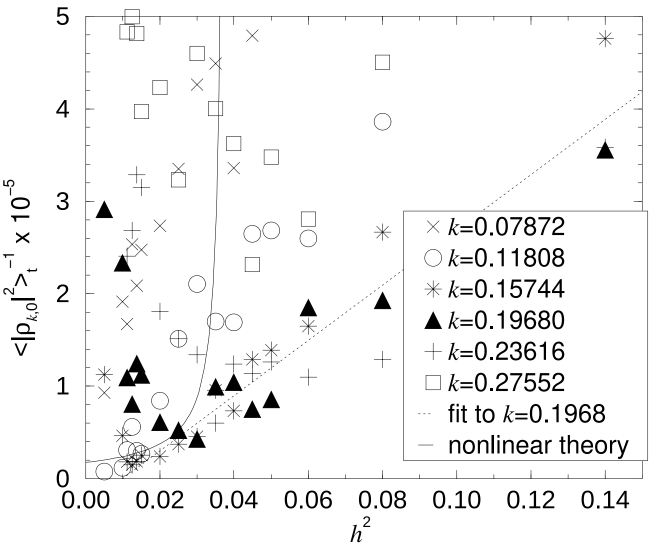

Figure 4.7: *Test of the linear and nonlinear model, see text.*

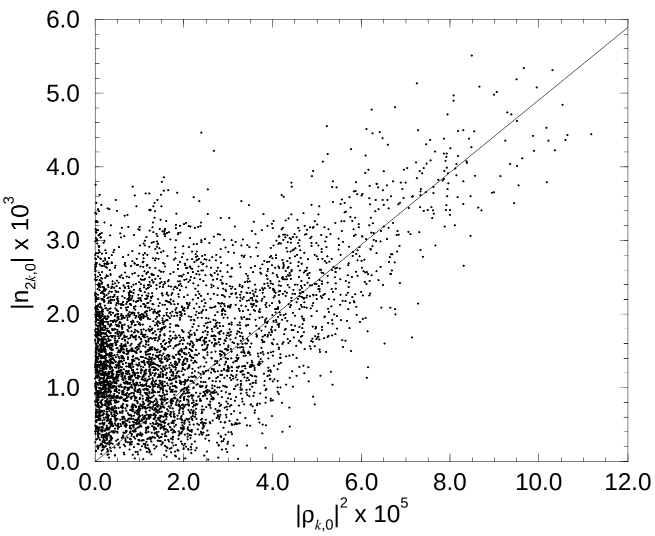

Figure 4.8: *Samples of pairs* $(|\tilde{n}_{2k,0}|, |\tilde{\rho}_{k,0}|^2)$ *at* $k = 0.19680$ *and* $h^2 = 0.025$ *from numerical simulations and the relation given by (4.22) (solid line).*

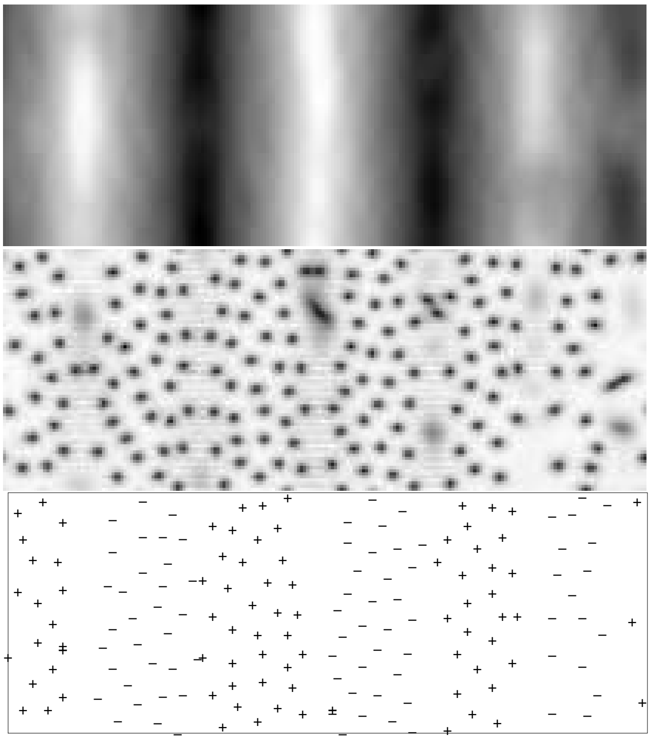

Figure 4.9: *Snapshot of the steady state corresponding to* $h^2 = 0.005$ *in Fig. 4.7. Top: values of* φ $(-2.33 \ldots 2.30)$ *encoded on a gray scale; center:* $|A|$*; bottom: defect positions and polarities.*

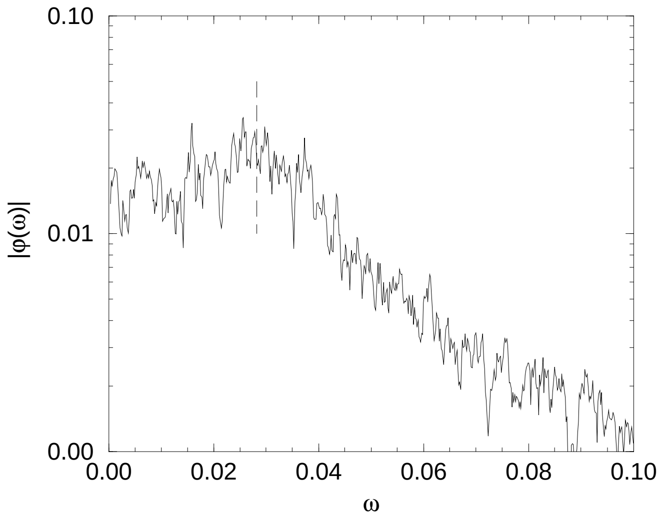

Figure 4.10: *Fourier transform of φ in a simulation of Eqs. (1.123,1.127) in the oscillatory regime. The frequency of the most unstable mode of Eqs. (4.4–4.6) is indicated by the dashed line. The parameters are given in Section 4.5.*

References

[1] H. Amm, R. Stannarius, and A. G. Rossberg. Optical characterization of chevron texture formation in nematic electroconvection. Preprint, May 1997.

[2] M.I. Barnik, L.M. Blinov, M.F. Grebenkin, and A.N. Trufanov. Dielectric Regime of Electrohydrodynamic Instability in Nematic Liquid Crystals. *Mol.Cryst.Liq.Cryst* 37:47, 1976.

[3] L. M. Blinov. *Electrooptical and Magnetooptical Properties of Liquid Crystals*. John Wiley, New York, 1983.

[4] E. Bodenschatz, W. Pesch, and L. Kramer. Structure and dynamics of dislocations in anisotropic pattern-forming systems. *Physica D* 32:135, 1988.

[5] E. Bodenschatz, W. Zimmermann, and L. Kramer. On electrically driven pattern-forming instabilities in planar nematics. *J. Phys.(Paris)* 49:1875, 1988.

[6] H. R. Brand and H. Pleiner. *J.Phys. (Paris)* 45:563, 1984.

[7] F. H. Busse. Non-linear properties of thermal convection. *Rep. Prog. Phys.* 41:1929, 1978.

[8] S. Chandrasekhar. *Liquid Crystals*. University Press, Cambridge, 1992.

[9] M. C. Cross. *Phys. Rev. A* 27:490, 1983.

[10] M. C. Cross and P. C. Hohenberg. Pattern formation outside of equilibrium. *Rev. Mod. Phys.* 65:851, 1993.

[11] P. G. de Gennes and J. Prost. *The Physics of Liquid Crystals*. Clarendon Press, Oxford, 1993.

[12] W. Decker. PhD thesis, Universität Bayreuth, 1995.

[13] E. Dubois-Violette, P.G. De Gennes, and O. Parodi. *J.Phys. (Paris)* 32:305, 1971.

[14] J. Guckenheimer and P. Holmes. *Nonlinear Oscillations, Dynamical Systems and Bifurcations of Vector Fields*, volume 42 of *Applied Mathematical Sciences*. Springer, New York, 1983.

[15] G. Heilmeier and W. Helfrich. *Appl. Phys. Lett.* 16:1955, 1970.

[16] A. Hertrich. Elektrohydrodynamische Instabilitäten in nematischen flüssigen Kristallen mit nichttrivialen Grundzuständen. PhD thesis, Universität Bayreuth, May 1995.

[17] A. Hertrich, W. Decker, W. Pesch, and L. Kramer. The electrohydrodynamic instability in homeotropic nematic layers. *J. Phys. France* II 2:1915, 1992.

[18] K. Hirakawa and S. Kai. Analogy Between Hydrodynamic Instabilities in Nematic Liquid Crystal and Classical Fluid. *Mol.Cryst.Liq.Cryst.* 40:261, 1977.

[19] D. Igner and J.H. Freed. Electrohydrodynamic instabilies observed in a nematic phase under oblique boundary conditions. *J.Chem.Phys* 76(12):6095, 1982.

[20] S. Kai, S. Hayashi, and Y. Hidaka. Pattern forming instability in homeotropically aligned liquid crystals. *J. Phys. Chem* 100(49):19007–190016, Dec 1996.

[21] S. Kai and W. Zimmermann. Pattern dynamics in the electrohydrodynamics of nematic liquid crystals. *Prog. Theor. Phys. Suppl.* 99:458, 1989.

[22] M. Kaiser. *Amplitudengleichungen für die elektrohydrodynamische Instabilität in nematischen flüssigen Kristallen.* Dissertation, Universität Bayreuth, 1992.

[23] M. Kaiser, W. Pesch, and E. Bodenschatz. Mean flow effects in the electrohydrodynamic convection in nematic liquid crystals. *Physica D* 59:320, 1992.

[24] L. Kramer and W. Pesch. Convection instabilities in nematic liquid crystals. *Annu. Rev. Fluid Mech.* 27:515, 1995.

[25] L. Kramer and W. Pesch. Electrohydrodynamic instabilities in nematic liquid crystals. In A. Buka and L. Kramer, editors, *Pattern formation in liquid crystals*. Springer, New York, 1995.

[26] A. Lindner. Diploma thesis, Universität Bayreuth, 1997.

[27] P. Manneville. *Dissipative Structures and Weak Turbulence.* Academic Press, New York, 1990.

[28] I. Melbourne. Derivation of the Time-Dependent Ginzburg-Landau Equation on the Line. University of Houston Research Report UH/MD-205 1995. To appear in J. Nonlin. Sci.

[29] I. Melbourne. Steady-state bifurcation with Euclidean symmetry. University of Houston Research Report UH/MD-214, 1996. To appear in Trans. AMS.

[30] N. D. Mermin and H. Wagner. Absence of ferromagnetism or antiferromagnetism in one- or two-dimensional istropic Heisenberg models. *Phys. Rev. Lett* 17(22), Nov. 1966.

[31] L. Nasta, A. Lupu, and M. Giurgea. Characteristics of Domains Appearing in Nematic Liquid Crystals Below the Threshold Voltage of Chevrons. *Mol.Cryst.Liq.Cryst.* 71:65, 1981.

[32] S. Nasuno, O. Sasaki, S. Kai, and W. Zimmermann. Secondary instabilities in electroconvection in nematic liquid crystals. *Phys. Rev. A* 46:4954, 1992.

[33] S. Nasuno, O. Sasaki, S. Kai, and W. Zimmermann. Stability diagram in electrohydrodynamic convection of nematics Electrohydrodynamic convection in nematics: the homeotropic case. In S. Kai, editor, *Pattern formation in complex dissipative systems and Global Dynamics*, page 275. World scientific, Singapore, 1992.

[34] A. C. Newell and J. A. Whitehead. Finite bandwidth, finit amplitude convection. *J. Fluid Mech.* 38:279, 1969.

[35] Orsay Liquid Crystal Group. *Mol.Cryst.Liq.Cryst.* 12:251, 1971.

[36] W. Pesch and L.Kramer. Nonlinear analysis of spatial structures in two-dimensional anisotropic pattern forming systems. *Z.Phys. B* 63:121, 1986.

[37] E. Plaut, W. Decker, A. G. Rossberg, L. Kramer, and W. Pesch. New Symmetry Breaking in Nonlinear Electroconvection of Nematic Liquid Crystals. *Phys. Rev. Lett* 79(12):2367–2370, Sep. 1997.

[38] E. Plaut and W. Pesch. Preprint, July 1997.

[39] E. Plaut and W. Pesch. Extended weakly nonlinear theory of Thermoconvection in a planar nematic layer. *Phys. Rev. E* 56(3):R2375–R2378, Sep. 1997.

[40] E. Plaut and R. Ribotta. Cascade of structures in the thermoconvection of a nematic in the director-dominated regime. *Europhys.Lett.* 38(6):441–446, May 1997.

[41] H. Pleiner and H. Brandt. Hydrodynamics and electrohydrodynamics of liquid crystals. In A. Buka and L. Kramer, editors, *Pattern formation in liquid crystals.* Springer, New York, 1995.

[42] S. Rasenat. PhD thesis, Universität Bayreuth, 1991.

[43] R. Ribotta and G. Durand. High Frequency Electrohydrodynamic Instabilies in Nematic Liquid Crystals. *J.Phys. (Paris) Colloque* C3:334, 1979.

[44] H. Richter. *Elektronisch induzierte Instabiliäten in homöotrop und planar angeordneten nematischen Flüssigkristallen.* PhD thesis, Universität Bayreuth, Feb. 1995.

[45] H. Richter, A.Buka, and I.Rehberg. *Spatio-Temporal Patterns in Nonequilibrium Complex Systems*, pages 343–352. Addison-Wesley Publishing Company, 1994.

[46] H. Richter, A.Buka, and I.Rehberg. Electrohydrodynamic convection in a homeotropically aligned nematic sample. *Phys.Rev. E* 51:5886, 1995.

[47] H. Richter, N. Klöpper, A. Hertrich, and A. Buka. Electroconvection in a Homeotropic Nematic under the Influence of a Magnetic Field. *Europhys. Lett.* 30:37, 1995.

[48] H. Riecke and L. Kramer. Surface-induced chemical oscillations and their influence on space- and time-periodic patterns. *J. Chem. Phys.* 83:3941, 1985.

[49] A. G. Rossberg and L. Kramer. Weakly Nonlinear Theory of Electroconvection in Homeotropically Oriented Nematic Liquid Crystals. *Phys. Scr.* T67:121, Dec 1996.

[50] M. Scheuring. Strukturbildung im dielektrischen Bereich von nematischen Flüssigkristallen. Diploma thesis, Universität Bayreuth, 1996.

[51] L. A. Segel. Distant side-walls cause slow amplitude modulation of cellular convection. *J. Fluid Mech.* 38:203, 1969.

[52] E. D. Siggia and A. Zippelius. Pattern selection in Rayleigh-Bènard convection near threshold. *Phys.Rev.Lett.* 47:835, 1981.

[53] P. Takáč, P. Bollerman, A. Doelman, A. van Harten, and E. S. Titi. Analyticity of essentially bounded solutions to semilinar parabolic systems and validity of the Ginzburg-Landau equation. *SIAM J. Math. Anal* 27(2):424–448, March 1996.

[54] P. Tóth. Elektrokonvektion in homöotropen Flüssigkristallen. Diploma thesis, Universität Bayreuth, August 1996.

[55] A. N. Trufanov, L. M. Blinov, and M. I. Barnik. New type of high-frequency electrohydrodynamic instability in nematic liquid crystals. *Sov.Phys.JETP* 51(2):314, 1980. original in Zh.Eksp.Teor.Fiz **78** 622 (February 1980).

[56] A. Weber, E. Bodenschatz, and L. Kramer. *Advanced Materials* 3:191, 1991.

Thanks

I would like to do this in German:

"Lieber Herr Prof. Kramer, es hat großen Spaß gemacht, mit Ihnen zusammenzuarbeiten. Hoffentlich erhalten noch viele Studenten diese Möglichkeit."

Außerdem gilt mein Dank Heidi, Elsebeth, allen Bayreuther Physikern und natürlich den freundlichen Franken.

Axel Roßberg